

7-22-2010

Inhibition studies of serine hydrolases by cyclic phosphates and phosphonates

Supratik Dutta

University of Missouri-St. Louis, sdvd6@gmail.com

Follow this and additional works at: <https://irl.umsl.edu/dissertation>



Part of the [Chemistry Commons](#)

Recommended Citation

Dutta, Supratik, "Inhibition studies of serine hydrolases by cyclic phosphates and phosphonates" (2010). *Dissertations*. 471.
<https://irl.umsl.edu/dissertation/471>

This Dissertation is brought to you for free and open access by the UMSL Graduate Works at IRL @ UMSL. It has been accepted for inclusion in Dissertations by an authorized administrator of IRL @ UMSL. For more information, please contact marvinh@umsl.edu.

Inhibition studies of serine hydrolases by cyclic phosphates and phosphonates

by

Supratik Dutta

M.S, Chemistry, University of Missouri, St. Louis, 2007

M.Sc, Organic Chemistry, University of Burdwan, 2001

B.Sc, Chemistry, University of Burdwan, 1999

A Dissertation

Submitted to the Office of Graduate studies of the

UNIVERSITY OF MISSOURI-ST. LOUIS

In partial fulfillment of the requirements for the degree of

DOCTOR OF PHILOSOPHY

in

CHEMISTRY

with an emphasis in Biochemistry

July 2010

Advisory committee

Dr. Cynthia M. Dupureur

Chairperson

Dr. Michael R. Nichols

Dr. Chung F. Wong

Dr. Bethany K. Zolman

Abstract

Inhibition studies of serine hydrolases by cyclic phosphates and phosphonates

(June 2010)

Supratik Dutta, M.S., University of Missouri, St. Louis, MO, USA.

Chair of Committee: Dr. C. M. Dupureur

The serine hydrolase superfamily is one of the largest known enzyme families comprising approximately 1% of the predicted protein product in human genome. This family of enzymes contains a catalytic triad that is mainly consists of serine, aspartic acid/glutamic acid and histidine residues in their active sites. It has been proposed that the potential drug targets for Alzheimer's disease and diabetes type 2 are enzymes that belong to this enzyme family.

Acetylcholinesterase (AChE) is an enzyme that catalyzes the breakdown of acetylcholine, a neurotransmitter that helps transport information from one nerve cell to another. Breakdown of acetylcholine in Alzheimer's disease patients enhances memory loss, which could be reduced if AChE is inhibited. Cyclophostin, a bicyclic phosphate, is a natural product inhibitor of AChE having an IC_{50} of 8×10^{-4} μ M. The laboratory-

synthesized mono- and bicyclic analogs of phosphonate analog of cyclophostin exhibited low μM potency against human AChE. It is established that these analogs covalently modify the active site of AChE and do not dissociate from the active site upon treatment with oximes. From a comparative analysis of kinetic data these compounds are less toxic and milder than the existing AChE inhibitors and can be used as potential chemotherapeutic agent against Alzheimer's disease.

Hormone-sensitive lipase (HSL) is another serine hydrolase enzyme that hydrolyzes lipids in the form of triglycerides. It is a homodimer of 84 kDa subunits and is mostly found in adipose tissues. HSL is a potential drug target for diabetes type 2. The activity of HSL must be inhibited in insulin deficient patients to lower the risk of associated cardiovascular disease. Cyclophostin is a natural product inhibitor of HSL. Laboratory-synthesized monocyclic phosphonate analogs of cyclophostin having varying C-chain length exhibited μM potency against rat HSL. The potency of these analogs improved upon introducing longer C-chain like C_{16} . This class of compounds showed an aggregation property that affected their potency against the enzyme. The attachment of the C-chain at the P-center of the monocyclic phosphonate analog considerably improved the potency (almost 10 fold).

HSL has not been crystallized yet, so the biophysical events triggering the translocation of the enzyme towards lipid storage modules upon phosphorylation are not well established. It is shown that the translocation of the enzyme happens due to the hydrophobic surface exposure of the protein upon phosphorylation. It is revealed from fluorescence data that at least S563 and S565 phosphorylation sites do not have a

significant effect on the exposure process. *In vivo* translocation experiments revealed that for translocation, the β -adrenergic hormone (forskolin) treatment is important for the co-localization of protein to the lipid.

DEDICATION

To my wife Sudakshina, my parents, Guria, Nupur and Tarakkaka.

ACKNOWLEDGEMENT

I would like to express my deepest gratitude to my advisor Prof. Cynthia Dupureur. I am indebted to her for the opportunity that she has given me to work on numerous projects towards the completion of my dissertation. This thesis would not have been possible without her invaluable guidance. I would like to sincerely thank Prof. Christopher Spilling for providing all the resources for the different projects. I am grateful for his inputs and helpful advice towards my research. I would also like to express my gratitude to Dr. Michael R. Nichols for providing me valuable information about maintaining cell culture facility and for his availability whenever I needed it. My sincere thanks go to the members of the Nichol's lab especially to Malou who has always been very helpful and supportive. Many thanks are due to Dr. Chung Wong who always had time to discuss my docking experiment related questions. I really appreciate his valuable and precise advice, which correctly oriented me many times. I also want to thank Dr. Sophie Alvarez in Danforth Plant Science Center for performing the MALDI-TOF experiments for me. Without the mass spectroscopic data the publication in BMC would not have been possible. I thank Prof. George Gokel for allowing me to use the DLS instrument in his lab. My sincere gratitude goes to Prof. Frederic Kraemer in Stanford for his generous donation of the rat HSL gene. I would like to thank my committee members Dr. Michael R. Nichols, Dr. Chung Wong and Dr. Bethany Zolman for reading my manuscript and also for their helpful comments.

Special thanks go to Dr. Saibal Bandhopadhaya and Raj K. Malla for synthesizing the required molecules for the project. My deepest and warmest gratitude

goes to my previous labmates Dr. Grigorios A. Papadakos, Dr. Fuqian Xie, Dr. Charulata Prasannan, Binod Pandey and Mary Keithly. Apart from working together I really enjoyed and appreciated their invaluable friendship. I would also like to express my thankfulness to my current labmate Elena Vasilieva for her support and friendship. I wish her all the luck for completion of her graduation. Many thanks also go to my good friends Laurel Mydock, Geeta Paranjape, Sneha Ranade, Sudeshna Roy and Sergey Sedinkin. It has really been a pleasure.

I would not have completed this thesis without the endless and loving support of my wife, Sudakshina. I also want to express my deepest gratitude towards my parents. In spite of the long distance they have always been understanding and encouraging. As a least sign of acknowledgement I would like to dedicate this work to them.

Finally I would like to thank the Department of Chemistry and Biochemistry in the University of Missouri St.Louis for the opportunity in graduate studies that I was provided and the NIH for the financial support of my projects.

TABLE OF CONTENTS

	Page
ABSTRACT	ii
DEDICATION	v
ACKNOWLEDGEMENTS	vi
TABLE OF CONTENTS	viii
LIST OF FIGURES	xi
LIST OF TABLES	xiv
LIST OF SCHEMES	xv
LIST OF ABBREVIATIONS	xvi
CHAPTER I INTRODUCTION	
1.1 Introduction to serine hydrolases	1
1.2 Introduction to Acetylcholinesterase (AChE)	3
1.3 Inhibitors of AChE	18
1.4 Introduction to Hormone-sensitive lipase (HSL)	27
1.5 Inhibitors of HSL	43
CHAPTER II MATERIALS AND METHODS	
2.1 Inhibition studies of AChE	48
2.2 Inhibition studies of rat hormone-sensitive lipase (HSL)	54

2.3	Hormone-sensitive lipase translocation to lipid droplets in 3T3-L1 adipocyte cells	62
2.4	1-anilino-naphthalene-8-sulphonate (1, 8-ANS) binding to rat HSL	65
2.5	Dynamic light scattering (DLS) experiment of HSL inhibitors in aqueous solution	68
2.6	Structure aided multiple sequence alignment (SSAMSA) of HSL and CRL using SwissPDB Viewer	68
CHAPTER III	INHIBITION STUDIES OF ACETYLCHOLINESTERASE IN PRESENCE OF BICYCLIC PHOSPHONATE ANALOG OF CYCLOPHOSTIN	
3.1	Acetylcholinesterase (AChE) inhibition and structure-activity relationship of laboratory synthesized organophosphates (OPs)	70
3.2	Active site serine modification of AChE by cyclic phosphonate	83
3.3	Inhibition studies of human AChE in presence of laboratory synthesized natural product cyclophostin	89
CHAPTER IV	INHIBITION STUDIES OF RAT HORMONE-SENSITIVE LIPASE AND ITS PHOSPHORYLATION-INDUCED TRANSLOCATION IN 3T3-L1 CELLS	
4.1	Structure-activity relationship of laboratory synthesized inhibitors of hormone-sensitive lipase HSL	97
4.2	<i>In vitro</i> fluorescence studies of rat HSL's hydrophobic surface exposure upon phosphorylation	102
4.3	<i>In vivo</i> studies of rat HSL translocation from cytoplasm to lipid droplets in 3T3-L1 cells	103
CHAPTER V	DISCUSSION	
5.1	Comparison of potency of laboratory synthesized OPs with the commercially available OPs against human AChE.	109

5.2 Probable reasons for less potency of compound 22 to 24 against rat HSL.	111
5.3 Phosphorylation induced translocation of rat HSL	117
REFERENCES	119
VITA	130

LIST OF FIGURES

	Page
Figure 1.1	Secondary structure of SHs. 2
Figure 1.2	Acylation and deacylation steps of SHs at the active site. 4
Figure 1.3	Hydrolysis of natural substrate acetylcholine (ACh) by AChE. 5
Figure 1.4	Mechanism of neuron to neuron information transfer and role of AChE 6
Figure 1.5	Crystal structure of a subunit of the recombinant human AChE. 8
Figure 1.6	ClustalW based multiple sequence alignment of human, electric eel, and house fly AChE. 10
Figure 1.7	Active site structure of recombinant AChE. 11
Figure 1.8	Reversible inhibitors of AChE. 20
Figure 1.9	Organophosphate inhibitors of SHs. 22
Figure 1.10	Formation of tetrahedral intermediate in the reaction between SH and OP. 23
Figure 1.11	Hydrolysis of triacylglycerol (TAG) and cholesterol ester by HSL. 29
Figure 1.12	Predicted structure of rat HSL. 32
Figure 1.13	Secondary structure of C-terminal domain of rat HSL. 34
Figure 1.14	Predicted secondary structure of regulatory loop domain. 35
Figure 1.15	Phosphorylation and translocation of HSL to lipid droplets. 39

	Page
Figure 1.16	Kyte and Doolittle hydropathy plot of rat HSL. 41
Figure 2.1	Reaction of AChE-organophosphate complex with oxime. 53
Figure 2.2	Western Blot analysis of recombinant HSL gene containing baculovirus infected Sf9 cell lysate. 56
Figure 2.3	SDS-PAGE gel from recombinant rat HSL purification using Ni-NTA beads. 59
Figure 2.4	A confocal image of YFP-HSL protein in pre-adipocyte 3T3-L1 cell. 64
Figure 2.5	BODIPY-C ₁₂ stained differentiated 3T3-L1 cells. 66
Figure 2.6	1, 8-ANS excitation and emission spectra. 67
Figure 3.1	Diastereospecificity of 2a and 2b against human and electric eel AChE. 73
Figure 3.2	Test of irreversibility of 2a -human/electric AChE reaction. 77
Figure 3.3	Kinetics of inhibition of human AChE in presence of 2a and 2b . 78
Figure 3.4	Kinetics of inhibition of human AChE in presence of 9 and 15 . 79
Figure 3.5	Kinetics of inhibition of human AChE in presence of DIFP. 80
Figure 3.6	Probable fate of human AChE- 2a complex. 84
Figure 3.7	Pralidoxime reactivation of human AChE- 2a complex. 86
Figure 3.8	MALDI-TOF evidence of covalent modification of human AChE active site serine. 88
Figure 3.9	Test of irreversibility of natural/unnatural isomer-human AChE reaction. 92

	Page
Figure 3.10 Kinetics of inhibition of human AChE in presence of natural and unnatural isomer.	93
Figure 3.11 Pralidoxime reactivation of human AChE-natural/unnatural isomer complex.	96
Figure 4.1 ANS binding to rat HSL to probe the hydrophobic surface exposure.	104
Figure 4.2 BODIPY-C12 stained differentiated YFP-HSL transfected 3T3-L1 cells.	106
Figure 4.3 FRET experiment to access HSL translocation to lipid droplet.	107
Figure 5.1 Structural difference of cyclipostin and compound 22-25 .	112
Figure 5.2 Backbone structure of C-terminal domain of rat HSL.	113
Figure 5.3 Simplified docking model of cyclipostin and 24 in HSL active site.	114
Figure 5.4 Dynamic Light Scattering (DLS) experiment of 24 .	116

LIST OF TABLES

	Page
Table 1.1 Substrate specificity of Human AChE.	16
Table 1.2 Cyclophostin and its cyclic phosphonate analogs.	26
Table 1.3 Expression and function of HSL at different tissues and cell types.	30
Table 1.4 Inhibitors of human HSL and their IC ₅₀ s.	45
Table 1.5 Structures of analogs of cyclipostin and their potency against rat HSL.	46
Table 3.1 IC ₅₀ s of organophosphates against AChE from different sources.	72
Table 3.2 Kinetic parameters of inhibition of human AChE by laboratory synthesized OPs.	81
Table 3.3 Potency of natural and unnatural isomer of cyclophostin against human AChE.	90
Table 3.4 Kinetic parameters of inhibition of human AChE by natural and unnatural isomer	94
Table 4.1 IC ₅₀ s of laboratory synthesized HSL inhibitors.	100
Table 5.1 Comparison of first order rate of inactivation (k _i) of OPs against human AChE.	110

LIST OF SCHEMES

	Page
Scheme 1.1 Kinetic Mechanism for AChE Catalysis that Incorporates an Induced-Fit Step.	13
Scheme 1.2 Extended model for substrate hydrolysis by AChE.	17

LIST OF ABBREVIATIONS

AChE, acetylcholinesterase; ACh, acetylcholine; ATCh, acetylthiocholine; DTNB, 5,5'-dithiobis-2-nitrobenzoic acid; OP, organophosphate; CAS, catalytic anionic site; PAS, peripheral anionic site; HSL, hormone-sensitive lipase; *p*-NPB, para nitro phenyl butyrate; TAG, triacylglycerol; DAG, diacylglycerol; MAG, monoacylglycerol; LPL, lipoprotein lipase; ABS, acyl binding site; ATGL, adipocyte triglyceride lipase; LD, lipid droplet; FABP, fatty acid binding protein; FRET, Forster resonance energy transfer; BODIPY, 4,4-difluoro-5-(2-thienyl)-4bora-3a,4a-diaza-*s*-indacene-3 dodecanoic acid; YFP, Yellow fluorescent protein; ANS, anilinonaphthalene sulfonate.

CHAPTER I

INTRODUCTION

1.1 Introduction to Serine hydrolase (SH):

Serine hydrolases (SHs) are a remarkably large and diverse family of enzymes that comprise approximately 1% of the protein products of the mammalian genome (Rawlings et al.; Nelson et al. 1999). These include almost 100 serine proteases (e.g., trypsin, thrombin, elastase) and more than 150 SHs that hydrolyze metabolites and peptides. The SH family consists of esterases (e.g., acetylcholinesterase (AChE)), lipases (e.g., hormone-sensitive lipase (HSL), cytosolic phospholipase A2 (cPLAs)), peptidases (e.g., dipeptidylpeptidase-IV (DPPIV)), and amidases (e.g., fatty acid amide hydrolase (FAAH)). SHs play an important role in many physiological and pathological processes, which include inflammation (Clark et al. 1995), cancer (DeClerck et al. 1997), neural plasticity (Yoshida and Shiosaka 1999), angiogenesis (Mignatti and Rifkin 1996), and diabetes (Gorrell 2005). Most of the SHs (>60%) contain the α/β -hydrolase fold secondary structure (**Fig. 1.1**) (Contreras et al. 1996); however, there are other subclasses of SHs which adopt different types of folds and catalytic machinery, including amidases (serine-lysine-lysine triad) (Bracey et al. 2002; Gorrell 2005) and patatin domain containing lipases (serine-aspartic acid dyad). Generally, SHs contain the serine-histidine-aspartic acid catalytic triad (Bracey et al. 2002; Rawlings et al. 2010); it utilize a conserved serine nucleophile to hydrolyze ester, thioester, and amide bonds in both proteins and small molecule substrates (e.g., metabolites). This reaction is done by attacking substrate esters or amides at the sp^2 carbon by a base-activated

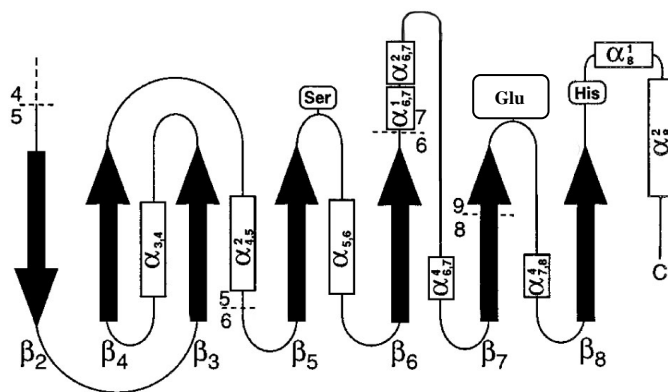


Figure 1.1: Secondary structure of SHs (A-26). The secondary structures of the SHs containing the α/β -hydrolase fold that consists of 8 α -helices (rectangular boxes) and 7 β -sheets (black arrows) in an alternate manner. This unique α/β -hydrolase fold structure brings the serine, glutamic acid, and histidine in proximity to create the catalytic triad for catalysis. Catalytic serine is located between β_5 and $\alpha_{5,6}$, whereas other catalytic triad residues glutamic acid and histidine are located at $\beta_7/\alpha_{7,8}^4$ and β_8/α_8^2 junctions, respectively. Adapted from (Contreras et al. 1996).

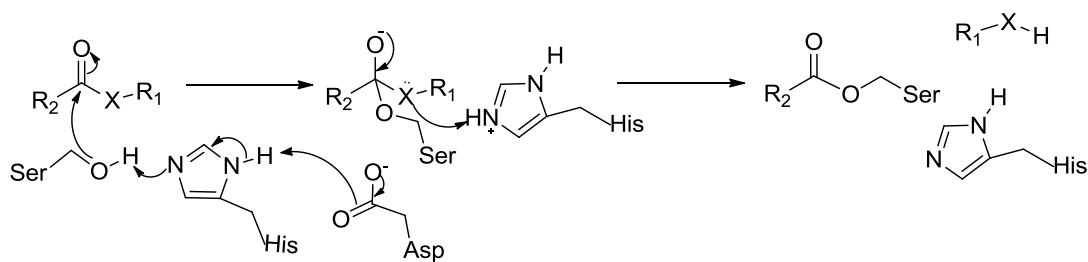
serine nucleophile (**Fig. 1.2**). An active site water molecule then cleaves the resulting acyl-enzyme intermediate to conclude the substrate hydrolysis and revive the hydrolase active form.

1.2 Introduction to Acetylcholinesterase (AChE):

1.2.1 Physiological function:

Acetylcholinesterase (acetylcholine acetylhydrolase, EC 3.1.1.7; abbreviated as AChE) and its natural substrate acetylcholine (ACh) function in the central and peripheral nervous system to transmit action potentials across neurons and neuromuscular synapses (Rosenberry 1975; Rosenberry 1975). AChE catalyses the hydrolysis of the cationic neurotransmitter ACh to choline and acetic acid (**Fig. 1.3**). In response to the action potential in a pre-synaptic neuron, ACh is released at the synapse (**Fig. 1.4**). Then, ACh binds to the acetylcholine receptor at the post synaptic neuron and opens the Na⁺ ion channel. After a series of reaction processes, the action potential triggers the post-synaptic neuron. Finally, ACh is hydrolyzed by extrinsic membrane bound AChE to acetic acid and choline (**Fig. 1.3**) and terminates the ACh receptor mediated ion-gating (Rosenberry 1975; Maelicke and Albuquerque 2000) (**Fig. 1.4**). In neuronal diseases like Alzheimer's disease (AD), the neuron cells suffer from severe damage and produce less ACh and in turn the whole ion-gating process hinders leading to acute memory loss. Researchers have targeted AChE to minimize the ACh hydrolysis and control the memory loss process in the AD disease condition.

Acylation



Deacylation

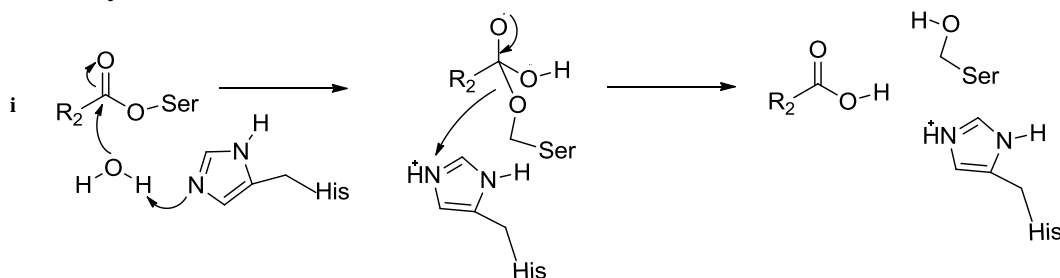


Figure 1.2: Acylation and deacylation steps of SHs at the active site. The SHs active site contains a catalytic triad, which consists of serine, histidine, and glutamic acid. By electron relay process, it hydrolyses the substrate esters ($X = O$ atom) or amides ($X = N$ -atom). As shown in the acylation reaction, the serine does the nucleophilic attack at the carbonyl C-center and forms an acyl-serine intermediate. The active site water molecule does the nucleophilic attack at the carbonyl C-center of acyl-moiety of acyl-serine and forms the ultimate reaction product as acid and alcohol (when substrate is ester) or amine (when substrate is amide).

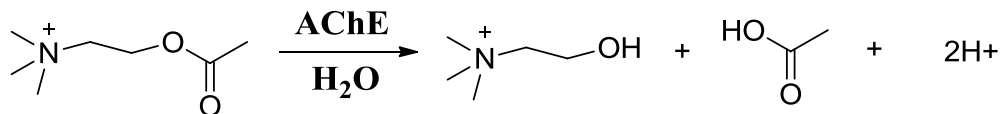


Fig. 1.3: Hydrolysis of natural substrate acetylcholine (ACh) by AChE.

Acetylcholine (ACh) is hydrolyzed by AChE to form acetic acid and choline. The mechanism of hydrolysis is given in **Fig. 1.2**. The positively charged choline moiety of ACh binds the catalytic anionic site residues and directs the business end (the acyl part) of the substrate to the catalytic triad to pursue the chemical hydrolysis step.

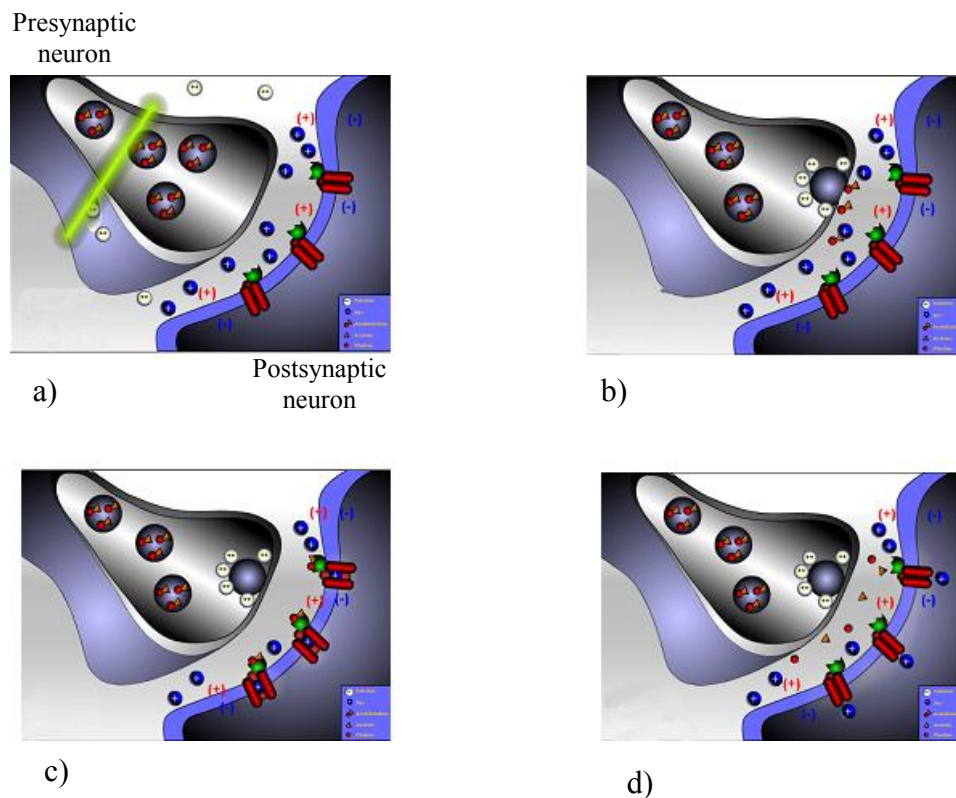


Fig. 1.4: Mechanism of neuron to neuron information transfer and role of AChE.

a) Signal comes as action potential (green line) in pre-synaptic neuron. The action potential attracts the Ca^{+2} ions (white spheres) to bind the ACh-containing (shown as combination of red sphere and yellow triangle) vesicles. b) Ca^{+2} ions rupture the vesicle to release the ACh to the synapse (junction between pre- and post-synaptic neuron). c) The ACh binds to the ACh-receptor on the post-synaptic neuron and opens the Na^{+} ion (shown as blue spheres) channel (shown as red rods). d) Na^{+} ions pass through the channel and thus carry electrical information generated in pre-synaptic neuron. Adapted from (Maelicke and Albuquerque 2000).

In addition to the involvement in terminating ACh-mediated neurotransmission, AChE engages itself in various physiological processes through its role in cell differentiation, regulation of cell proliferation, and cell survival. The effect of AChE in these process depends upon the type of cell involved, the differentiation state, and the binding with protein partners (Soreq et al. 1994). It is reported that suppression of AChE gene in hematopoietic stem cell increases the tendency of cell proliferation, which directly indicates the involvement of AChE in apoptotic processes (Robitzki et al. 1998; Ben-Ari et al. 2006). The exact mechanism of AChE's function in apoptosis is still under investigation. Scientists have found some evidence of involvement of AChE in type 2 diabetes mellitus through insulin resistance state and lipid metabolism process (Sridhar et al. 2006).

1.2.2 AChE structure:

Recombinant human AChE is a homotetramer of 64 kDa subunits. The molecular weight of the protein varies from species to species e.g., electric eel AChE has a molecular weight of 70 kDa and house fly AChE has a molecular weight of 76 kDa. Each monomer of human AChE contains 579 amino acids. **Fig. 1.5** shows the monomeric subunit of recombinant human erythrocyte AChE (1B41.pdb). The structure contains an α/β -hydrolase fold, a common secondary structural element in SH (Ollis et al. 1992). The active site Ser203 is located at the junction between β_5 and $\alpha_{5,6}$, whereas other catalytic triad members, Glu334 and His447 are located at β_7 and $\alpha_{1,8}$, respectively (**Fig. 1.1 and Fig. 1.5**). The AChE tertiary structure is stabilized by three

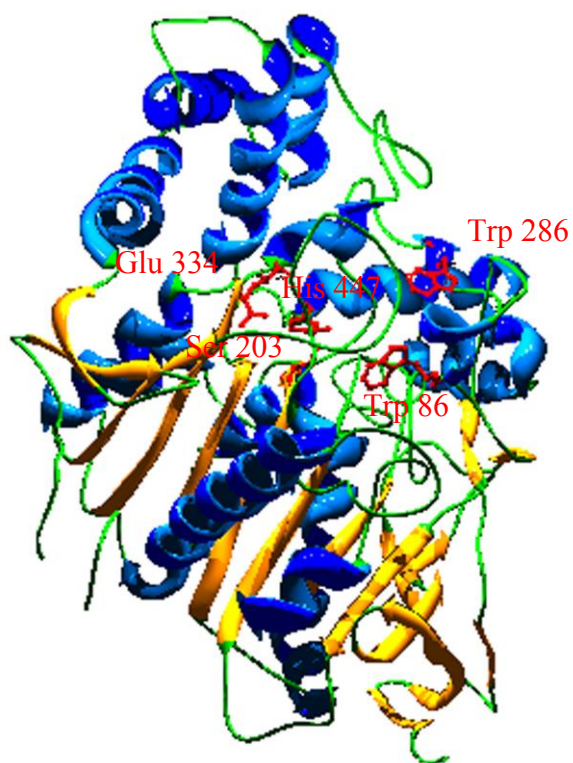


Fig. 1.5: Crystal structure of a subunit of the recombinant human AChE (B41.pdb). The tertiary structure of a subunit of recombinant human AChE is shown in the Figure. The alternate α -helices (in blue) and β -sheets (in yellow) array can be seen in the structure as a part of α/β -hydrolase fold secondary structure. The catalytic site residues Ser203, Glu334, His447, Trp286, and Trp86 are shown in red. The raw structure B41.pdb has been downloaded from Protein data bank and modified using the SwissPDB Viewer structural tool.

pairs of disulfide loops: Cys69-Cys96, Cys257-Cys269, and Cys409-Cys529. It is believed that the motion of Cys69-Cys96 loop plays a key role in the allosteric conformational change of Trp286 upon peripheral ligand binding to the peripheral anionic binding site (P-site) (Barak et al. 1995).

The amino acid sequence of AChE from mammals differs from other eukaryotes and insects. The human AChE amino acid sequence is 65% similar (**Fig. 1.6**) to that of the electric eel AChE, whereas it is only 33% homologous to the house fly AChE amino acid sequence (**Fig. 1.6**). The low homology between human and house fly AChE has provided an opportunity for designing highly efficient and specific insecticides (Weill et al. 2002; Pang 2006).

The active site of the AChE is buried in a gorge (**Fig. 1.7**). The catalytic triad is located at the bottom of the gorge. The active site catalytic triad members are Ser203, Glu334, and His447. As discussed above, the catalytic triad hydrolyses ACh by an electron relay mechanism.

In addition to the catalytic triad residues, there are other important residues that are involved in substrate binding and transition state stability. Trp286 at peripheral anionic site (PAS or P-site) is one of them (**Fig. 1.7**). Trp286 transiently binds the ACh substrate and makes an initial selection of the substrate. There are other P-site members like Asp74, Tyr77 and Tyr133 that also contribute to substrate binding at the active site gorge. Trp86 and Phe 338 (**Fig. 1.7**), which set up the catalytic anionic site (CAS), undergo a π -cation interaction with the positively charged choline moiety

```

Human -----MRPPQCLLHTPSLA 14
Eel -----MKILDALLFP----- 10
Fly  MARSVRTPISSSSSSSSRSWSPPSSSSFYLLSSFKASLTPSSSSSVAHHLAARNNDI 60
      .
      *

Human SPLLLLLLWLLGGGVGAEGREDAELLVTVRGGRLRGIRLKTTPG-GPVSAFLGIPFAEPPM 73
Eel  ---VIFIMFFIHLSIAQT---DPELTIMTRLGQVQTRLPVDFDRSHVIAFLGIPFAEPP 64
Fly  CRGLFATLVILLRMSALTSAMTDHLTVQTTSGPVRGRSVTVQG-RDVHVFVGIPYAKPPV 119
      : : : : . * : . * : * : . . * * * * : * * :
Human GPRRFLPPEPKQPWSGVVDATTFQSVCYQYVDLTYPGFEGTEMWNPNRELSDECLYLNW 133
Eel  GKMRFKPPEPKKPWNDFDARDYPSACYQYVDTSYPGFSGTEMWNPNRMSDECLYLNW 124
Fly  DDLRFKRPVPAEPWHGVLDATRLPATCVQERYEYFPGFSGEEMWNPNTNVSDECLFMNIW 179
      . * * * * : * * * * : * * * * * * * * * * * * * * * * * * *
Human TPYPRPTSP-----TPVLVWIYGGGFYSGASSLDV 163
Eel  VPATPRPHN-----LTMVWIYGGGFYSGSSSLDV 154
Fly  APAKARLRHGRGTNGGEHSSKTDQDHLIHSATPQNTTNGLPILIIWIYGGGFMTGSATLDI 239
      . *
      : : : * * * * * * * * * * * * * * * * * * * * *
Human YDGRFLVQAERTVLVSMNYRVGAFGLALPGSR-----EAPGNVGLLDQRLALQWQENV 218
Eel  YDGRYLAHSEKVVVSMNYRVSAFGFLALNGSA-----EAPGNVGLLDQRLALQWQDNI 209
Fly  YNAEIMSAVGNVIVASFQYRVGAFGLHLSVMPGFEEAEAPGNVGLWDQALALRWLKENA 299
      * . . : . : : * : * * * * * * * * * * * * * * * * * * * * * *
Human AAFGGDPTSVTLFGESAGAASVGMHLLSPSRGLFHRAVLQSGAPNGPWATVGMGEARRR 278
Eel  HFFGGNPKQVTIFGESAGAASVGMHLLSPDSRPKFTRAILQSGVPNGPWRTVTSFDEARRR 269
Fly  RAFGGNPEWMTLFGESAGSSSVNAQLMSFVTRGLVKKRGMMSQATMNAFWSHMTSEKAVEI 359
      * * * * * * * * * * * * * * * * * * * * * * * * * * * * * *
Human ATQLAHLVGCPPGGTGGNDTELVACLRTPAQVVLVNHVHVLVPEESVFRFSFVPPVDGDF 338
Eel  AIKLRGLVGCPE---DGNDDLIDCLRSKQPQLIDQEWLVLVLPFSGLFRFSFVPPVIDGVV 325
Fly  GKALVNDNCNNAQLPENPAQVMACMRQVDAKTIISVQQWNSYS--GILSYPSAPTIDGAF 417
      . * . . * . . . * . . . * . . . * . . . * . . . * . . . * . . . *
Human LSDTPEALINAGDFHGLQVLVGVVKGDEGSYFLVYGAPG-FSKDNESLISRAEFLAGVRVG 397
Eel  FPDTPPEAMLNNGNFKDTQILLGVNQNEGSYFLIYGAPG-FSKDNESLITREDFLQGVKMS 384
Fly  LPADPMTLLKTADLSGYDILIGNVKDEGTFFLLYDFIDYFDKDDATSLPRDKYLEIMNNI 477
      . * : : : : : . . : * * : * * * * * * . . * * * : : * * : .
Human VPQVSDLAEEAVVLHYTDWLHPEDPARLREALSDVVDHNVVCPVAQLAGR----- 448
Eel  VPHANEIGLEAVILQYTDWMDENPIKRNREAMDIDVGDHNVVCPVQHFQAKMYAQYSILQG 444
Fly  FQKASQAEREAIFQYTSWEGNPG-YQNQQQIGRAVDGHFFTCPTNEYAQA----- 527
      . : . : * * : : * * * . : : : . * * * . * * * . *
Human ---LAAQG-----ARVYAYVEHRASTLSWPLWVGVPVHGVEIEFIFGI 488
Eel  QTGTASQGNLWGNSSGASNSGNSQVSVLYMFDHRASNLVWPEWVGVIHGVEIEFVFGI 504
Fly  ---LAERG-----ASVHYYYFTHRTSTSLWGEWVGVLHGDEIEYFFGQ 567
      * : *
      . * * * * * * * * * * * * * * * * * * * * * * *
Human PLDPSRNYTAAEKIFAQRLMRYWANFARTGDPNEPRD---PKAPQWPPYTAGAQQYVSLD 545
Eel  PLEKRLNYTLEEKLSRRMMKYWANFARTGNPNINVDGSDSRRRWPFVFTSTEQKHVGLN 564
Fly  PLNNSLQYRPVERELGKRLNSVIEFAKSGNPAVDGE-----EWPNFSKEDPVYYVFS 620
      * * : * * . : : * : . : * * : * * : . * * : : * * : : .
Human LRP--LEVRRGLRAQACAFWNRFLPKLLSATDTLDEAERQWKAEFHRWSSYMVHWKNQFD 603
Eel  TDS--LKVHKGKLSQFCALWNRFLPRLNVTENIDDAERQWKAEFHRWSSYMMHWKNQFD 622
Fly  TDEKIEKLQRGPKAKRCSFWNDYLPKVRSWIGSECENKSSSTASAAIYEMKMQLTLVAV 680
      : : : * : : * * * * * * : . . : : . * . : . * : .
Human HYSKQDRCSDL- 614
Eel  HYSKQERCTNL- 633
Fly  AIIILTMVNSIFQ 692
      : :

```

Fig. 1.6: ClustalW based multiple sequence alignment of human, electric eel, and house fly AChE. The human AChE (Swiss-Prot P22303), electric eel AChE (Swiss-Prot ID O42275), and house fly AChE (TrEMBL Q8MXC6) are aligned using ClustalW. * = completely identical amino acids; : = any two are identical.

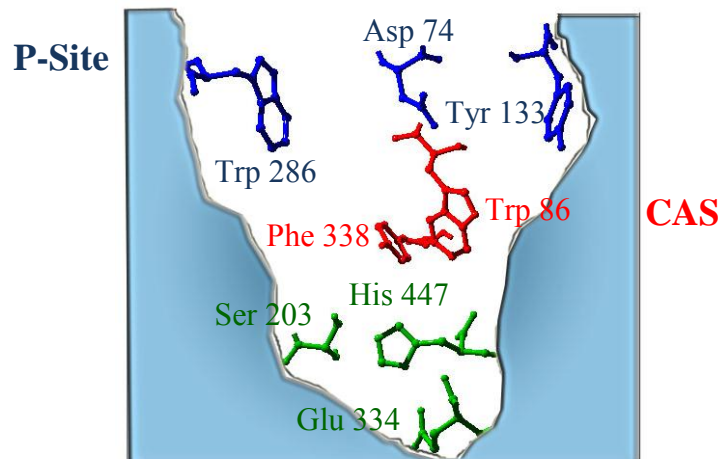


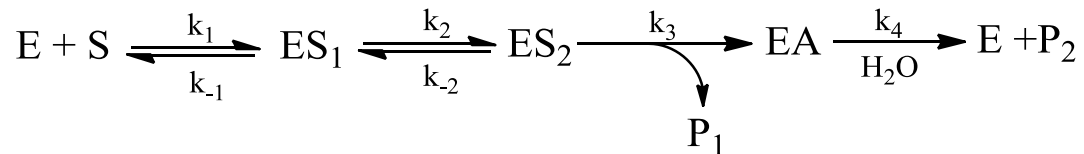
Fig. 1.7: Active site structure of recombinant human AChE. The figure shows the active site gorge of the human AChE. At the bottom of the gorge the catalytic triad residues Ser203, Glu334, and His447 (in green) are located. At the upper edge of the gorge the P-site residues Trp286, Asp74, and Tyr133 (in blue) are located, whereas, on one of the walls of the gorge the catalytic anionic site residues Phe 338 and Trp86 (in red) can be seen. The figure has been generated from 1B41.pdb using SwissPDB Viewer structural tool.

of ACh and direct the business end of the substrate to the catalytic triad for catalysis. There are several conserved aromatic residues whose aromatic ring constitutes 70% of the inner surface of the active site gorge, thereby contributing to form the required geometry of the gorge. Another important component of the AChE active site architecture is an involvement of hydrogen bond donors that can stabilize the tetrahedral transition state of enzyme-substrate complex by accommodating the negatively charged carbonyl oxygen. Structural and modeling studies (Sussman et al. 1991; Shafferman et al. 1992; Ordentlich et al. 1993) revealed an oxyanion hole formed by peptidic NH groups of Gly-121, Gly-122, and Ala-204. Residues Gly-121, Gly-122, and Gly-120 are part of a flexible “glycine loop” which forms one of the active site gorge walls adjacent to the catalytic serine. The glycine loop not only accommodates the oxyanion hole but it is one of the most crucial determinants of the active site geometry (Raves et al. 1997).

1.2.3 General catalytic mechanism:

AChE catalysis occurs through an acyl-enzyme mechanism that involves nucleophilic serine and acid-base histidine residue as shown in **Fig. 1.2**. Froede and Wilson (1984) showed the existence of formation of acyl-enzyme intermediate by trapping the acetyl-enzyme formed during the AChE catalyzed hydrolysis of ACh and acetylthiocholine (ATCh) at $[S]_0 \gg K_m$ (Froede and Wilson 1984). They also showed that acylation and deacylation are both involved in the rate limitation of the reaction.

Terrone Rosenberry (Rosenberry 1975; Rosenberry 1975) proposed a kinetic mechanism of AChE catalysis, which involves an induced-fit step (**Scheme 1**) (Rosenberry 1975). It was suggested that for neutral substrates, an induced-fit



Scheme 1: Kinetic Mechanism for AChE Catalysis that Incorporates an Induced-Fit Step. E = AChE, S = substrate, EA = acyl-enzyme, P₁, P₂ = products, ES₁ = Michaelis complex. ES₂ = induced-fit complex. k₁ and k₋₁ are the forward and reverse rate constant for the formation of Michaelis complex; k₂ and k₋₂ are the forward and reverse rate constant for the formation of induced-fit complex; k₃ and k₄ are the rate for the formation of acyl-enzyme and reactivation of the enzyme. Adapted from (Rosenberry 1975; Rosenberry 1975).

conformational change happens after substrate binding but prior to chemical catalysis. In **Scheme 1**, k_3 and k_4 are the chemical step rate constants for acylation and deacylation, respectively. Rosenberry et al (Rosenberry 1975) solved the steady state kinetic parameters (k_E and k_{ES}) for the mechanism of **Scheme 1** as **equation 1** and **equation 2**, respectively.

$$k_{ES} = \frac{k_2 k_3 k_4}{k_2 k_3 + k_4 (k_2 + k_{-2} + k_3)}$$

Equation 1

$$k_E = \frac{k_1 k_2 k_3}{k_2 k_3 + k_{-1} (k_{-2} + k_3)}$$

Equation 2

where, k_{ES} and k_E are steady rate constants to emphasize the initial states to which the rate constants refer, i.e., bound states and free enzyme state, respectively. It is seen from eqn. 2 that k_E represents the conversion of free enzyme and free substrate to a transition state(s) in the acylation stage of catalysis, whereas the rate constant k_{ES} represents the conversion of bound states (ES_1 and/or ES_2 and/or EA) to transition states for acylation and/or deacylation. Thus, k_E always emphasizes the acylation reaction dynamics, whereas k_{ES} tracks the acylation and/or deacylation.

It has been shown that AChE has outstanding catalytic power; the turnover number k_{ES} is $> 10^4 \text{ sec}^{-1}$ (Rosenberry 1975), which is one of the highest turnover numbers reported for enzyme catalysis. Moreover, for the natural substrate ACh, k_E is $> 10^8 \text{ M}^{-1} \text{ sec}^{-1}$ (Rosenberry and Bernhard 1971; Rosenberry 1975) and thus the diffusion of ACh to the AChE active site is possibly rate determining. The high second

order rate constant indicates that AChE is one of the evolutionary perfect enzymes. **Table 1.1** shows the substrate specificity of AChE in terms of the k_E , a steady state kinetic parameter representing the conversion of free enzyme and free substrate to a transition state(s) in the acylation stage of catalysis, and K_m , the concentration of substrate to reach $V_{max}/2$ rate. It is revealed from **Table 1.1** that AChE shows more specificity towards ACh, ATCh, and acetylselenocholine compared to other esters.

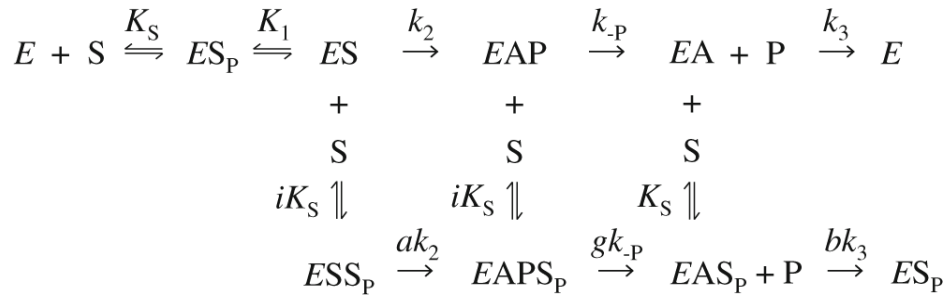
From kinetic (Nachmansohn and Wilson 1951), fluorescence (Rosenberry et al. 2008), and X-ray crystallographic data (Sussman et al. 1991), it has been established that AChE catalysis is not as simple as shown in **Scheme 1**. It has been shown that the catalytic mechanism of AChE depends upon the binding of substrate not only at the acyl-binding site (A-site) but also at the P-site (discussed in detail in the next section). Considering the involvement of P-site, Rosenberry (Rosenberry 2010) has proposed an alternative mechanism (**Scheme 2**) of AChE catalysis, which is considered an extended version of classical Michaelis-Menten model for AChE-catalyzed substrate hydrolysis. In **Scheme 2**, the initial enzyme–substrate complex (ES) converts to an acylated enzyme intermediate (EA), which is then hydrolyzed to give product (P). The scheme includes two additional intermediates on the catalytic pathway, an initial complex with substrate bound to the P-site (ESP) and an intermediate EAP between ES and EA. In EAP, the enzyme has been acylated but the product P has not yet dissociated from the A-site. Moreover, the scheme considers certain ternary complexes, in which the intermediate also binds substrate at the P-site (ESS_P , $EAPS_P$, and EAS_P). This makes the rate constants for inter conversion of the intermediates to the next to be changed

Table 1.1: Substrate specificity of Human AChE.

Substrate	k_E ($M^{-1}.s^{-1}$)	K_m (mM)
Acetylcholine (ACh) ^a	1.00×10^8	0.046
Acetylthiocholine (ATCh) ^b	1.58×10^8	0.040
Acetylselenocholine (ASeCh) ^c	3.62×10^8	0.020
Acetylazacholine (AACh) ^d	2.50×10^3	2.00
Ethyl acetate ^a	7.90×10^1	N.A
Phenyl acetate ^{a, d}	5.00×10^6	N.A

N. A = Not applicable.

^a (Rosenberry 1975); ^b (Froede and Wilson 1984); ^c (Moore and Hess 1975); (Moore and Hess 1975)^d(Hillman and Mautner 1970)



Scheme 2: Extended model for substrate hydrolysis by AChE. E = AChE, S = substrate, EA = acyl-enzyme, P = product, ES_p = initial complex where substrate bound to peripheral binding site (P-site), EAP = an intermediate between ES and EA, where the enzyme is acylated but the P is not yet dissociated from the complex, all ks represent the rate constants and the Ks represents the equilibrium constants. iKs are the equilibrium constants which represent the equilibrium between the enzyme-substrate initial complex and another substrate molecule, this constant represents the inhibition situation when a already bound substrate inhibits the incoming substrate to bind and involves in catalysis.

Adapted from (Rosenberry 2010)

in these ternary complexes by the relative factors a , g , and b respectively. The most important aspect of this scheme is the substrate trapping by P-site. The P-site transiently binds the substrate before it forms the ES complex, and confirms that most of the substrates which come across the P-site end up to the A-site for catalysis (Szegeletes et al. 1999; Mallender et al. 2000; Johnson et al. 2003). In this way, the low affinity P-site highly contributes towards the catalytic efficiency of the AChE active site. However, the initial binding of substrate at P-site poses a substantial threat for catalytic efficiency at high concentration of substrate, most of the time this condition leads to the 'steric blockade' (Szegeletes et al. 1999).

1.3 Inhibitors of AChE:

As discussed above, AChE is utilized as a drug target in Alzheimer's diseases (AD), glaucoma, and myasthenia gravis because of its role in hydrolyzing ACh in active neurons (Millard and Broomfield 1995). In neuronal diseases, the patient suffers from memory loss that occurs due to the destruction of neurons. In this condition, the ailing neuron produces less ACh and hinders the normal process of neuron to neuron information transfer, which ultimately leads to severe memory loss. In this abnormal situation, if the hydrolysis of ACh by AChE occurs normally then the concentration of ACh at the synapse (**Fig. 1.4**) decreases and the process of information transfer is compromised. Researchers have proposed that AChE can be targeted to control this abnormality (Parnetti 1995; Taylor 1998; Cutler and Sramek 2001). Inhibition of AChE will decrease the ACh hydrolysis rate, as a result the concentration of ACh at the synapse will remain nearly constant and preserve the normal process of information transfer. For

the last 30 years, several inhibitors have been synthesized for AChE. Some of them are reversible and most of them are irreversible inhibitors.

It has always been a point of discussion among scientists whether reversible or irreversible inhibitors are more effective for controlling abnormal memory loss in patients (Taylor 1998). A large number of scientists think that reversible inhibitors are suitable drug candidates because they can be easily excreted from the body upon excess use of fluid, which leads to fewer side effects .

1.3.1 Reversible inhibitor of AChE:

There are a large number of reversible inhibitors of AChE available on the market. Most of them are laboratory synthesized and specifically designed for the AChE active site. The inhibitors are designed in such a way that they can specifically target the P-site and/or CAS in AChE active site (Kryger et al. 1999; Bourne et al. 2003; Alonso et al. 2005; Johnson and Moore 2006). The reversible inhibitors extensively used in AChE inhibition studies as well as neuronal disease drugs include physostigmine, neostigmine, rivastigmine, donepezil, tacrine, and huperzine (**Fig. 1.8**). The IC_{50} s of these compounds against human AChE are in the low nM range (Lahiri et al. 2004; Eckert et al. 2006; Belluti et al. 2009). In some of the inhibitors (neostigmine, tacrine) a positively charged quaternary N-atom has been introduced to facilitate the substrate like π -cation interaction with the anionic site (Pauling and Petcher 1971; Harel et al. 1993). On the other hand, some of them contain aromatic substitutions that facilitate the π - π interaction with the P-site and CAS aromatic residues (Harel et al. 1993). Inhibitors like propidium, which has a phenanthrene-like aromatic moiety linked with choline by a carbon chain

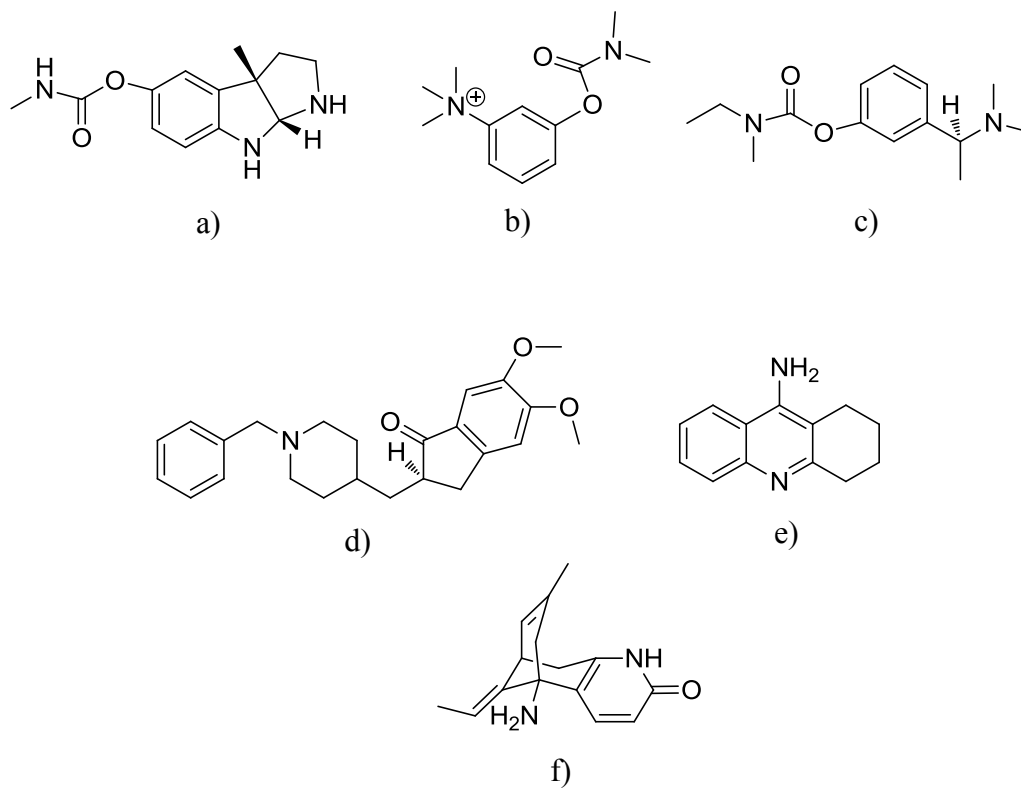


Fig. 1.8: Reversible inhibitors of AChE. a) Physostigmine, b) Neostigmine, c) Rivastigmine, d) Donepezil (AriceptTM), e) Tacrine (CognexTM), and f) Huperzine. Except huperzine (a sesquiterpene, isolated from a plant called *Huperzia Serratta*), all the compounds are laboratory synthesized. Mostly, these inhibitors bind to the P-site and/or CAS site of the AChE active site. Among all the inhibitors shown, only donepezil and tacrine are approved as drugs for AD.

linker, can bind simultaneously to the P-site and CAS site at the AChE active site (Radic et al. 2008). Such a compound can arrest the internal dynamics of the AChE active site and stabilize the inactive form of the enzyme. To date, donepezil (AriceptTM) and tacrine (CognexTM), which are very efficient AChE reversible inhibitors, have been approved as drugs for AD.

1.3.2 Organophosphates as irreversible inhibitors of AChE:

Organophosphates (OPs) act as a pseudo-substrate for SHs. This class of compounds have been widely used as SH inhibitors (Kam et al. 1993; Glynn et al. 1994; Winkler et al. 1996). The rate of hydrolysis of the natural substrate is reduced (generally several orders of magnitude) when OPs phosphorylate the SHs. It is well established in the literature that OPs covalently modify the active site nucleophilic serine of SHs and irreversibly inhibit the enzymes (Harel et al. 1991; Glynn et al. 1994; Winkler et al. 1996; Chambers and Oppenheimer 2004). OPs, like diisopropylfluorophosphate (DIFP) have been used as activity-based probes (ABP) to characterize the SH family members (Liu et al. 1999; Kidd et al. 2001). Besides, DIFP, other OPs like diethylfluorophosphate (DEFP), paraoxon, tabun, soman, and VX (**Fig. 1.9**) are extensively used in the literature for SH characterization and inhibition studies.

OPs exhibit two important features that are used for global characterization of SHs (**Fig. 1.10**). First, OPs use several conserved features of the SH active site, including a highly nucleophilic serine O-atom (susceptible to the reaction with highly electrophilic P-atom of OP) and the oxyanion hole which stabilizes the SH-substrate

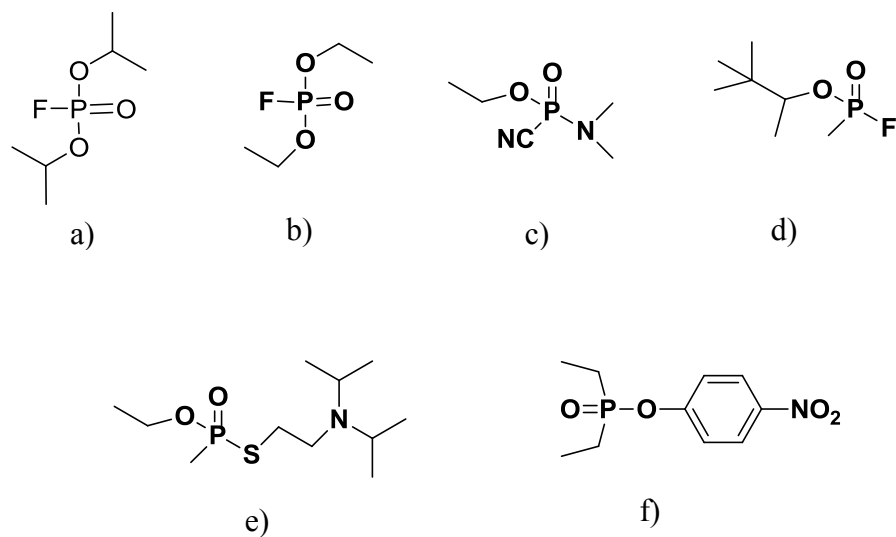


Figure 1.9: Organophosphate inhibitors of SHs. a) Diisopropylfluorophosphate (DIFP), b) Diethylfluorophosphate (DEFP), c) Tabun, d) Soman, e) VX, and f) Paraoxon. Though these OPs are mainly designed to inhibit acetylcholinesterase (AChE) and butyrylcholinesterase (BuChE), other SHs like lipases and some other proteases are also inhibited by them (Casida and Quistad 2004; Casida et al. 2008). These classes of compounds are considered as nerve agents because they target the AChE at cholinergic neurons to prevent the same to reach the resting state.

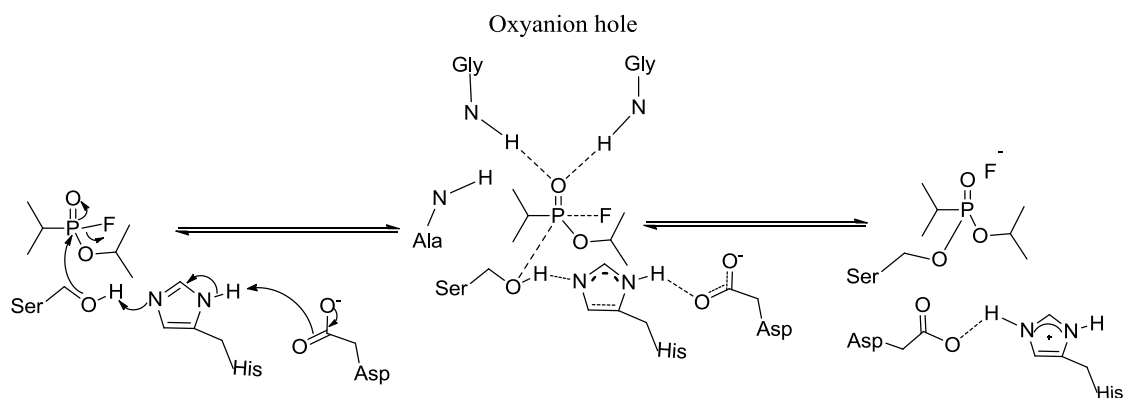


Figure 1.10: Formation of tetrahedral intermediate in the reaction between SH and OP. SH – OP reaction occurs through the formation of tetrahedral intermediate similar to the intermediate that forms when SH reacts with its natural substrate. The intermediate has an anionic character and can be stabilized by oxyanion hole forming peptidic NH-group of glutamic acid and alanine in the SH active site. The similarity of the intermediate structure of SH-OP complex and SH-substrate complex has been utilized to design mechanism-based OP inhibitor against SH.

tetrahedral intermediate (resembled by similar tetrahedral structure of OPs) (**Fig. 1.10**) to attain high target selectivity of SH class of enzymes. Second, OPs exhibit extremely low cross-reactivity with other classes of hydrolases, including aspartyl-, cysteinyl-, and metallo-hydrolases (Bouma et al. 1980).

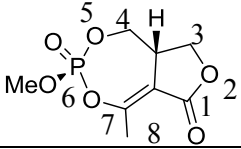
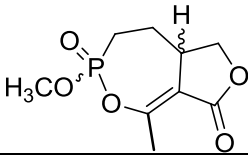
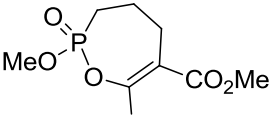
Organophosphates (OPs) or phosphonates are extensively used as AChE irreversible inhibitors. As mentioned above, this class of compounds covalently modifies the AChE active site by reacting with the active site serine. The tetrahedral intermediate of the AChE–OP complex is very similar to the AChE–ACh complex which is stabilized by the oxyanion hole forming residues (**Fig. 1.10**). Soman, VX, sarin, and DIFP (**Fig. 1.9**) are efficient irreversible inhibitors for AChE. They have low nM IC_{50} s against human AChE (Worek et al. 2004). Their bimolecular rates of inactivation (k_i) are in the range of 10^5 – 10^8 $M^{-1} \text{ min}^{-1}$, which tags them as highly efficient inactivators of AChE. Even though the AChE-OP reaction has been shown to be a purely irreversible type, reactivation of AChE can occur ($\sim 0.02 \text{ min}^{-1}$) (Aldridge and Reiner 1969; Sultatos 1994; Worek et al. 2004), provided the process of aging has not occurred. Aging is one of the poorly understood reactions in which one alkoxy substituent of OP is hydrolyzed, leaving the mono-alkoxy phosphate bound irreversibly to the active site serine of AChE (Sultatos 1994). The process of aging is more likely when the alkyl substituent of the alkoxy group of OP has more than two carbon atoms. In the absence of aging, the phosphorylation of AChE by OPs is often kinetically described as a Ping Pong Bi Bi reaction that reduces to Ordered Uni Bi reaction when the second substrate, water, is present in excess (Segel 1975).

Researchers have extensively used OPs to probe and to characterize the AChE active site structure (Liu et al. 1999; Kidd et al. 2001; Patricelli et al. 2001). Barak et. al. first proposed that covalent modification at the active site serine by DIFP led to an allosteric conformation change at P-site Trp286 and Tyr133 which ultimately led to an altered binding of P-site binding ligands like propidium and edrophonium (Barak et al. 1995). This was the first evidence of allostery in AChE active site.

OPs can cause neurotoxic syndrome (NS) in human and other animals. One of the well characterized and fatal NSs is caused by the inhibition of acetylcholinesterase (AChE) at cholinergic synapses (Glynn 1999). However, it has been reported that proper dosage of OPs can prevent several neuronal disease conditions like AD (Taylor 1998). The above mentioned neurotoxic property of OPs have been deliberately used to target insect neuronal system for the development of pesticides (Weill et al. 2002; Pang 2006).

The search for an efficient natural product inhibitor of AChE is ongoing owing to an increase in life expectancy of human population, increased incidence of neuronal disorder diseases like AD, glaucoma, and other clinical interests. To date, several natural product inhibitors of AChE have been reported; most of them are alkaloid (huperzine, amaryllidaceae), carbamate (physostigmine), or peptide-based (fasciculin) (Hostettmann et al 2006; (Bourne et al. 1995). The only phosphate-based natural product inhibitor of AChE reported in the literature is cyclophostin (Kurokawa et al. 1993) (**Table 1.2** and **Table 3.1** in **Chapter III**). Kurokawa et. al. (A) first isolated this compound from the NK901093-70 strain of bacterium *Streptomyces*

Table 1.2: Cyclophostin and its cyclic phosphonate analogs.

Name	Structure
Cyclophostin ^a	
Phosphonate analog of Cyclophostin ^{b, c}	
Mono cyclic phosphonates analog of Cyclophostin ^{b, c}	

^a(Kurokawa et al. 1993); ^b(Bandyopadhyay et al. 2008); ^c (Kurokawa et al. 1993; Dutta et al.).

lavendulae and characterized it as a bicyclic phosphate containing seven membered phosphate ring fused with five membered lactone ring. The compound was reported to exhibit the IC_{50} of $8 \times 10^{-4} \mu\text{M}$ against grasshopper AChE (Kurokawa et al. 1993). Although the biosynthetic pathway for the synthesis of cyclophostin or the function of the metabolite in *Streptomyces lavendulae* is still unknown, cyclophostin has gathered a lot of importance due to its highly efficient inhibition of AChE. Due to extremely low yield from the natural source, organic synthetic chemists have taken the challenge to synthesize this bicyclic entity. Kurokawa et al. (1993) did not report the exact mechanism of action of cyclophostin against AChE. In this study, we have reported the mode of action of cyclophosphonate analogs of cyclophostin (**Table 1.2** and **Table 3.1**) and some diastereoisomers of cyclophostin (**Table 3.3**) against human, electric eel and house fly AChE.

1.4 Introduction to Hormone-sensitive lipase (HSL):

1.4.1 General background:

Free fatty acids (FFAs) are the main source of energy for most mammalian cells and tissues. The majority of the FFAs found in plasma originate from the adipose tissue where the FFA is stored as triglycerides (TGs). Up to 150 g of fatty acids, which corresponds to nearly half of the daily caloric need, can be obtained from adipose tissue (Holm et al. 2000; Yeaman 2004). TG hydrolysis occurs through three consecutive reaction steps and is catalyzed by three extremely important metabolic enzymes: triacylglyceride lipase (TGL), hormone-sensitive lipase (HSL) and monoglyceride lipase (MGL). TGL hydrolyzes the TGs and MGL hydrolyzes the (monoacylglycerides) MGs,

whereas HSL has broad substrate specificity and can catalyze the hydrolysis of TGs (**Fig. 1.11**), diglycerides (DGs), monoacylglycerides (MGs), cholesteryl esters (**Fig. 1.11**) as well as retinyl esters (Kraemer and Shen 2002). Its activity towards diglycerides is 10 and 5 fold higher than that toward tri- and monoacylglycerides (Kraemer and Shen 2002). Moreover, the hydrolysis of TGs and DGs, but not the DGs, is a c-AMP dependent protein kinase A (PKA) mediated phosphorylation dependent. HSL is not known to show any phospholipase activity (Kraemer and Shen 2002).

Initially it was believed that HSL is an intracellular adipocyte-specific triacylglycerol lipase but now it has been shown that HSL is expressed in multiple other locations, including macrophages, pancreatic β -cells, corpus luteum (steroidogenic tissue), and intestinal mucosa (Cook et al. 1982; Grober et al. 2003).

Due to HSL's broad lipid substrate specificity, it exhibits multiple functions in lipid metabolism (**Table 1.3**). HSL activity is regulated by several mechanisms, including reversible phosphorylation by different types of protein kinases, interaction with different protein partners, and translocation to different locations within the adipocyte cell (Stralfors and Belfrage 1983; Osterlund et al. 1999; Su et al. 2003; Sztalryd et al. 2003). It is believed that altered expression of HSL in different cells and tissues may be linked with numerous pathological states, including type II diabetes, obesity, and atherosclerosis (discussed in section e) (Ylitalo et al. 2000; Hoffstedt et al. 2001; Teruel et al. 2005; Palou et al. 2009).

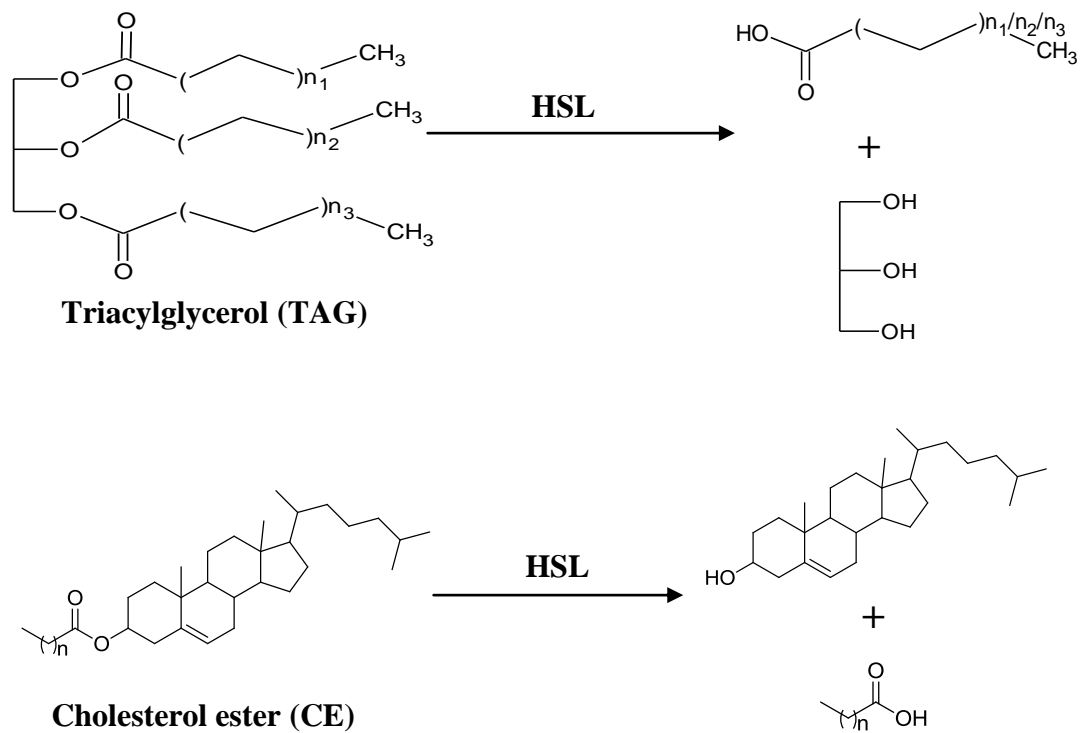


Fig. 1.11: Hydrolysis of triacylglycerol (TAG) and cholesterol ester (CE) by HSL. HSL hydrolyzes the ester function both at TAG and CE to produce fatty acid and glycerol or cholesterol respectively. The TAG hydrolysis generally happens in adipose tissues and the CE hydrolysis occurs in macrophages.

Table. 1.3: Expression and function of HSL at different tissues and cell types ^a.

Cell type	Major product	Main function
Adipocyte	Fatty acid	Export for oxidation
Muscle	Fatty acid	Oxidation
Pancreatic β -cells	Fatty acid	Signal transduction
Macrophage	Cholesterol	Export via high density lipoprotein (HDL)

^aAdapted from (Yeaman 2004).

1.4.2 Structure of and biochemical properties of HSL:

After cDNA cloning of HSL, it was revealed that the enzyme has low sequence homology with other mammalian lipases (Holm et al. 1988; Holm et al. 1988). However, HSL, having 775 amino acids, showed better sequence identity with the lipase from the bacteria called *Moraxella* TA 144 (Feller et al. 1991; Langin et al. 1993). Moreover, sequence similarity was found with several other bacterial lipases, acetylcholinesterase (AChE), and lipoprotein lipase (LPL) which led to the idea that it belongs to the lipase/esterase super family of enzymes (Hemila et al. 1994).

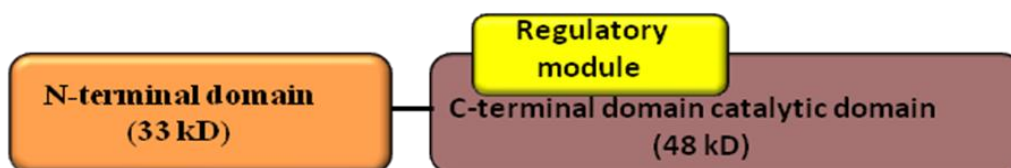
HSL is a serine hydrolase (SH) and can be inhibited by common SH inhibitor diisopropylfluorophosphate (DIFP) (Fredrikson et al. 1981). It contains the Gly-X-Ser-X-Gly motif, having an active site serine that is found in other SH family members (Cook et al. 1981; Holm et al. 1988). The studies also identified the catalytic triad residues as Ser423, Asp703, and His 733 in the rat HSL amino acid sequence (**Fig. 1.12A**) (Hemila et al. 1994; Holm et al. 1994). Sequence analyses, limited proteolytic digestions and molecular modeling studies revealed a multi domain structure for HSL (**Fig. 1.12B**). The first 300 amino acids constitute the N-terminal domain and the rest of 300-767 amino acids constitute the C-terminal domain that includes the regulatory loop having 150 amino acids (Hemila et al. 1994; Contreras et al. 1996). The N-terminal domain, which does not have any similarity with other proteins or peptides, is proposed to be a docking domain for HSL-interacting protein partners and also involved in ‘nose to tail’ dimerization of the protein (Osterlund et al. 1996; Osterlund et al. 1999). It is shown that the fatty acid binding protein-4 (FABP-4) docks at the N-terminal

A



Primary structure of rat HSL

B



Domain structure of rat HSL

Fig. 1.12: Predicted structure of rat HSL. A) Primary structure of HSL: Orange, violet, and yellow blocks represent the N-terminal domain, C-terminal domain, and regulatory loop domain amino acid sequences respectively. The catalytic residues are indicated as Ser423, Asp703, and His733. Probable phosphorylation sites at regulatory loop domain are Ser563, Ser565, Ser659, and Ser660 (Yeaman 2004). B) Domain structure of HSL: The color coding is the same as A). The N-terminal domain (33 kD) is composed of 300 amino acids, whereas the C-terminal domain (48kD) is composed of 467 amino acids. The regulatory module (16.5 kD) is a part of the C-terminal domain having 150 amino acids (residues 521 to 669). The N-terminal and C-terminal domain is connected by a hinge region that is composed of 20 amino acids (315-335) (black line). Adapted from (Holm et al. 1988; Yeaman 2004).

domain of the HSL and regulates product inhibition by opening up the product release door at the C-terminal domain (Osterlund et al. 1999; Kraemer and Shen 2002; Jenkins-Kruchten et al. 2003; Ali et al. 2005).

Molecular modeling studies revealed that HSL contains an α/β -hydrolase fold at the C-terminal domain and the regulatory loop domain runs from residue 521 to 669 between $\alpha^2_{6,7}$ and $\alpha^4_{6,7}$ (**Fig. 1.13**) (Contreras et al. 1996; Osterlund et al. 1996) in the same domain. The regulatory domain of HSL is a unique structural component that contains several phosphorylation sites and is only found in this enzyme. To date no other lipase is known that is regulated by phosphorylation; it is still an outstanding question how the phosphorylation of serine residues in the regulatory domain controls the intrinsic activity of HSL catalytic domain, manages the interaction with different substrates and products, and regulates the translocation of the enzyme to and from the lipid droplets. It has been speculated that the regulatory domain of HSL is actually an evolutionary modification of lid domain found in other lipases like *Candida rugosa* lipase and human pancreatic lipase (Brocca et al. 2003; Passolunghi et al. 2003). But having no homology with lid domain amino acid sequence and with other proteins or peptides, the idea of the regulatory loop being a modified lid has been discarded. The loop has three helical regions (**Fig. 1.14**); the most important region is the one which contains the 563 and 565 phosphorylation sites. It is proposed that upon phosphorylation the distortion of the helical structure occurs, which ultimately leads to a global conformational change which in turn triggers the translocation of the HSL to the lipid droplets (Contreras et al. 1996; Ben Ali et al. 2004).

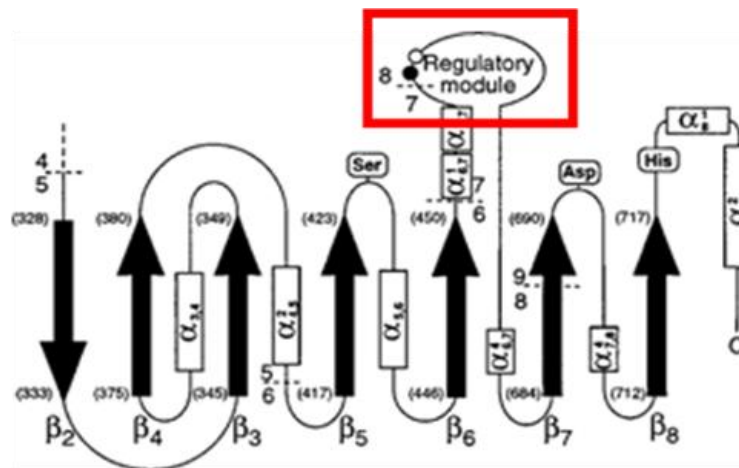


Fig. 1.13: Secondary structure of C-terminal domain of rat HSL. The secondary structure of the C-terminal domain of rat HSL contains α/β -hydrolase fold which consists of 8 α -helices (rectangular boxes) and 7 β -sheets (black arrows) in alternate manner. This unique α/β -hydrolase fold structure brings the Ser423, Asp703 and His733 in proximity to create the catalytic triad for catalysis. Catalytic Ser423 is located between β_5 and $\alpha_{5,6}$, whereas, other catalytic triad residues Asp703 and His733 are located at $\beta_7/\alpha_{7,8}$ and $\beta_8/\alpha_{8,8}$ junctions, respectively. The red box represents the regulatory region which is located between $\alpha_{2,7}$ and $\alpha_{4,5}$, and contains the phosphorylation sites S563, S565, S659, and S660 (Contreras et al. 1996).

Adapted from (Contreras et al. 1996).

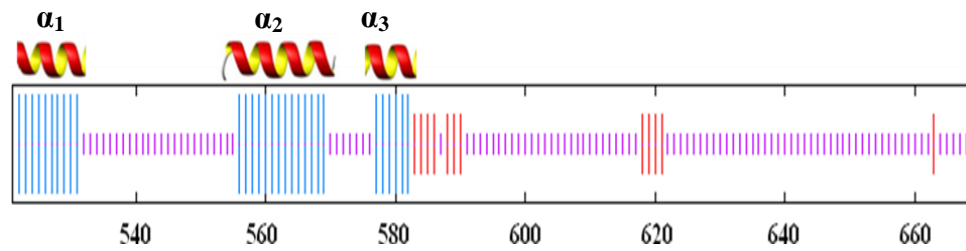


Fig. 1.14: Predicted secondary structure of regulatory loop domain. The amino acid sequence of the regulatory loop domain (521-669) has been fed to the Hierarchical Neural Network method (HNN) freeware tool and the predicted secondary structure has been obtained. The blue bars represent the α -helical region, whereas the red and purple bars represent β -sheets and random coil respectively. In the structure, there are three distinct α -helical regions α_1 , α_2 , and α_3 . Among them α_2 contains the basal and regulatory phosphorylation sites S563 and S565.

As discussed above, HSL hydrolyzes the lipid substrate with broad substrate specificity. It is shown that HSL prefers *sn* 1-ester and 3-ester bonds when it hydrolyzes the triacylglycerol (Fredrikson and Belfrage 1983). It is reported that HSL does not have preference for the fatty acid in the triacylglycerol; it shows increasing activity with decreasing chain length of the fatty acid group (Raclot et al. 2001). Moreover, HSL is active against short chain esters like, p-nitro phenyl butyrate, vinyl acetate, vinyl propionate *in vitro*. Activity of the enzyme against these compounds is retained even after lipase activity is destroyed by limited proteolysis (Smith et al. 1996). This phenomenon indicates to the fact that for lipase activity, HSL needs to have properly aligned hydrophobic acyl chain binding site/s that is not essential for short chain ester binding and hydrolysis.

1.4.3 Phosphorylation of HSL:

As mentioned above, the most important feature of HSL is its regulation by phosphorylation, induced by β -adrenergic receptor agonists or hormones. It is seen that the HSL lipolysis of triacylglycerol can be enhanced up to 2-fold upon hormone induced c-AMP-dependent protein kinase phosphorylation *in vitro* (Fredrikson et al. 1981; Cook et al. 1982). The same trend for other short chain substrates has not been seen yet but it is reported that cholesteryl ester hydrolysis can also be enhanced by phosphorylation of HSL (Cook et al. 1982; Cook et al. 1983; Greenberg et al. 2001). It is possible that for short chain substrate, the assay condition is not sensitive enough to detect those changes.

Mutational studies and structural analysis have revealed that there are four distinct c-AMP-dependent protein kinase sites in HSL regulatory domain: Ser563,

Ser565, Ser659, and Ser660 (Stralfors and Belfrage 1983; Stralfors et al. 1984; Anthonsen et al. 1998). Ser565 is considered as the basal phosphorylation site and Ser563 as regulatory phosphorylation site. It is proposed that Ser565 phosphorylation site prevents the regulatory site Ser563 from being phosphorylated and thwarts the HSL lipolysis of lipid droplets (Vossler et al. 1997; Shen et al. 1998; Zhang et al. 2003). Thus, Ser565 is sometimes considered to be an anti-lipolysis regulation element in HSL. There is strong evidence that Ser565 is phosphorylated exclusively by cAMP-dependent protein kinase *in vivo* but *in vitro* this site can be phosphorylated by several other kinases too (Garton et al. 1989; Moore et al. 2005; Watt et al. 2006; Krintel et al. 2009). Mutations at Ser563 and Ser565 to alanine do not completely abolish the cAMP-dependent phosphorylation and in turn the activation of HSL; this data suggests that Ser660 and Ser659 also play a vital role in phosphorylation-induced activation of HSL (Anthonsen et al. 1998; Su et al. 2003; Krintel et al. 2008). Recently, it has been established that phosphorylation at Ser649 and Ser650 in human HSL (corresponding to Ser659 and Ser660 in rat HSL) is the major determinant of lipolytic activity of the enzyme *in vitro*, but they have less contribution in non-lipolytic activity under non-phosphorylated condition (Krintel et al. 2008). Moreover, the cAMP-dependent pathway activates mitogen-activated protein kinase (MAPK) and extra-cellular signal-regulated protein kinase (ERK) that can phosphorylate the Ser600 site and can enhance the activity of HSL almost 2-fold (Garton et al. 1989; Greenberg et al. 2001; Donsmark et al. 2004).

1.4.4 Phosphorylation induced translocation of HSL:

As mentioned above, the lipolytic activity of the HSL increases up to 2-3 fold *in vitro* upon phosphorylation. On the contrary, it has been established that the lipolytic rate increases up to 100 fold when tested in rat adipose cells (Nilsson et al. 1980; Londos et al. 1985; Grober et al. 1997). This discrepancy in lipolytic rate happens mostly due to the involvement of other protein/s. The most important one is the hydrophobic lipid coating protein, perilipin. Perilipin is one of the most abundant adipocyte lipid binding proteins that binds the surface of lipid droplets and regulates lipolysis (Londos et al. 1999; Londos et al. 1999). It is established that perilipin forms a barrier for HSL so that non-phosphorylated enzyme cannot perform lipolysis (Brasaemle et al. 2000; Brasaemle et al. 2009; Wang et al. 2009). Under basal conditions, HSL stays in the cytoplasm and perilipin protects the lipid droplets by forming a protein coat (Wang et al. 2009). It has been shown that HSL physically interacts with the N-terminal domain of perilipin (Shen et al. 1999; Wang et al. 2009) *in vivo*. However, this is not the sole factor that prevents non-stimulated HSL from translocating to the lipid droplets; binding of perilipin to other protein partners like α/β -hydrolase fold containing protein 5 (Abdh5) also contributes to form the barrier (Yamaguchi; Granneman et al. 2007; Granneman et al. 2009). Upon catecholamine-induced phosphorylation (mainly the cAMP-dependent pathway), HSL translocates to the lipid droplets and at the same time phosphorylated perilipin leaves the lipid droplet surface, thus facilitating the access of HSL to the lipid droplets (**Fig. 1.15**). It is also proposed that perilipin induces a structural change in the lipid droplet by breaking it into small droplets so that the total accessible surface area increases

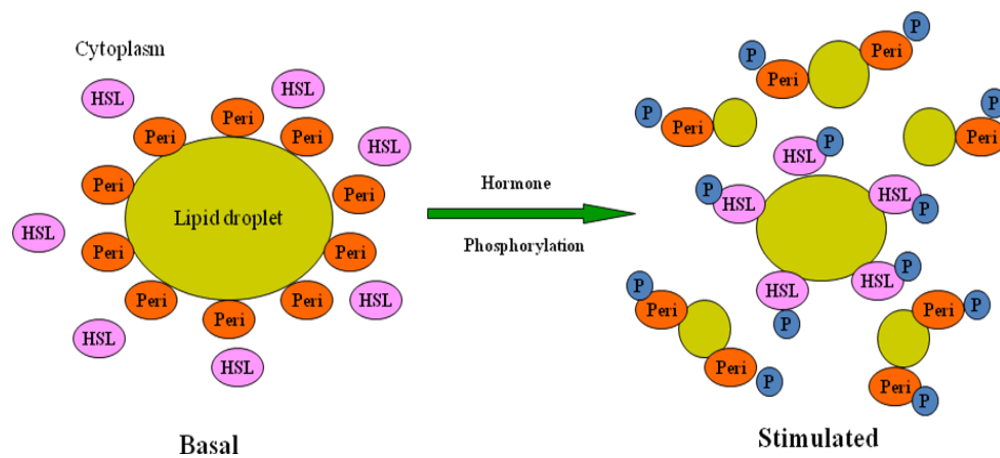


Fig. 1.15: Phosphorylation and translocation of HSL to lipid droplets. The picture shows the common mechanism of phosphorylation and translocation of HSL to the lipid droplets in adipocyte tissue. Under basal conditions, the non-phosphorylated HSL resides in the cytoplasm and the lipid droplets are well protected by the lipid-coat protein perilipin. After hormone induction, HSL and perilipin both get phosphorylated mainly by cAMP-dependent protein kinase-A. Due to phosphorylation, perilipin releases the barrier around the lipid droplets and divides the bigger lipid droplet into smaller droplets so that the overall accessible surface area of the droplets increases (Sztalryd et al. 2003; Shen et al. 2009). HSL translocates from the cytoplasm to the droplet surface and does the hydrolysis of lipid.

(Su et al. 2003; Marcinkiewicz et al. 2006). Mutagenesis studies have confirmed that simultaneous phosphorylation of both HSL and perilipin is required to perform successful translocation and lipolysis of HSL (Su et al. 2003; Sztalryd et al. 2003; Shen et al. 2009).

As mentioned above, HSL is primarily a cytosolic enzyme under basal conditions. It has been shown both *in vitro* and *in vivo* that hormone-induced phosphorylation triggers the translocation of HSL to the hydrophobic lipid droplets (Su et al. 2003; Miyoshi et al. 2006; Martin et al. 2009). It has been proposed that a major conformational change triggers the translocation of HSL upon phosphorylation (Holm et al. 1988). Many scientists have proposed that the phosphorylation primarily leads to some sort of electrostatic interaction that ultimately induces the exposure of hydrophobic surface area (Holm et al. 1988; Anthonsen et al. 1998). C Holm et al.(1988) has long been proposed that an eight amino acid hydrophobic patch (F₇₃₄LSLAALC₇₄₁) at the C-terminal domain of the rat HSL (**Fig. 1.16**) might be involved in the exposure process (Holm et al. 1988; Krintel et al. 2009). Recently, it has been shown that the conformational change is indeed a form of hydrophobic surface exposure of the enzyme (Krintel et al. 2009). This is one of the phenomena under investigation in this dissertation.

Even though the *in vitro* studies have elucidated most of the complicated phosphorylation related regulation of HSL, the mechanism of regulation of HSL activity *in vivo* is not that simple. Recently it has been shown that not only cAMP-dependent or independent pathways regulate HSL, but there are numerous other protein partners like

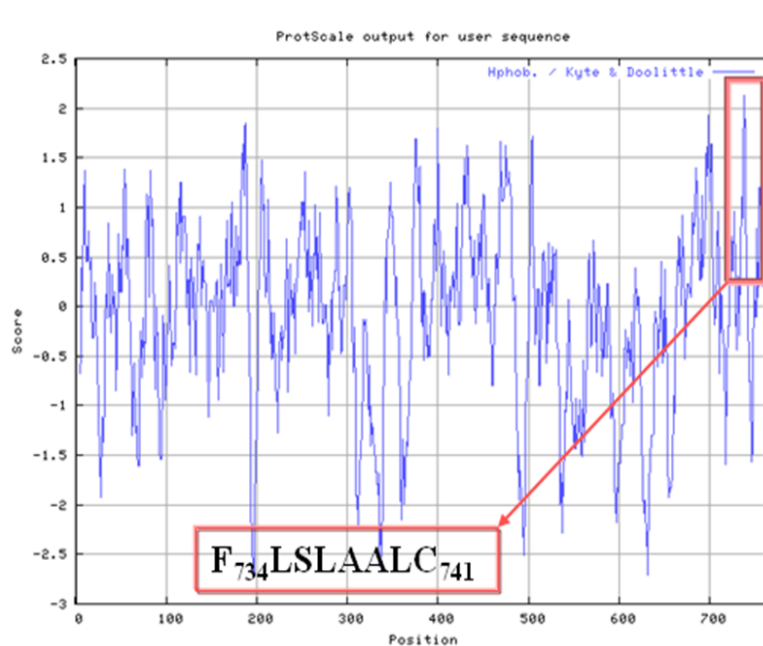


Fig. 1.16: Kyte and Doolittle hydropathy plot of rat HSL primary sequence. The rat HSL primary sequence has been fed to the freeware tool of Kyte and Doolittle hydropathy region predictor (Kyte and Doolittle 1982). The parameter sets are followed: amino acid window size: 9; weight variation model: linear; relative weight of the window edges compared to window center: 100. Apart from the hydrophobic acyl-binding site (ABS) (residue 442-453) predicted by the modeling studies (secondary structure aided multiple sequence alignment of rat HSL using *Candida rugosa* lipase as template), the plot predicted an additional lipid binding patch from F₇₃₄-C₇₄₁. C Holm et al. (1988) proposed that this patch might play a vital role in phosphorylation induced translocation of HSL to the lipid droplets (Holm et al. 1988; Krintel et al. 2009).

fatty acid binding protein (FABP) (Holm et al. 2000), lipotransin (Syu and Saltiel 1999), and vimentin (Shen et al. 2009; Shen et al.) which physically interact with the enzyme and play a vital role in regulating HSL's activation and translocation.

1.4.5 HSL as potential drug target for diabetes type –II:

It is well established in the literature that insulin exerts anti-lipolytic activity by activating phosphodiesterase and modulating the cAMP-dependent pathway (Kitamura et al. 1999; Rondinone et al. 2000; Hasegawa et al. 2002). In addition, insulin also activates the ERK signaling pathway; so it is of great debate whether insulin's main role is to induce phosphorylation or dephosphorylation of Ser600 (Londos et al. 1985). It is proposed that insulin's action has both cAMP-dependent and cAMP-independent components; it is highly probable that in addition to phosphodiesterase activation, it might induce the phosphorylation of phosphatases and ultimately regulate the anti-lipolytic activity of HSL (Stralfors and Honnor 1989; Resjo et al. 2002). It has been observed in adipocyte tissues *in vivo* and *in vitro* that phosphatases, like protein-phosphatase-2A (PP2A), protein-phosphatase-2C (PP2C), and protein-phosphatase-1 (PP1), do dephosphorylate at least at the Ser563 site (Wood et al. 1993; Clifford et al. 1998) of HSL.

Insulin regulates lipid hydrolysis by binding to the insulin receptor and by activating the PDE3B enzyme to minimize the cAMP-dependent protein kinase-A action (Nilsson et al. 1980; Londos et al. 1985; Rondinone et al. 2000). It is a well established fact that diabetes type-II patients suffer from insulin resistance state in which the normal secretion of insulin becomes inadequate to exert insulin response in liver, muscle and

adipocyte cells (Hotamisligil et al. 1995; Groop et al. 1996; Gonzalez-Sanchez and Serrano-Rios 2007). Under these conditions, the triacylglycerol hydrolysis increases and ultimately hinders the process of glucose storage in liver and uptake in muscles. In this way the concentration of glucose increases in the blood and patients suffer from acute type-II diabetes disease condition. To help control this, scientists have proposed to inhibit the activity of HSL to minimize the triacylglycerol hydrolysis and ultimately to manage the increasing glucose content in the blood (Reynisdottir et al. 1995; Ylitalo et al. 2000; Claus et al. 2005). Scientists have also noticed an altered mRNA expression level of HSL in diabetic and obese patients *in vivo* (Klannemark et al. 1998; Smih et al. 2002). This gives an additional support for the involvement of HSL in obesity and diabetes disease conditions.

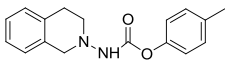
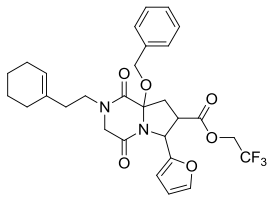
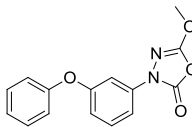
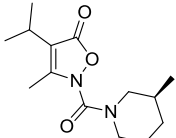
1.5 Inhibitors of HSL:

According to the American Diabetes Association estimation in 2009, about 20 million people alone in North America have been diagnosed with diabetes and among 90% of them have been affected by diabetes type-II. As discussed above, HSL being a potential diabetes type-II drug target, it has become important to find a potent HSL inhibitor. As the three dimensional structure of HSL has not been established, the high throughput screening of laboratory-synthesized compound libraries against HSL has been a usual method for finding potent inhibitors. To date, several potential HSL inhibitors have been synthesized and characterized. Most are carbazate, pyrrolopyrazinedione, oxadiazolone (compound 7600), and urea-based laboratory synthesized compounds. As

shown in **Table. 1.4**, the carbazate, pyrrolopyrazinedione-based compounds, and compound 7600 are most potent (IC_{50} in lower nM range) inhibitors of HSL (Slee et al. 2003; de Jong et al. 2004; Ben Ali et al. 2006). From the sequence similarity of *Alicyclobacillus acidocaldarius* esterase with the HSL C-terminal domain and the mass spectroscopic data available for esterase-compound 7600 complex, it is proposed that HSL's active site serine O-atom either attacks the ester carboxylic C-atom present in the molecules (carbazates) or opens the oxadiazolone ring (compound 7600) to covalently modify its active site (Claus et al. 2005; Ben Ali et al. 2006). It is speculated that the additional aromatic substitutions in the inhibitors (carbazate, pyrrolopyrazinedione, oxadiazolone) facilitate the initial binding of the inhibitor to the active site hydrophobic residues of HSL (Ben Ali et al. 2006). To date, no reversible inhibitor (binder) has been reported for HSL except BAY (**Table. 1.4**) which showed surprising reversible character, having a time-dependent inactivation mechanism against the enzyme (Claus et al. 2005).

Apart from laboratory synthesized inhibitors, the search is still on to find a natural product inhibitor for HSL. Vertesy et. al., first reported a natural product inhibitor of HSL, cyclipostin (**Table. 1.5**), that was isolated from the fermentation product of *Streptomyces species* DSM 13381 (Vertesy et al. 2002). They reported the isolation of several analogs of this compound having the IC_{50} s against rat adipocyte HSL in low nM range (Vertesy et al. 2002). The exact mechanism of action of these compounds against HSL has not yet been reported. As shown in **Table. 1.5**, the core structure of the cyclipostin is identical to the AChE inhibitor cyclophostin, having long

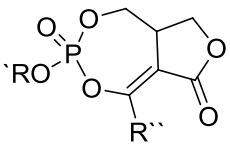
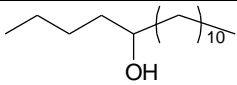
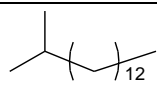
Table. 1.4: Inhibitors of human HSL and their IC₅₀s.

Class of compound	Commercial Name	Structure	IC ₅₀ (nM)	
			Esterase assay	Lipase assay
Carbazates ^a	N.A.		N.D.	19
Pyrrolopyrazinedione ^b	N.A.		120	180
Oxadiazolone ^c	Compound 7600		N.D.	60
Isoxazononyl urea ^d	BAY		N.D.	5

IC₅₀s are against human HSL; N.A.- Not Applicable; N.D.- Not determined.

^a(de Jong et al. 2004); ^b(Slee et al. 2003); ^c(Ben Ali et al. 2006); ^d(Claus et al. 2005).

Table 1.5: Structures of analogs of cyclipostin and their potency against rat HSL^a.

Core Structure of Cyclipostin	Analog			IC ₅₀ (nM)
	Name	R'	R''	
	A		CH ₃	20
	P		CH ₃	30
	P2		CH ₃	40
	S		CH ₂ CH ₃	20

^aAdapted from (Vertesy et al. 2002)

oxy-alkyl chain attached to the central P-atom. This makes the structure highly suitable for the hydrophobic HSL active site. In addition to the long C-chain substitutions, these compounds have a highly reactive seven-membered phosphate ring that can covalently modify the active site serine residue (very similar to the modification mentioned in AChE active site in **Chapter III**).

One of the goals of this dissertation is to test different phosphonates analogs (**Chapter IV**) of cyclipostin against rat HSL and determine the mechanism of inhibition.

CHAPTER II

MATERIALS AND METHODS

2.1 Inhibition studies of acetylcholinesterase (AChE):

Acetylcholinesterase (AChE) from electric eel and recombinant human, acetylthiocholine iodide (ATCh), 5,5'-dithiobis-2-nitrobenzoic acid (DTNB), and pralidoxime iodide were purchased from Sigma Co, Saint Louis, MO. P6-DG desalting resin was obtained from Pierce. ZipTip pipette tips were obtained from Millipore. All the organophosphates and phosphonates were supplied by our collaborator Dr. Spilling at the University of Missouri, Saint Louis, MO.

2.1.1 AChE assay:

Both electric eel and human recombinant AChE were quantitated utilizing the extinction coefficients 101,550 and 119, 656 $M^{-1}cm^{-1}$ respectively, calculated from their amino acid sequences (Pace et al. 1995). AChE (34 nM) was assayed utilizing Ellman's protocol (Ellman et al. 1961) using 160 μM acetylthiocholine (ATCh) as substrate and 300 μM 5,5'-dithiobis-2-nitrobenzoic acid (DTNB) as coloring reagent in 100 mM sodium phosphate, pH 8.0, at 25°C in total volume of 1.6 ml in 3 ml cuvette. A micro spinner was placed at the bottom of the cuvette for continuous mixing. The thiocholine formed by enzyme hydrolysis reacts with DTNB and forms thionitrobenzoate anion, which gives absorption at 412 nm. The assay was conducted using an HP8453 diode array spectrophotometer. The absorbance at 412 nm was monitored every 2 seconds for 30 seconds, and the slope (abs/sec) was

calculated using first 12–15 absorbance points to get the initial velocity of the reaction. The abs/sec was then converted to $\mu\text{mol}/\text{min}$ using the thionitrobenzoate extinction coefficient of $14,150 \text{ M}^{-1}\text{cm}^{-1}$.

2.1.2 Test of IC_{50} s of organophosphates (OPs) with AChE:

The organophosphate and phosphonate inhibitors were solubilized in isopropanol (IP) and used in such a way so that the final concentration of the IP does not go beyond 5% in the enzyme-inhibitor reaction medium. The AChE from electric eel or human (34nM) was incubated with the inhibitor at increasing concentrations (in μM range) in 20 mM Tris, 1% BSA, pH 7.5 at 25°C for 30 mins. The residual activity of the enzyme was assayed by Ellman's assay using acetylthiocholine (ATCh) ($500 \mu\text{M}$) as substrate and as a function of inhibitor concentration. The substrate concentration maintained well above the K_m of $46 \mu\text{M}$ for AChE (Radic et al. 1993). The % residual activity was calculated and plotted against the inhibitor concentration. The IC_{50} was determined as the concentration of inhibitor at 50% residual enzyme activity.

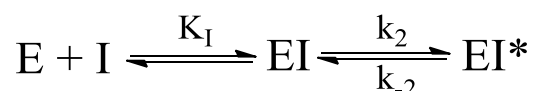
2.1.3 Test of irreversibility of enzyme-inhibitor reaction:

AChE from electric eel or human was incubated with inhibitor for 30 mins at 25°C in 20 mM Tris, pH-7.5 and passed through the P6DG gel filtration column (1 ml in volume and pre-equilibrated with 20mM Tris, pH 7.5). The eluted enzyme was requantitated and assayed for residual activity. P6DG is a desalting gel filtration column through which small molecules can be separated from a macromolecule; the protein elutes in the void volume leaving behind the small molecules like organophosphate or

phosphonates. If the enzyme-inhibitor reaction is purely reversible, then the eluted enzyme shows reactivation because of efficient separation of enzyme from inhibitor. For irreversible or covalent modification of the enzyme, the eluted enzyme remains inactivated. The activity of the enzyme was expressed as $\mu\text{M}/\text{min} \cdot \mu\text{M}$ of enzyme so that the activity was always normalized by enzyme concentration.

2.1.4 Time dependent irreversible experiment:

To obtain the irreversible inhibition kinetic parameters like the inhibition rate constants (k_i) and the inhibition equilibrium constant (K_i), time dependent inhibition experiments were performed. The loss of enzyme (here AChE) activity was measured as a function of pre-incubation time (min) and inhibitor concentrations (μM or nM) at 25°C . The pre-incubation time was incremented by 5 mins up to 30 mins with few exceptions. The time-dependent loss of % residual activity of the enzyme is described below (**Eqn 1**), assuming the enzyme-inhibitor reaction fits the irreversible two-step **Model 1**, having a reversible second order first step followed by a reversible first order second step.



Model 1: E = Enzyme, I = Inhibitor, EI = Enzyme-inhibitor complex, EI* = Enzyme-inhibitor dead-end complex, K_1 = inhibition equilibrium constant, k_2 = forward rate constant for inactivation, and k_{-2} = reverse rate constant for inactivation (Callan OH 1996; Walker et al. 2001).

$$A_t = A_0 [(1 - k_{-2}/k_{obs}) * e^{-(k_{obs} * t)} + k_{-2}/k_{obs}] \quad \text{Eqn. 1}$$

This equation represents a mono-exponential decay, where A_t equals the % residual activity at pre-incubation time (t), A_0 represents the % residual activity at zero time i.e., the initial activity in the absence of inhibitor), and the observed rate of decay is k_{obs} .

The measured % residual activity as a function of pre-incubation time (min) and inhibitor concentrations (μM or nM) was globally fit with **Eqn.1** using Scientist software to obtain the observed rate constant (k_{obs}) and reverse rate constant for inactivation (k_{-2}). The dependence of the observed rate constant (k_{obs}) on inhibitor concentration is defined as:

$$k_{obs} = k_2 * [I] / (K_I + [I]) + k_{-2} \quad \text{Eqn. 2}$$

where k_{obs} = observed rate constant, K_I = inhibition equilibrium constant, k_2 = forward rate constants for inactivation, and k_{-2} = reverse rate constant for inactivation.

The observed rate constant (k_{obs}) at different inhibitor concentrations ($[I]$) was plotted against inhibitor concentration $[I]$ with estimation of k_{-2} from the global fit and fit using Kaledagraph software to **Eqn. 2** to obtain the estimated value of inhibition equilibrium constant (K_I) and forward rate constant for inactivation (k_2).

Model 1 was intentionally designed to represent the global two-step reversible model. Most of the irreversible inhibitors showed an extremely low k_{-2} value and were also analyzed using **Model 2**. We also calculated pseudo-first order rate constant (k_i) for each inhibitor by dividing K_I from k_{inact} .



Model 2: E = Enzyme, I = Inhibitor, EI = Enzyme-inhibitor complex, EI* = Enzyme-inhibitor dead-end complex, K_I = inhibition equilibrium constant, k_{inact} = rate constant inhibition catalysis.

2.1.5 Oxime reactivation reaction:

The oxime reactivation experiments were conducted using pralidoxime iodide (shown in **Fig. 2.1**) as the oxime source. First, the AChE from electric eel or human (34 nM) was incubated with OP for 30 mins at 25°C in 20 mM Tris, pH-7.5, then pralidoxime (final concentration 35 mM) was added to the reaction mixture and the residual activity of the enzyme was assayed at different incubation times (up to 2 hrs).

2.1.6 MALDI-TOF analysis of proteolytic fragment of AChE:

For the trypsinization of AChE – inhibitor complex, 10 µg of the enzyme was first incubated with inhibitor (1 mM) at 25°C for 30 mins in 20 mM Tris, pH 7.5 and centrifuged through a Microcon YM-3 (Millipore) (to get rid of excess inhibitor so that it does not affect the activity of trypsin) and denatured by incubating the retentant with 0.1% SDS at 90°C for 45 mins. The denatured enzyme was then incubated with 2 µg of trypsin at 37 °C for 2 h in 50 mM sodium phosphate, at pH 8.0 and 20% acetonitrile (CH₃CN) (Wong et al. 2000; Kropp and Richardson 2007). After incubation, the trypsinized AChE samples were lyophilized (if necessary) or analyzed. The control

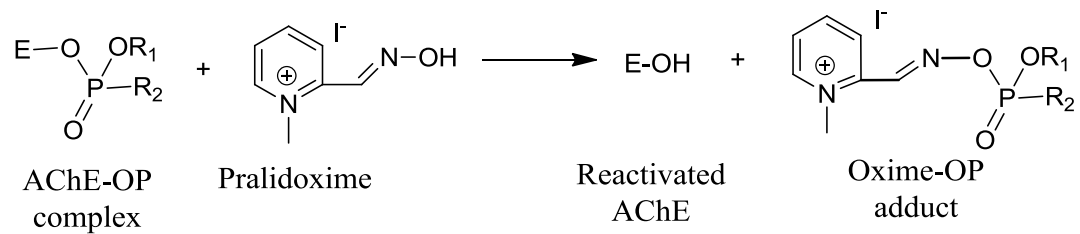


Fig. 2.1: Reaction of AChE-organophosphate complex with oxime.

Adapted from (Wong et al. 2000).

sample (enzyme without the inhibitor) was also denatured and trypsinized by the above process.

Lyophilized samples (both inhibitor treated and untreated) were suspended in 20 μ l of 20% CH₃CN solution containing 0.1%TFA, and incubated at room temperature for 10 mins. ZipTip (Millipore) C4 tips were activated in 70% CH₃CN/0.1% TFA for 10 mins and washed 4 times with 20 μ l of 20% CH₃CN/0.1% TFA. The 20 μ l of trypsinized AChE was adsorbed to the tips by 15 cycles of 10 μ l of aspirate and dispense steps. Step gradient elution was performed by 3 cycle of 10 μ l of aspirate and dispense steps at different CH₃CN concentrations (e.g., 20, 25, 30, 35, 40, 60, and 80%) (15 μ l each) containing 0.1% TFA. 5 μ l of each elution fraction was mixed with 5 μ l of of trans – 3,5-dimethoxy-4-hydroxycinnamic acid (Sigma; 10mg/ml saturated solution in 40% CH₃CN and 0.1%TFA) and spotted on MALDI-TOF/ MS target. The spot was dried and placed inside the MALDI-TOF/MS probe for data collection. Otherwise the Zip Tipped samples were lyophilized and submitted to the Mass-spectrometric facility of Danforth Plant Science Centre, Saint Louis, MO for MALDI-TOF analysis with Applied Biosystems Voyager-DE STR MALDI instrument.

2.2 Inhibition studies of recombinant rat hormone-sensitive lipase (HSL):

2.2.1 Cell culture:

The *Spodoptera frugiperda* (Sf9) cells were grown in TNM-FH medium supplemented with 10% heat inactivated FBS, 100 units/ml penicillin G, and 100 μ g/ml streptomycin at 27°C. The cells were maintained in T-150 flasks (Fisher Scientific) and subcultured in 1:3 ratio whenever it reached 90% confluency.

2.2.2 Hormone-sensitive lipase preparation and purification:

The rat hormone-sensitive lipase gene was obtained from Dr. F.B Kraemer's lab at Stanford. The gene was cloned into a pcDNA3 vector using *HindIII* and *XbaI* sites. The HSL gene was subcloned in the pAcHLT-A baculovirus transfer vector (BD Biosciences), having N-terminal 6X-His Tag gene at a *SmaI* blunt cloning site. The pAcHLT-A-HSL construct was transformed into TOP10F' *E. Coli* competent cells for large scale DNA production.

Recombinant baculovirus containing the HSL gene was made us the HSL gene from the pAcHLT-HSL plasmid and the linearized Baculogold DNA (BD Biosciences; Cat. No. 21100D). The transfection into Sf9 insect cells was accomplished by utilizing the Ca^{II}-phosphate precipitation method using a BaculoGold Transfection Kit (BD Biosciences; Cat. No. 560129). The successful formation of recombinant baculovirus containing the HSL gene was confirmed by Western Blot analysis using a anti –rabbit HSL polyclonal antibody as the primary antibody (Cayman Chemicals Ltd.), and anti-rabbit horseradish peroxidase (Promega) as the secondary antibody on the virus-infected cell lysate (**Fig. 2.2**) (Kraemer and Shen 2002; Kropp and Richardson 2007).

Next, the recombinant virus was further proliferated to get a high titer virus solution. From an end point dilution assay (BDBiosciences Baculovirus expression manual), the virus titer was estimated as 1 e7 pfu/ml. For semi-large scale protein production, 7 e7 Sf9 cells were grown in T-150 (Fisher) flasks in TNM-FH medium

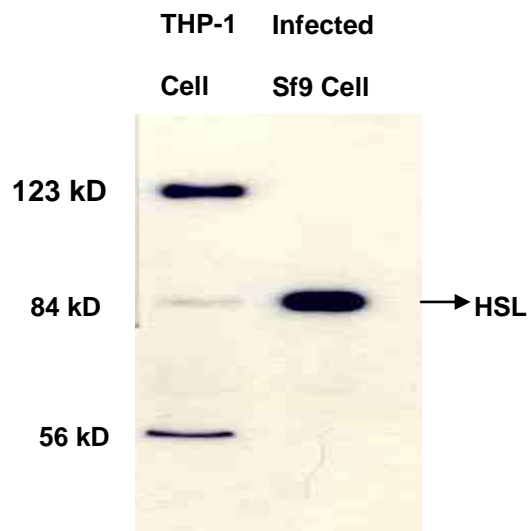


Fig. 2.2: Western Blot analysis of recombinant HSL gene containing baculovirus infected Sf9 cell lysate. Sf9 cells were infected with recombinant viral containing HSL gene. After 3 days of incubation, the cells were lysed by using 1% digitonin (w/v) in 50 mM Phos, pH 7.5. SDS PAGE was performed on a denatured Sf9 cell lysate sample with a THP-1 cell lysate sample as a positive control. The Western Blot was performed by using anti –rabbit HSL antibody as the primary antibody (Cayman Chemicals Ltd.) and anti-rabbit Horseradish Peroxidase (Promega) as secondary antibody. Lane 1 is the Western blot of THP-1 lysate having all the three HSL isoforms (123 KD, 84 KD, and 56 KD). Lane 2 is the same for HSL gene cloned baculovirus infected Sf9 cell lysate. In lane 2 Sf9 expressed recombinant HSL can be seen at 84 KD.

containing 10% FBS, 100 units/mL penicillin G, and 100 $\mu\text{g}/\text{mL}$ streptomycin in 27°C incubator (without CO_2) and infected with the recombinant virus at 5 m.o.i (multiplicity of infection; virus-to-cell ratio) (Ben Ali et al. 2004). 3 days after infection, the cells were harvested by centrifugation at 5,500 g for 7 mins and the cell pellet was collected and preserved at -80°C freezer for further analysis. As HSL is not a secreted enzyme, the supernatant was discarded.

For protein production, the cell pellet was resuspended in a 3 pellet equivalent volume of homogenization buffer containing 50 mM phosphate, pH 7.5, 25 mM sucrose, 1 mM β -mercaptoethanol, 10% glycerol, and protease inhibitor cocktail (antipain, pepstatin, and leupeptin at final concentrations of 2, 1, and 2 $\mu\text{g}/\text{mL}$, respectively, Sigma; Cat. No. P8849) (Ben Ali et al. 2004). The cell homogenate was sonicated (2 mins at 2 setting followed by 2 mins at 4 setting with 30 sec interval in ice between each treatment) using Branson Sonifier 250 sonicator and centrifuged at 15,000 rpm for 15 mins at 4°C.

As the expressed protein contained N-terminal 6X-His Tag, the resulting supernatant was collected and incubated with Ni-NTA beads (pre-equilibrated with 50 mM Phos, pH 7.5, 20% glycerol, 0.3 NaCl, 1 mM β -mercaptoethanol, and protease inhibitor cocktail (buffer A)) for 45 mins at 4°C. Next, the recombinant HSL-bound Ni-NTA beads were washed with 4 bead volumes of buffer A containing 5 mM imidazole to prevent non-specific binding. The protein was then eluted via imidazole concentration step gradient from 50 mM to 250 mM imidazole in buffer A (elution volume 300 μl)

(Fig. 2.3). The fractions were evaluated by SDS-Page and the most pure elution fractions were pooled and dialyzed using Slide-A-lyzers (Pierce) against buffer A containing no imidazole. The purified HSL was quantitated by UV spectrophotometry (Hewlett Packard 8453) using an extinction coefficient of $52,090 \text{ M}^{-1} \text{ cm}^{-1}$, calculated from its amino acid sequence (Pace et al. 1995).

2.2.3: HSL assay:

The assessment of HSL activity was done in two ways; a) by esterase assay, and b) by lipase assay. Both assays were done to determine HSL activity, and they are described below.

a) Lipase Assay:

The lipase assay of HSL was conducted by using 9, 10 - ^3H labeled triolein (Perkin Elmer). Triolein is a trioleylglycerol which is hydrolyzed by HSL to form free oleic acid. The basis of the assay is to monitor the release of radio-labeled free oleic with time to obtain the rate of reaction. The triolein was introduced to the enzyme through liposomes. The liposome containing substrate was formed by mixing phosphatidylcholine, phosphatidylinositol, and unlabelled triolein in a 1:3:1 ratio (Belfrage and Vaughan 1969). 500 μM of 20 ml triolein solution was prepared by adding 20 μg of phosphatidylcholine, 75 μg of phosphatidylinositol, 8855 μg of unlabeled triolein and 191cpm/fmol of ^3H labeled triolein in chloroform. The chloroform was evaporated by using rotavap in an N_2 environment and adding 20 ml of buffer containing 25 mM Tris pH 7.4, 150 mM NaCl, 0.2 mM EDTA, and 1mM β -ME. As liposome formation is energetically unfavorable, the mixture was sonicated (2 mins at 2 settings

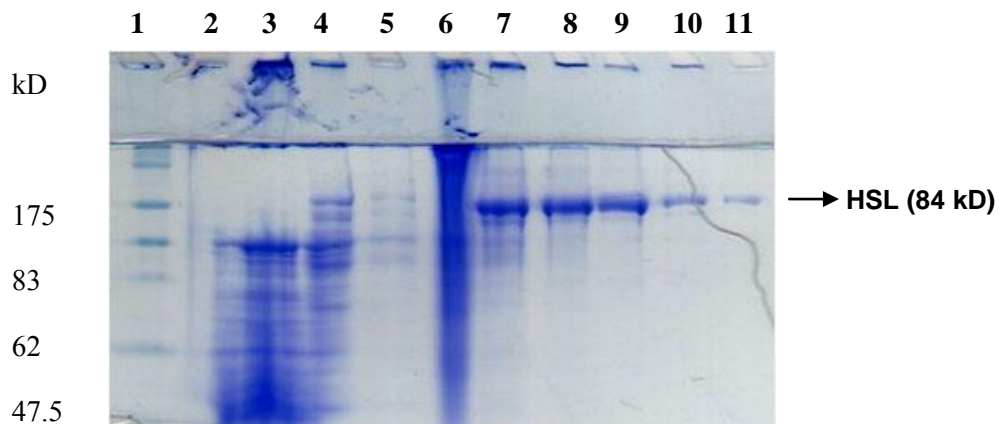


Fig. 2.3: SDS-PAGE gel from recombinant rat HSL purification using Ni-NTA beads. Step gradient of imidazole from 50 mM to 250 mM was used to elute the Ni-NTA bound 6X-His tag HSL. The SDS PAGE was performed on denatured elution fractions and the above image was acquired. SDS gel image shows the amount of protein present in each fractions and their purity. Lane 1 is protein molecular weight marker (NEB), lane 2, 3, 4, and 5 are crude extract, flow through of loading, washing 1, and washing 2 respectively. Lane 6, 7, 8, 9, 10, and 11 are elution at 50, 100, 150, 200 and 250 mM imidazole solution. The purified HSL can easily be seen at 84 kD.

and 2 mins at 4 setting) by a Branson sonifier (Belfrage and Vaughan 1969). The sonified solution was then cooled to room temperature, and 0.1 % BSA was added. The resulting emulsion was used as a stock solution of substrate.

The reaction of HSL with liposome-containing substrate was conducted on a 600 μ l scale. 480 μ l of the substrate was incubated with 120 μ l of 100 nM HSL (depending on the concentration required) at 37°C for 40 mins. The reaction was quenched by adding 600 μ l of methanol:chloroform:heptane (1.41:1.25:1) solvent mixture and 300 μ l of 50 mM potassium carbonate - potassium borate - potassium hydroxide buffer at pH 10. The resulting mixture was vigorously vortexed for 7 mins and centrifuged at 13,000 rpm for 10 mins. The extraction was repeated. The upper aqueous layer containing radiolabeled free fatty acid was collected, and the radioactivity was determined via liquid scintillation. The reaction was monitored for 30 mins, and every 5 mins 100 μ l of the aliquot was withdrawn and quenched by the above mentioned solutions, and the radioactivity was evaluated. The rate was calculated from the slope of cpm vs. time, and the rates were expressed in terms of μ mol/min per mg of enzyme.

b) Esterase Assay:

The esterase activity of HSL was determined by using water soluble *p*-nitrophenyl butyrate (*p*-NPB) as a substrate. For the assay of HSL (100 nM), *p*-NPB in 100% acetonitrile was added to 100 mM Phos pH 7.2, 150 mM NaCl, and 0.5% Triton X-100 at 25°C (Shirai et al. 1982). HSL hydrolysis of *p*-NPB obtained yellow color *p*-nitrophenol, which absorbs at 400 nm. The increase in absorbance at 400 nm was

recorded every 30 secs for 5 mins. The reaction rate was calculated in abs/sec using first 6 to 8 absorbance points and converting to $\mu\text{mol}/\text{sec}$ by utilizing the extinction coefficient of *p*-nitro phenol as $14,200 \text{ M}^{-1}\text{cm}^{-1}$ at 400 nm.

2.2.4 Test of IC₅₀s of organophosphates (OPs) with HSL:

The HSL activity was tested in the presence of two types of organophosphates; one having long carbon chain fatty acid-like substituents and another without (e.g., DIFP, compound **2a**, **2b**).

The water insoluble carbon chain substituted inhibitors were introduced to the enzyme through liposomes. First, a stock solution of phosphatidylcholine (PC) and phosphatidylinositol (PI) mixture, having a concentration of $1.4 \mu\text{M}$ and $4.2 \mu\text{M}$ (respectively) was prepared in chloroform. Varying volumes of 148 mM inhibitor isopropanol solution were mixed with $9.33 \mu\text{l}$ of PC/PI solution to make 1 ml liposome-embedded inhibitor solution of different concentrations. Solvent was evaporated, and 1 ml of buffer containing 25 mM Tris pH-7.4, 150 mM NaCl was added to it. Next the mixture was sonicated for 2 mins at 2 setting and 2 mins at 4 setting. Thus, different concentrations of inhibitor solutions (e.g., 100 , 200 , 400 , 800 , and $1600 \mu\text{M}$) were made keeping the PC/PI composition constant. For IC₅₀ determination, 100 nM of HSL was incubated with liposome-embedded inhibitor solution at varying concentration for 30 mins at 37°C . The residual activity of the enzyme after the reaction was determined by assaying the enzyme-inhibitor mixture using either lipase or esterase assay method described above. The lipase and esterase assays were conducted using $50 \mu\text{M}$ of triolein and 5 mM *p*-NPB, which were 15 and 10 fold higher than their respective K_{ms} , $3.4 \mu\text{M}$

and 0.59 mM (Osterlund et al. 1996; Shen et al. 1998). The IC₅₀ was determined as the concentration of inhibitor at 50 % residual activity of the enzyme.

2.3 Hormone-sensitive lipase translocation to lipid droplets in 3T3-L1 adipocyte cells:

2.3.1 Cell culture:

The 3T3-L1 cells (ATCC) were grown in Dubelcco's Modified Eagle Medium (DMEM) supplemented with 10% FBS (Hyclone), 2 mM L-glutamine, 100 U/ml penicillin, and 100 µg/ml streptomycin at 37°C in 5% CO₂. The cells were sub-cultured every three days at the density of 7000 cells/cm². The cells were fed with the new medium every couple of days and never allowed to be more than 70% confluent.

2.3.2 Differentiation of 3T3-L1 cells:

The pre-adipocyte 3T3-L1 cells were obtained from ATCC. For the HSL translocation experiment, the cells are required to be differentiated and to have mature lipid droplets and a well-defined cytoplasm and nucleus.

For differentiation, the cells were grown to confluency in DMEM medium containing 10% FBS, 100 U/ml penicillin, and 100 µg/ml streptomycin at 37°C in 5% CO₂. At two days of post-confluency, the cells were stimulated with medium containing 10% FBS, 175 nM insulin (Sigma), 0.5 mM 3-isobutyl-1-methylxanthine (IBMX; Sigma), 0.25 µM dexamethasone (Sigma), 2 mM L-glutamine, 100 U/ml penicillin, and 100 µg/ml streptomycin (Wolins et al. 2006). After two days of incubation at 37°C in 5% CO₂, the medium was changed to insulin medium containing 200 nM insulin, 10%

FBS, 2 mM L-glutamine, 100 U/ml penicillin, and 100 µg/ml streptomycin. It generally took 7-8 days post confluency to achieve full differentiation of 3T3-L1. The differentiated cells were maintained in normal DMEM growth medium.

2.3.3 Expression of YFP-fused HSL in 3T3-L1:

The rat HSL gene was subcloned in to the pTag-YFP (Evrogen) vector at the C-Terminal of YFP at the HindIII/XbaI site. The pTagYFP-HSL construct was then transfected into 3T3-L1 cell using Lipofectamine 2000 (Invitrogen; Cat. No. 11668-027) transfection reagent. 0.8 µg of pTagYFP-HSL and 2 µl of Lipofectamine 2000 were mixed together and incubated for 5 mins at 25°C, and the mixture was added to the wells of 24 well plates having 2×10^5 3T3-L1 cells. After 8 hrs of incubation at 37°C in 5% CO₂, the transfection medium was replaced with growth medium and incubated for another 24 hrs at the same temperature. Two days post transfection the cells were screened for transfected cells in the presence of antibiotic, geneticin (600 µg/ml) (Bayers' Chemical). Next, the expression of YFP-HSL was verified by performing Western Blot or by direct imaging of YFP expression (**Fig. 2.4**) through Carl Zeiss 700 Laser Scanning Confocal Microscope at Centre for Nanoscience, UMSL.

2.3.4 Lipid droplet staining by BODIPY-C₁₂ in 3T3-L1 cells:

The lipid droplets in differentiated 3T3-L1 cells were stained by BODIPY-C₁₂ dye. First, 500 µl of 8 % BSA (final concentration 2 %) was sonicated (2 mins at 2 settings) with 10 µl of oleic acid (final concentration 1.8 mM) in phosphate buffer saline (PBS), then the resulting emulsion was mixed with BODIPY-C₁₂ (20 µg/ml), 2 µl of 167

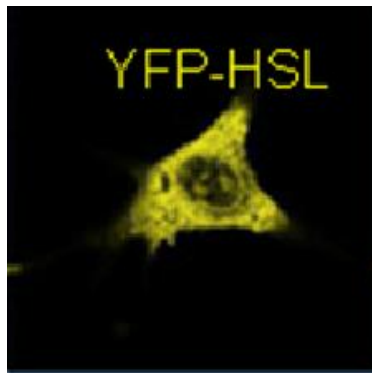


Fig. 2.4: A confocal image of YFP-HSL protein in pre-adipocyte 3T3-L1 cell. 3T3-L1 cells were transfected by pTagYFP-HSL DNA and screened for positively transfected cells using geneticin (600 $\mu\text{g/ml}$). After the screening process, the transfected cells were grown for additional 2 days in growth medium. Next the cells were subcultured in a MatTek dish and a confocal image was collected using a Carl Zeiss 700 Laser Scanning Confocal Microscope. The excitation wavelength was 508 nm and the emission was detected at 520 – 610 nm.

μM of insulin and 100 μl of 0.5 M glucose. The total volume of the mixture was adjusted to 2 ml. The whole solution was laid on the differentiated 3T3-L1 cell bed in MatTek (MatTek corp.) dish and incubated for 2.5 hours. The cell density in the MatTek dish was maintained such that the cells could get plenty of space to spread their cell structure. After the incubation, the cells were gently (no vigorous agitation) washed three times with PBS and confocal images were taken. **Fig. 2.5** shows the BODIPY stained lipid in the differentiated 3T3-L1 cells.

2.4 1-anilinonaphthalene-8-sulphonate (1, 8-ANS) binding to rat HSL:

1-anilinonaphthalene-8-sulphonate (1, 8-ANS) (Molecular Probes) is a small organic molecule that is non-fluorescent in water but fluoresces when comes in contact with any organic solvent or hydrophobic surface of protein (Parker et al. 1967; Tanaka et al. 2006). The excitation and emission wavelength of protein-bound 1, 8-ANS is reported as 375 nm and 480 nm, respectively (Parker et al. 1967) (**Fig. 2.6**). A Fluorolog 3 spectrofluorimeter (Horiba Jobin Yvon) was used to perform the experiments. A nitric acid cleaned quartz cuvette (NSG scientific) was used and 25°C temperature was maintained during the experiments using an external water bath.

Normally, 100 μM of 1, 8-ANS was reacted with 1 μM of HSL at 25°C in membrane filtered 50 mM Tris, pH 7.5 solution in a total volume of 700 μl and the fluorescent emission spectrum was taken at 487 nm by exciting the ANS at 380 nm. The rat HSL was dephosphorylated by incubating it with 2 units of PP2ase (Promega) in the same buffer condition at 25°C for 30 mins. For consecutive phosphorylation of the

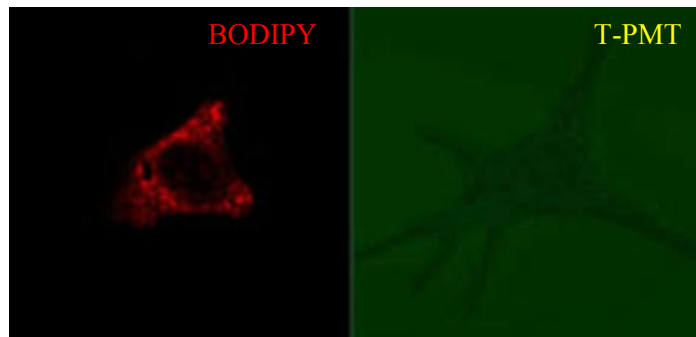


Fig. 2.5: BODIPY-C₁₂ stained differentiated 3T3-L1 cells. The normal 3T3-L1 cells were differentiated (protocol mentioned in the text) and then the cells were stained with BODIPY-C₁₂ (20 $\mu\text{g/ml}$) for 1 hr at 37°C (protocol in the above text). The cells were washed with PBS three times and confocal images were taken. The picture at left was taken using Zeiss confocal imaging microscope (CNS, UMSL) in track 1 with the following parameter set: Lense: 63X, laser power master gain = 350, pin hole = 1AU, excitation at 500 nm and emission at 510 nm in Smart setup. For normal cell picture at right in track 2 the parameters sets were following: lense: 63X, laser power master gain = 304, pin hole = 1AU, transmitted light (T-PMT) in Smart setup.

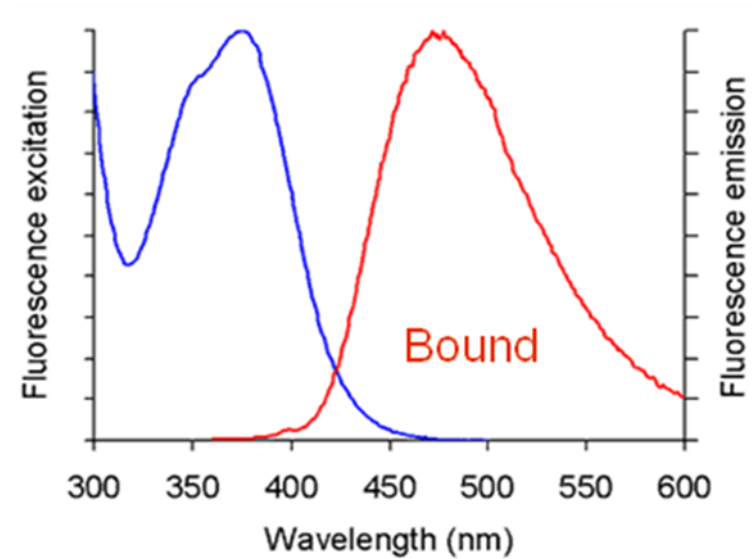


Fig. 2.6: 1, 8-ANS excitation and emission spectra. The blue curve represents the excitation spectra of 1, 8-ANS, whereas the red curve represents the emission spectra of the same when it is bound to any hydrophobic entity like protein hydrophobic surface or any organic solvent. Adapted from (Parker et al. 1967).

enzyme, first it was treated with 10 nM of okadaic acid (a PP2ase inhibitor) for 15 mins and then incubating it with 200 μ M ATP, 10 mM MgCl₂, and 10 units of c-AMP dependent PKA at 25°C for 30 mins in same reaction buffer stated above.

2.5 Dynamic light scattering (DLS) experiment of HSL inhibitors in aqueous solution:

According to the classical theory of light scattering, when light passes on the molecule, the electric field of the light induces an oscillating polarization of electrons in the molecule. The molecules then become a secondary source of light and scatter the impinging light. The frequency shifts, the angular distribution, the polarization, and the intensity of the scatter light are determined by the size, shape and molecular interactions in the scattering material (Brookhaven Instruments; Berne and Pecora 1975).

All DLS experiments were conducted using a Particle sizer (Brookhaven Instruments) located in Dr. George Gokel's lab in Center for Nanosciences (CNS) at UMSL. A solution of compound **24** or the liposome containing **24** (**Chapter IV**) was prepared in 50 mM Tris, pH=7.5 at 25°C. The reaction volume was maintained as 1.2 ml in disposable cuvettes. After the sample was exposed to the laser source in the machine, it automatically generated a plot of autocorrelation function vs time (μ s) plot; the actual data was generated from the secondary plot of intensity vs diameter (**Fig. 5.3**). The autocorrelation function ($G\tau$) relates to the diffusion co-efficient (D) like **Eqn 3** (Berne and Pecora 1975),

$$G(\tau) \propto e^{-2DK^2\tau}$$

$$K = \frac{4\pi\eta}{\lambda} \sin\left(\frac{\theta}{2}\right)$$

Eqn 3

where $G(\tau)$ = autocorrelation function, τ = time in μ secs, D = diffusion co-efficient, K = measurement vector, η = refractive index of the solution (1.33 for water), λ = wave length of the laser (generally 632.4 nm), θ = angle of scattering.

Again, the diffusion co-efficient (D) can be related to the diameter of the particle or molecule by **Eqn 4**,

$$D = \frac{k_B T}{3\pi\eta d}$$

Eqn 4

where d = diameter of the particle or molecule (m), T = absolute temp, η = diluent viscosity (water = 8.94×10^{-4} kg/(ms) and k_B = Boltzmann constant (1.3807×10^{-23} J/K).

2.6 Structure aided multiple sequence alignment (SSAMSA) of HSL and CRL using SwissPDB Viewer:

SSAMSA has been done using SwissPDB Viewer's (Guex and Peitsch 1997) special tool named 'magic fit'. In this process the amino acid sequence of CRL (used as template) is fed to the program and the C-terminal amino acid sequence of rat HSL (1-367) is then provided. When 'magic fit' is turned on the program used the SSAMSA and other energy minimization method to come up with a suitable secondary structure of the HSL according to the template provided (**Fig 5.2**).

CHAPTER III

INHIBITION STUDIES OF ACETYLCHOLINESTERASE IN PRESENCE OF THE BICYCLIC PHOSPHONATE ANALOG OF CYCLOPHOSTIN

3.1 Acetylcholinesterase (AChE) inhibition and structure-activity relationship of laboratory synthesized organophosphates (OPs):

As discussed in **Chapter I**, acetylcholinesterase (AChE) belongs to the serine hydrolase (SH) superfamily of enzymes. This family of enzymes contains serine as one of the catalytic amino acids in their active sites. Including serine, the active site of the enzyme contains two other highly important amino acid residues, aspartic acid and histidine, which are involved in hydrolyzing the natural substrate acetylcholine (ACh) (Rosenberry 1975). ACh, the natural substrate of AChE, is a neurotransmitter which helps transporting information from one neuron to another (Maelicke and Albuquerque 2000). It has been proposed that AChE can be a drug target for neuronal disorder diseases (Millard and Broomfield 1995; Cutler and Sramek 2001). In AD patients, the accelerated hydrolysis of ACh enhances the risk of memory loss, which could be prevented if the hydrolyzing enzyme AChE is inhibited. Most of the inhibitors available for AChE are laboratory synthesized (Lahiri et al. 2004; Eckert et al. 2006; Belluti et al. 2009). There are very few natural product inhibitors of AChE known to scientists; they are physostigmine, huperzine-A, and fasciculin (**Fig. 1.8** in **Chapter I**). Organophosphates (OP) are one of the most extensively used inhibitors of AChE (Kam et al. 1993; Winkler et al. 1996; Glynn 1999). OPs like soman, tabun, VX, and paraoxon

are all laboratory synthesized compounds (**Fig. 1.9** in **Chapter I**), which are utilized to study AChE inhibition (Worek et al. 2004).

3.1.1 Test of IC₅₀s for laboratory synthesized organophosphates (OP) against human and electric eel AChE:

Cyclophostin is a bicyclic phosphate, which is reported to be one of the most potent organophosphate based natural product inhibitors of AChE (**Table 1.2** in **Chapter I** and **Table 3.1**) (Kurokawa et al. 1993). As listed in **Table 3.1** the IC₅₀ of cyclophostin is 0.8 nM against insect AChE. Our collaborator synthesized the bicyclic phosphonate analog of cyclophostin along with a variety of other cyclic and acyclic phosphonates (see **Table 3.1**). The potencies of all laboratory synthesized compounds were tested against human and electric eel AChE using Ellman's assay (Ellman et al. 1961). The IC₅₀s of all the laboratory synthesized compounds are listed in **Table 3.1** (Bandyopadhyay et al. 2008; Dutta et al. 2010).

As reported in (Bandyopadhyay et al. 2008), one diastereoisomer of bicyclic phosphonate analog of cyclophostin was more potent (**2a**) than the other one (**2b**), when tested against both human and electric eel AChE. The diastereospecificity of **2a** and **2b** against human and electric eel AChE is shown in **Fig. 3.1A** and **B**. The IC₅₀ for **2a** against house fly AChE is 0.8 μM, almost 10 times more potent than **2a** against human AChE. Though the species specific potencies of compound **2a** and **2b** were quite attractive in terms of designing more potent inhibitors, the highest potency of **2a** against house fly AChE (IC₅₀ 0.8 μM) was still 1000 times less than the potency of natural product (**1**) against insect AChE (IC₅₀ 8 e-4 μM) (Kurokawa et al. 1993).

Table 3.1: IC₅₀s of organophosphates against AChE from different sources.

Compound	Structure	IC ₅₀ , μM		
		Human	Eel	Fly
1 ^a		N.D		8e-4
2a ^{b,c}		3	70	N.D
2b ^{b,c}		30	400	N.D
3a ^{b,c}		≈ 35	150	N.D
3b ^{b,c}		≈ 6	100	N.D
9 ^c		7	300	N.D
10 ^c		600	N.D	N.D
15 ^c		5	N.D	N.D
21b ^c		70	N.D	N.D
21a ^c		>1000	N.D	N.D
DIFP ^c		0.12	N.D	N.D

N. D = Not Determined.

^a(Kurokawa et al. 1993); ^b(Bandyopadhyay et al. 2008); ^c(Dutta et al. 2010)

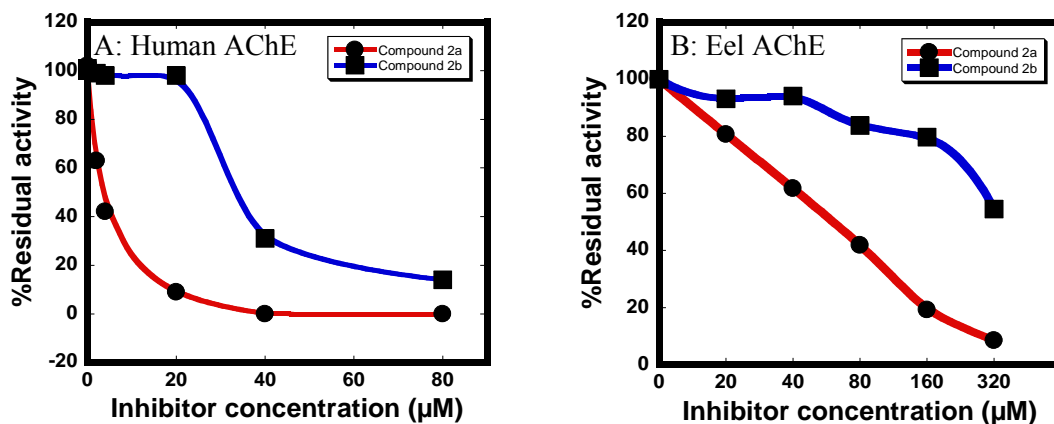


Fig. 3.1: Diastereospecificity of 2a and 2b against human and electric eel AChE.

A: 34 nM human AChE was incubated with 1, 2.5, 5, 10, 20, 40, and 80 μM of **2a** and **2b** for 30 mins at 25°C. The % residual activity of the enzyme was obtained using Elman's assay and plotted against inhibitor concentration. The data points are connected to guide the eyes. B: 34 nM electric eel AChE was incubated with 20, 40, 80, 160, and 320 μM of **2a** and **2b** for 30 mins at 25°C and is the same as in A. Adapted from (Dutta et al. 2010).

The relative configuration of the most potent inhibitor **2a** is opposite compared to the natural product (**1**); in **2a** the methoxy group attached to the central P-atom and the H-atom at junction C4 are located on opposite faces of the molecule, whereas for **1** it is at the same face. We have to keep in mind that the synthesis of the bicyclic phosphonate analogs were done using achiral phosphono carbonate (Bandyopadhyay et al. 2008), and as a result, the individual compounds **2a** and **2b** are actually a mixture of two isomers. Even though the relative configuration of **1** is similar to **2b**, it is possible that one of the isomers constituting compound **2b** is particularly unsuitable for the AChE active site and contribute the less potency. In addition, we should not forget about the contribution of O5 in **1** for enhancing its electrophilicity of P6 compared to the presence of C5 in **2a** (see the numbering in **1**).

Interestingly, the monocyclic compounds **3a**, **3b**, and **9** that lack the lactone ring showed similar IC_{50} s (35, 6, and 7 μ M for human AChE and 150, 100, and 300 μ M for eel AChE) to the bicyclic analogs (Dutta et al. 2010). It seemed from the IC_{50} that the lactone ring did not have much contribution towards the potency of the bicyclic compound, but binding constant data (discussed in later sections) indicates that there is considerable contribution from the lactone ring in this regard. Interestingly, reduction of the ester in **9** to **10** (an alcohol) decreased the potency up to 100 fold, a phenomenon which indicates the electron withdrawing contribution of ester in augmenting the leaving group characteristics of the enol from the P-center (Bandyopadhyay et al. 2008). It is also possible that carbonyl carbon of the ester is involved in some hydrogen bond-accepting contacts with the AChE active site residues (see later sections). Moreover,

compound **17b**, the E isomer of the compound pair having intact lactone ring, showed much better activity (70 μM) than the Z isomer, compound **17a**. This indicates that not only a cyclic phosphonate-like structure is necessary, but there is also a requirement of structural alignment between P-center and lactone ring for better inhibitory potency against AChE.

Though the results from **Table 3.1** illustrate the structure activity relationship of cyclic and acyclic phosphonates against AChE, the optimum potency of the laboratory synthesized compounds could not exceed the potency of conventional AChE inhibitor, DIFP. This phenomenon has both advantages and disadvantages in terms of AChE inhibitor designing in future (discussed later).

3.1.2 Mechanism of inhibition of human and electric eel AChE by cyclic phosphonates:

Kurokawa T et al. (1993) reported the inhibitory potency of cyclophostin against AChE in terms of IC_{50}s . They did not perform any mechanistic studies to establish the mode of action of the inhibitor against AChE. To establish the mechanism of inhibition, rigorous and detail analysis of inhibition was conducted. Generally, the OPs inhibit the AChE in an irreversible manner (**Fig. 1.10** in **Chapter I**). I tested the most potent inhibitor in our hand, compound **2a**, for its irreversible nature of inhibition.

The AChE from human and electric eel were incubated with compound **2a** for 30 mins at 25°C and passed through a P6DG column; the eluted enzymes in the void volume were quantitated and tested for activity (see experimental detail in **Chapter II**). P6DG retains the small molecules and lets the macromolecule elute at the void volume. If the

inhibitor is reversible, which means the interaction of inhibitor with the active site of the enzyme is non-covalent, then the eluted enzyme shows reactivation due to the small molecule partitioning in the desalting column. An irreversible inhibitor, which covalently modifies the enzyme active site and/or other sites, remains attached with the eluted enzyme and thus the enzyme is not re-activated even upon desalination. **Fig. 3.2a** and **3.2b** show the irreversible nature of compound **2a** against human and electric eel AChE on the time scale of the experiment.

To determine the exact mechanism of inhibition, % residual activity of the enzyme was recorded as a function of inhibitor concentration and incubation time for all potent compounds (IC_{50} in low μM range) against human AChE (**Fig. 3.3**, **Fig. 3.4**, and **Fig. 3.5**).

To elucidate the mechanism of inhibition, **Model 1** (explained in **Chapter II**) is utilized rather than the conventional Kitz and Wilson irreversible inhibition model (Kitz and Wilson 1962). The **Model 1** was more general and can explore the reversible inactivation step. Observed rate constants (k_{obs}) were determined by the global fit of the % residual activity vs pre-incubation time data using Scientist program. The k_{obs} s were then plotted against the inhibitor concentrations to obtain the equilibrium inhibition constant (K_I), forward rate constants for inactivation (k_2), and reverse rate constants for inactivation (k_{-2}). The K_I of **2b** is almost 10 times the K_I of **2a** (considering the experimental error involved in the analysis) (**Table 3.2**), reflecting the IC_{50} data (Dutta et al. 2010). Interestingly, the forward rate constants for inactivation (k_2) for both **2a**

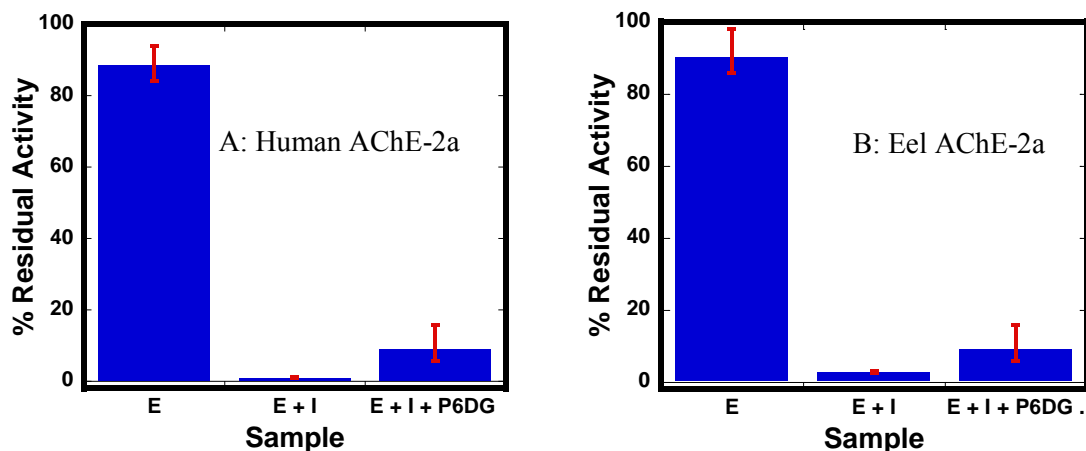


Fig. 3.2: Test of irreversibility of 2a-human/electric AChE reaction. A: 34 nM human AChE was incubated with 20 μ M of **2a** for 30 mins at 25°C in 20 mM Tris-Cl, pH-7.5 and passed through a P6DG desalting column. The enzyme was collected at the void volume, re-quantitated and assayed for activity. E represents the activity of enzyme incubated in buffer for 30 min and subjected to desalting. E + I represents the % residual activity of enzyme treated with inhibitor for 30 min but not desalted. For E + I the average activity for three trials was 0.2% of initial activity. E + I + desalt represents the activity of enzyme incubated with inhibitor for 30 min and purified by desalting gel. B: The same analysis was done with 34 nM electric eel AChE in presence of 200 μ M of **2a**. All the designations in the plot are same as A. For E + I the average activity for three trials was 1.0 % of initial activity. Error bars were generated from three independent experiments. Adapted from (Dutta et al. 2010)

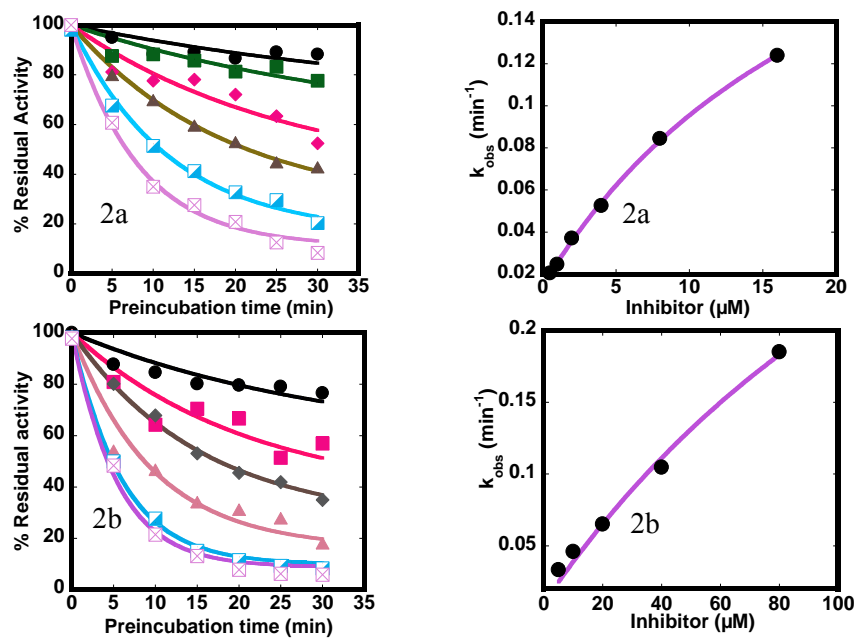


Fig. 3.3: Kinetics of inhibition of human AChE in presence of 2a and 2b. The left column shows the % residual activity as of function of pre-incubation time. Right column shows k_{obs} (min^{-1}) as a function of inhibitor (μM). The k_{obs} in the right column were obtained from the % residual activity vs pre-incubation time plot at the left column using **Model 1** (see **Chapter II**). The data in the k_{obs} (min^{-1}) vs inhibitor (μM) plot were fit with **Eqn 2** (see **Chapter II**) to obtain K_I , k_2 , and k_{-2} . Upper panel shows the kinetic study of **2a** against human AChE; **2a** = 0.5 (black circles), 1.0 (green squares), 2.0 (pink diamonds), 4.0 (brown triangles), 8.0 (half filled squares), and 16.0 μM (crossed violet squares). The lower panel shows the kinetic study of **2b** against human AChE; **2b** = 5 (black circles), 10 (pink squares), 20 (grey diamonds), 40 (brown triangle) 80 (half filled blue squares), and 160 μM (crossed violet squares). Adapted from (Dutta et al. 2010).

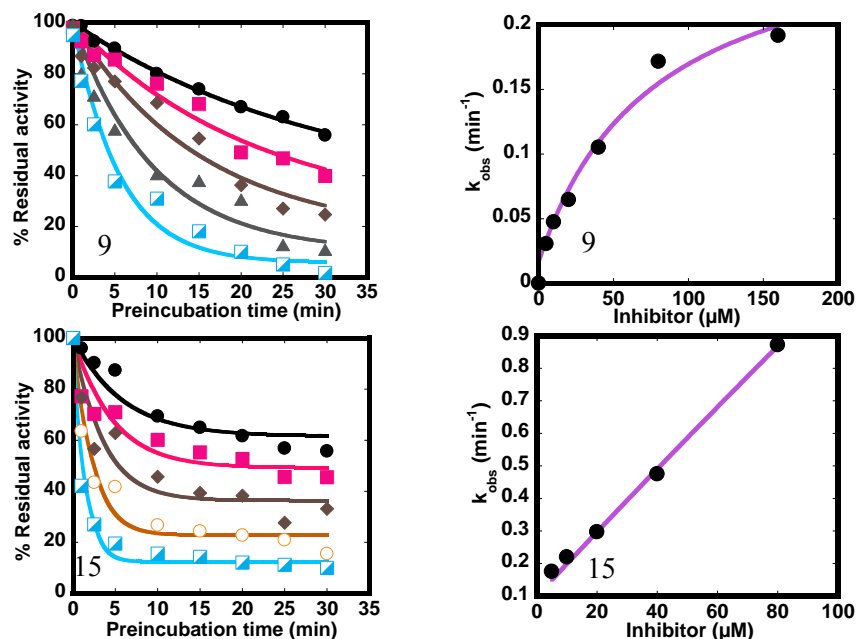


Fig. 3.4: Kinetics of inhibition of human AChE in presence of 9 and 15. The left column shows the % residual activity as a function of pre-incubation time. Right column shows the k_{obs} (min^{-1}) as a function of inhibitor (μM). The k_{obs} s in the right column were obtained from the % residual activity vs pre-incubation time plot at the left column using **Model 1**. The data in k_{obs} (min^{-1}) vs inhibitor (μM) plot at the right column were fit with **Eqn 2** (see **Chapter II**) to obtain K_i , k_1 , and k_2 . Upper panel shows the kinetic study of **9** against human AChE; **9** = 5 (black circles), 10 (pink squares), 20 (brown diamonds), 40 (grey triangles), and 80 μM (half filled blue squares). The lower panel shows the kinetic study of **15** against human AChE; **15** = 5 (black circles), 10 (pink squares), 20 (brown diamonds), 40 (orange open circle), and 80 μM (half filled blue squares). Adapted from (Dutta et al. 2010).

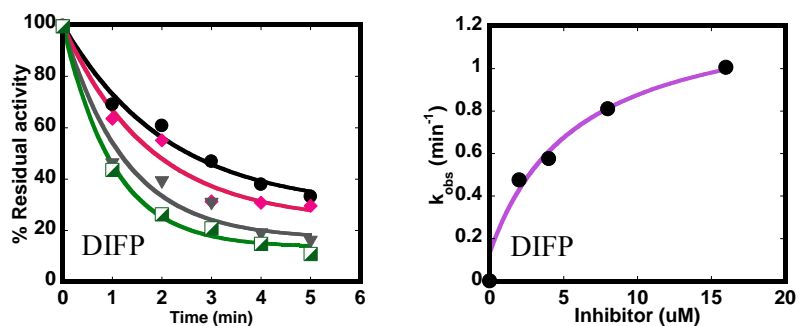
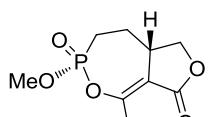
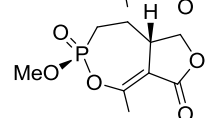
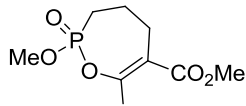
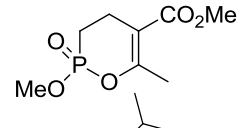
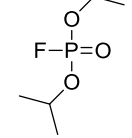


Fig. 3.5: Kinetics of inhibition of human AChE in presence of DIFP. The left panel shows the % residual activity as a function of pre-incubation time. Right panel shows the k_{obs} (min^{-1}) as a function of inhibitor (μM). The k_{obs} in right column were obtained from the % residual activity vs pre-incubation time plot on the left column using **Model 1**. The data in k_{obs} (min^{-1}) vs inhibitor (μM) plot at the right were fit with **Eqn 2** (see **Chapter II**) to obtain K_I , k_2 , and k_{-2} . $\mathbf{9} = 2$ (black circles), 4 (pink diamonds), 8 (grey inverted triangle) and 16 μM (half filled green squares). Adapted from (Dutta et al. 2010).

Table 3.2: Kinetic parameters of inhibition of human AChE by laboratory synthesized OPs.

Compound	Structure	Kinetic parameters		
		K_I (μM)	k_2 (min^{-1})	k_{-2} (min^{-1})
2a		24 ± 6.0	0.3 ± 0.06	0.02
2b		140 ± 58	0.4 ± 0.1	0.01
9		76 ± 20	0.2 ± 0.03	0.01
15		312 ± 134	4.2 ± 1.5	0.13
DIFP		6.0 ± 1.0	1.0 ± 0.1	0.13

Adapted from (Dutta et al. 2010).

and **2b** are similar, indicating the fact that the initial binding of the compounds to the active site of AChE was the determining factor for potency. Ten fold reverse rate constants for inactivation (k_{-2}) for both **2a** and **2b** compared to forward rate constant (k_2) confirmed the irreversible nature of the mechanism. The data indicate that distereomeric preference of **2a** by AChE is due to some specific initial contacts between **2a** and active site amino acid residues, which ultimately led to a successful inhibition. Moreover, compound **2a** showed 3-fold more affinity towards AChE than compound **9**, a monocyclic seven membered ring phosphonate, indicating the necessity of bicyclic entity or the lactone ring towards inhibitory activity. From a SAR point of view, if the ring strain is the sole reason for the reactivity of cyclic phosphonate, then reducing the ring size would give more potency against AChE.

Interestingly, compound **15**, a six membered monocyclic phosphonate, showed almost 10 times less affinity for AChE than compound **2a**. But the sole reactivity of compound **15** was reflected in its 14 times higher inactivation rate constant. It seems from the analysis that the seven-membered ring structure was optimum for moderate activity of the cyclic phosphonate. Though the six-membered ring phosphonate, compound **15**, showed similar activity with **2a** in terms of IC_{50} , the less tight initial binding of **15** could affect its specificity towards AChE active site, and thus might become a poor candidate as a potent inhibitor.

In terms of reactivity, DIFP shows 3 times higher affinity and 1 order of magnitude higher inactivation rate constant toward human AChE active site than **2a**. DIFP being a very strong nerve agent and already rejected as a drug option for

Alzheimer's disease, the milder option of **2a** may give an extra edge for successful drug discovery in the future.

3.2 Active site serine modification of AChE by cyclic phosphonate:

3.2.1 Oxime reactivation of OP-AChE complex:

Oxime is an antidote for nerve agents like sarin, soman, and VX (Marrs et al. 2006). As shown in **Fig. 2.1** in chapter II, oxime nucleophilically attacks the P –atom of OP-AChE complex and reactivates AChE by replacing the OP moiety from the active site. But sometimes even oxime cannot reactivate the inactivated OP-AChE complex because of a post complex modification of OP-AChE (**Fig. 3.6**). The common post complex modification is the aging reaction (Sultatos 1994). In the aging process, the active site water attacks the central phosphonate P and eliminates the O-alkyl group,

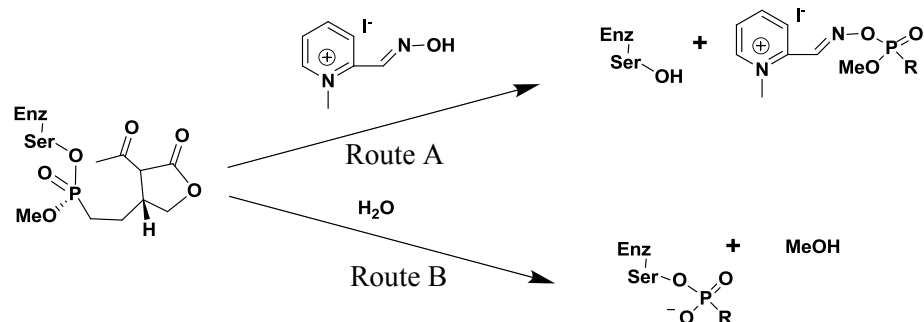


Fig. 3.6: Probable fate of human AChE-2a complex. Route A: **2a** covalently modifies the human AChE active site serine and forms a complex similar to the structure shown at the extreme left of the above picture. Pralidoxime can reactivate the **2a** inhibited human AChE by attacking the P-center. Nucleophilic attack of the oxime O-atom at the P-center of the complex may yield reactivated enzyme and OP-pralidoxime complex.

Route B: The AChE-**2a** adduct can also be attacked by an active site water molecule and may yield an inactivated enzyme having a less electrophilic P-centre. The resulting complex may be hard to reactivate even after oxime treatment.

which makes the P-centre less electrophilic and less vulnerable to oxime reactivation. If the OP-AChE complex undergoes aging, the oxime reactivation of inactivated AChE becomes difficult and it becomes almost impossible to reactivate the enzyme. Sarin and VX are the best examples of OPs that undergo productive aging reactions (Millard et al. 1999; Nachon et al. 2005).

Fig. 3.7 shows that the reaction of 35 mM pralidoxime at two different incubation times (30 and 120 mins) with the **2a**-AChE complex showed no more than 5% reactivation, considering pralidoxime's own effect of inhibition on AChE (Dutta et al. 2010). The reactivation of eel AChE was more significant (~13 % of actual enzyme activity) compared to human AChE; it is may be due to the lower activity of **2a** toward eel AChE or a slight difference in the active site geometry and constituent amino acid residues.

The above fact suggests to several possible mechanistic outcomes. The small reactivation could be either due to the aging process showed in **Fig. 3.6** or due to the modification of enzyme at sites other than the active site of the enzyme. It has been previously reported that the structure of the oxime also influences the reactivation process (Musilek et al. 2008; Kassa et al. 2009). Trp86, in the vicinity of the active site catalytic triad, participates in a π -cation interaction with an aromatic oxime and facilitates the nucleophilic attack of oxime O-atom on the P-centre of the OP-AChE complex (Sanson et al. 2009). It is possible that after the covalent modification by **2a**, the conformation of Trp86 changed, which in turn hinders the binding of the oxime to the Trp86 and results in poor reactivation of OP-AChE complex. The reactivation rate

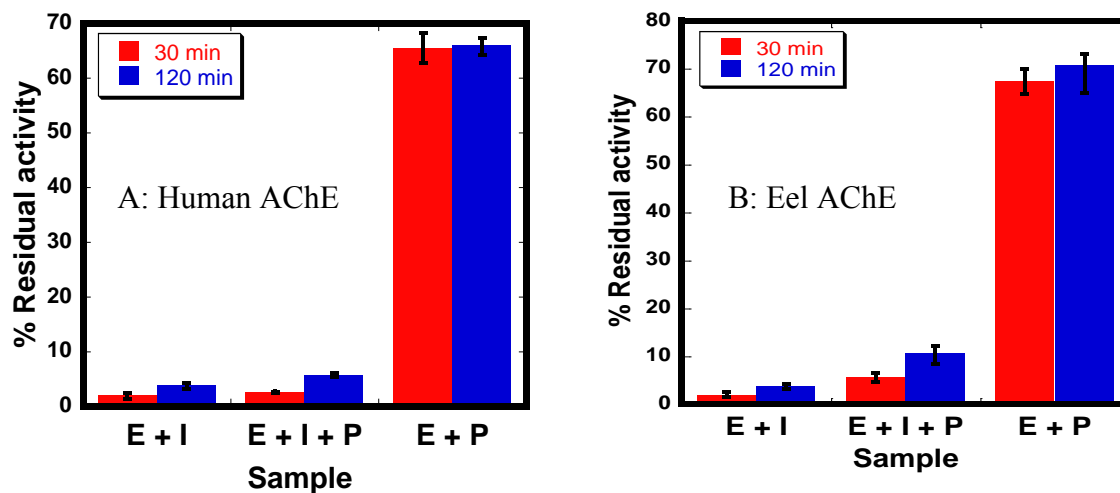


Fig. 3.7: Pralidoxime reactivation of human AChE-2a complex. A: 34 nM human AChE was incubated with 10 μ M of **2a** for 30 mins at 25°C in 20 mM Tris-Cl, pH-7.5. 35 mM pralidoxime was introduced and % residual activity of enzyme was determined. E + P, enzyme and pralidoxime control. E + I, enzyme and inhibitor control. E + I + P, enzyme and inhibitor and pralidoxime (see **Chapter II** for detail). All rates are expressed relative to the enzyme control at the same time point in the experiment. B: Same analysis was done using 34 nM electric eel AChE in presence of 150 μ M of **2a** and 35 mM pralidoxime. Adapted from (Dutta et al. 2010).

of **2a**-AChE complex by pralidoxime is evaluated to be 0.04 min^{-1} which is very close to the value of 0.05 min^{-1} , the reactivation rate found for DIFP-AChE complex by pralidoxime (Worek et al. 2004). This indicates that the low reactivation is not unique for **2a**-AChE complex; reactivation experiments using different oximes or mutational studies may be needed to yield some evidence to explain this. Finally, it can be concluded from **Fig. 3.7** data that pralidoxime has very little or no effect on reactivating the OP-AChE complex.

3.2.2 Mass Spectrometric analysis of trypsinized inhibitor-AChE complex:

To established covalent modification at the active site serine, human AChE-**2a** complex was subjected to proteolysis by trypsin, ZipTip purification and MALDI-TOF mass spectrometry (Dutta et al. 2010).

The theoretical mass of the peptide fragment (L_{178} - R_{219}) containing the active site serine is 4269.8 Da. The mass is calculated by feeding the human AChE amino acid sequence in to the MSDigest program (UCSF, bioinformatics tools) in trypsin mode of proteolysis. A peptide with a mass of 4267.9 Da was obtained from the MALDI-TOF data of trypsinized human AChE (**Fig. 3.8**). The mass shifted to 4500 Da when trypsinized human AChE-**2a** complex was subjected to MALDI-TOF (**Fig. 3.8**). **2a** has a molecular weight of 232 Da and existence of 4500 Da fragment in human AChE-**2a** MALDI-TOF data indicates covalent modification at the active site serine yielding a (4267.9+232) Da fragment.

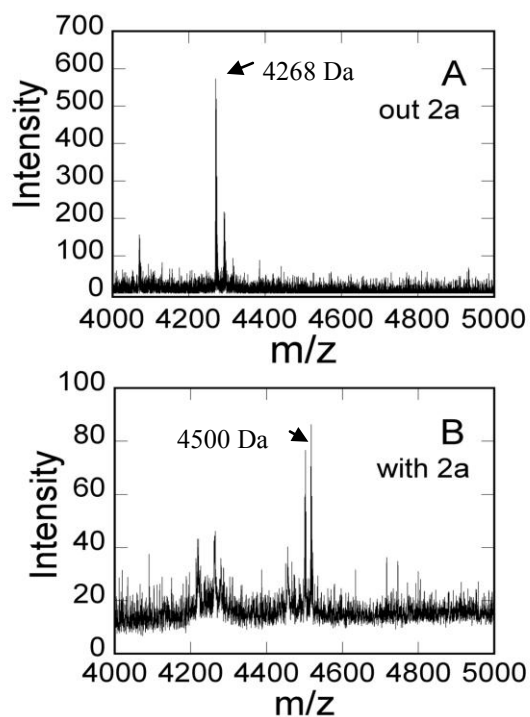


Fig. 3.8: MALDI-TOF evidence of covalent modification of human AChE active site serine. A: The figure shows the expected peak at 4268 Da for the (L₁₇₈-R₂₁₉) peptide fragment containing the active site serine. B: Human AChE was incubated with **2a** for 30 mins at 25°C and analyzed similarly. The figure shows the peak at 4500 Da, which can be attributed to modification of the (L₁₇₈-R₂₁₉) peptide fragment by **2a** (232 Da). Adapted from (Dutta et al. 2010).

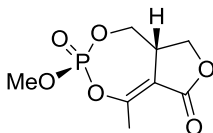
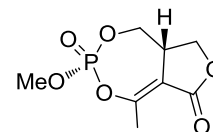
3.3 Inhibition studies of human AChE in presence of laboratory synthesized natural product cyclophostin:

3.3.1 Test of IC₅₀s of the natural and unnatural product of cyclophostin:

Like the phosphonate analog of cyclophostin, our collaborator supplied us with two diastereoisomeric forms of the natural product. This was because the phosphate starting material is achiral and can only yield two of the four isomers. In the structure of natural product cyclophostin, the methoxy group and the ring junction hydrogen are on the same side of the molecule. Our collaborator synthesized two isomers of cyclophostin, a) natural isomer of cyclophostin, having methoxy group and the ring junction hydrogen that are on the same side of the molecule, and b) unnatural product of cyclophostin, having the methoxy group and the ring junction hydrogen on opposite sides of the molecule (**Table 3.3**).

Like the cyclophosphonate analogs of cyclophostin, the IC₅₀s of both of the isomers were determined using Ellman's assay (Ellman et al. 1961). The IC₅₀ obtained for both of the isomers were around 40 nM (**Table 3.3**). Improved potency of the natural product compared to cyclophosphonate analog of cyclophostin was expected but not to the extent it actually exhibited (almost 1000 times more). Surprisingly, unlike **2a** and **2b**, the natural and unnatural product showed no diastereospecificity. It is possible that the presence of oxygen at the position 5 of the natural product makes the P-centre highly electrophilic, which minimizes the diastereospecificity towards the AChE active site. Synthesis and activity tests of the other two isomers of the natural product may

Table 3.3: Potency of natural and unnatural isomer of cyclophostin against human AChE.

Compound			IC ₅₀ (nM)
26	Natural Product		40
27	Unnatural Product		35

Natural product isomer of cyclophostin: The junction H-atom and the OMe group attached to the P-centre are on the same side of the molecule.

Unnatural product isomer of cyclophostin: The junction H-atom and the OMe group attached to the P-centre are on the opposite side of the molecule.

bring some light to this issue.

3.3.2 Mechanism of inhibition of human AChE by natural (compound 26) and unnatural cyclophostin (compound 27):

Since there is not much difference between the structure of the cyclic phosphonate analog of cyclophostin and the natural product, the test of irreversibility of the reaction of natural product and human AChE was performed. Both natural and unnatural isomers (100 nM) were incubated with human AChE and subjected to P6DG desalting column purification as discussed above. The eluted fractions of enzyme at the void volume for both isomers were re-quantitated and assayed. **Fig. 3.9** shows that for both isomers, the enzyme obtained after elution was inactive, again indicating the irreversible type of inactivation of this class of compound.

To determine the exact mechanism of inhibition, % residual activity of enzyme was recorded as a function of inhibitor concentration and incubation time for both the isomers against human AChE (**Fig. 3.10**). To obtain the equilibrium inhibition constant (K_I), forward rate constants for inactivation (k_2), and reverse rate constants for inactivation (k_{-2}), **Model 1** was utilized and the data were analyzed the same way described above for compound **2a** inhibition of AChE. The natural product and the unnatural product isomer showed similar equilibrium inhibition constant (K_I) which is consistent of their corresponding IC_{50} s (**Fig. 3.10 and Table 3.4**). Surprisingly, the forward rate constants for inactivation (k_2) for both isomers were only 2-3 times higher

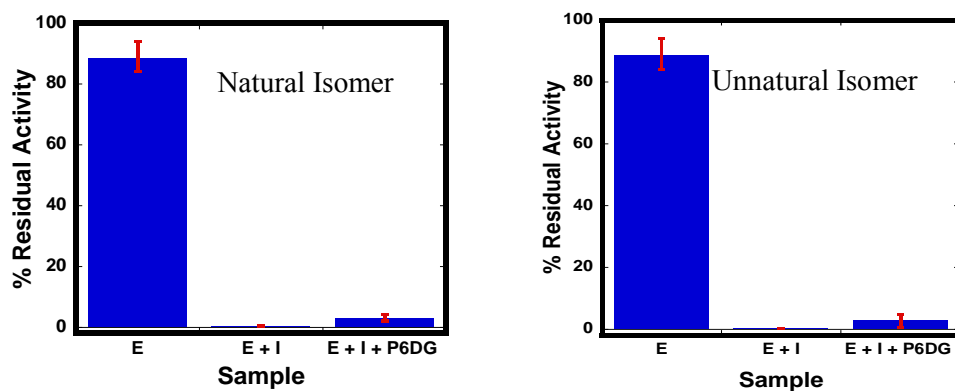


Fig. 3.9: Test of irreversibility of natural/unnatural (26/27) isomer-human AChE reaction.

A: 10 nM human AChE was incubated with 150 nM of natural isomer **26** for 30 mins at 25°C in 20 mM Tris-Cl, pH-7.5 and passed through P6DG desalting column. The enzyme was collected at the void volume, re-quantitated and assayed for activity. E represents the activity of the enzyme incubated in buffer for 30 min and subjected to desalting. E + I represents the % residual activity of enzyme treated with inhibitor for 30 min but not desalted. The average activity for three trials was 2.0 % of initial activity. E + I + P6DG represents the activity of enzyme incubated with inhibitor for 30 min and purified by desalting gel. B: The same analysis performed with 10 nM human AChE in presence of 150 nM of unnatural isomer **27**. Error bars were generated from three independent experiments.

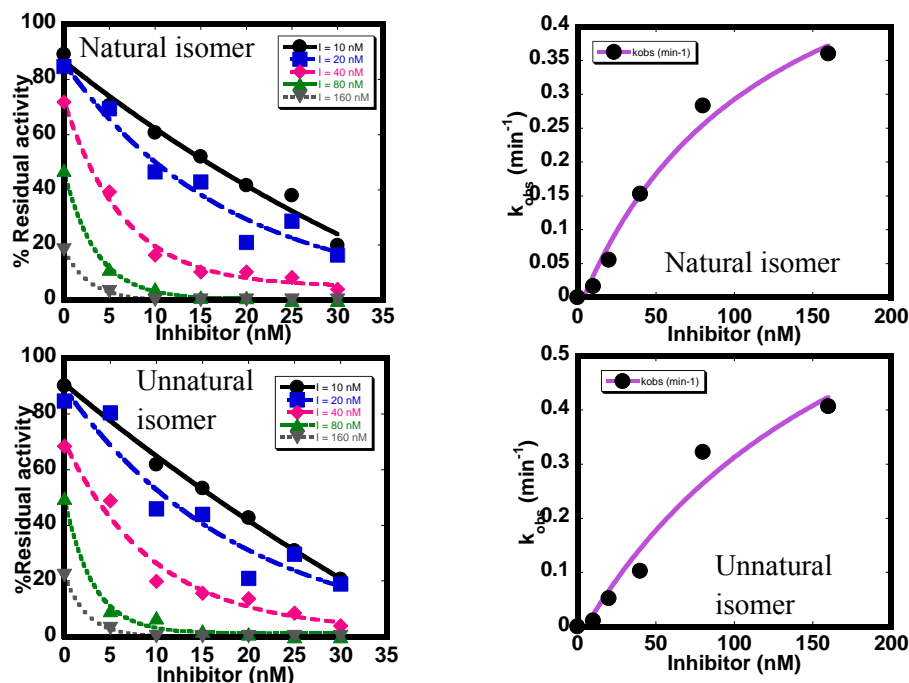
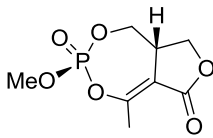
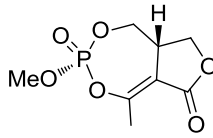


Fig. 3.10: Kinetics of inhibition of human AChE in presence of natural and unnatural isomer (26 and 27). The left column shows % residual activity as a function of pre-incubation time. Right column shows the k_{obs} (min^{-1}) as of function of inhibitor (nM). The k_{obs} s in right column were obtained from the % residual activity vs pre-incubation time plot at the left column using **Model 1**. The data in k_{obs} (min^{-1}) vs inhibitor (nM) plot at the right column were fit with **Eqn 2** (see **Chapter II**) to obtain K_i , k_2 , and k_{-2} . Upper panel shows the kinetic study of natural product **26** against human AChE; natural product = 10 (black circle), 20 (blue squares), 40 (pink diamonds), 80 (green triangles), and 160 nM (grey inverted triangle). The lower panel shows the kinetic study of unnatural product **27** against human AChE; unnatural product = 10, 20, 40, 80, and 160 nM (symbols as above). Human AChE = 10 nM.

Table 3.4: Kinetic parameters of inhibition of human AChE by natural (26) and unnatural isomer (27).

Compound		Kinetic Parameters		
		K_I (nM)	k_2 (min ⁻¹)	k_{-2} (min ⁻¹)
26		115±60	0.7±0.1	0
27		224±95	0.9±0.2	0

than that of the most potent μM range cyclophosphonate analogs of cyclophostin. It was bit surprising that the natural product having highly electrophilic phosphate P-centre did not show much difference in forward rate constants for inactivation (k_2) compared to phosphonate analog. The low values of reverse rate constants for inactivation (k_{-2}) for both the isomers explain a little bit of the above stated paradox. It is possible that insignificantly low values of reverse rate constants for inactivation (k_{-2}) contributed more towards the high potency of the natural product rather than the forward rate constants for inactivation (k_2) values.

3.3.3 Oxime reactivation of natural/unnatural product (26/27)-AChE complex:

Like cyclic phosphonate analogs, the natural and unnatural product isomers of cyclophostin exhibit a similar mechanism of inhibition against AChE, but with higher potential. Assuming that the isomers also covalently modify the active site serine, oxime reactivation experiments were conducted. Human AChE was incubated with natural/unnatural isomers of cyclophostin and subsequently reacted with pralidoxime and assayed for the activity. Like cyclicphosphonate case, both the isomers showed only residual reactivation (**Fig. 3.11**). The best way to address this issue is to get high resolution mass spectroscopy data of the trypsinized natural/unnatural isomer-AChE complex and look for probable peaks generated due to the mechanism route shown in **Fig. 3.6** or other mechanisms. It would also be instructive to perform reactivation kinetic studies of the complex using different oximes, to check for oxime specificity of the reaction.

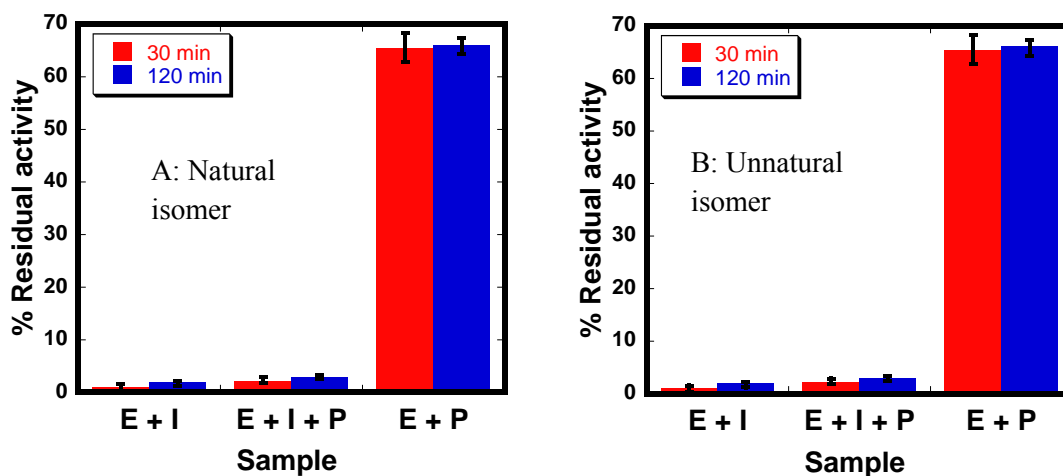


Fig. 3.11: Pralidoxime reactivation of human AChE-natural/unnatural isomer complex. A: 10 nM human AChE was incubated with 100 nM of natural isomer **26** for 30 mins at 25°C in 20 mM Tris-Cl, pH-7.5. 35 mM pralidoxime was introduced and % residual activity of enzyme was checked. E + P, enzyme and pralidoxime control. E + I, enzyme and inhibitor control. E + I + P, enzyme and inhibitor and pralidoxime (see **Chapter II**). All rates are expressed relative to the enzyme control at the same time point in the experiment. B: Same analysis was done with 10 nM human AChE in presence of 100 nM of unnatural isomer **27** and 35 mM pralidoxime.

CHAPTER IV

INHIBITION STUDIES OF RAT HORMONE-SENSITIVE LIPASE AND ITS PHOSPHORYLATION-INDUCED TRANSLOCATION IN 3T3-L1 CELLS

4.1 Structure-activity relationship of laboratory synthesized inhibitors of hormone-sensitive lipase HSL:

As discussed in **Chapter I**, hormone-sensitive lipase (HSL) is another SH family member like AChE. The active site of HSL contains a conserved serine residue, which acts as the nucleophile to attack the substrate's electrophilic centre (carbonyl C-atom). Though the exact geometry and structure of HSL's active site is still not known, it is shown from the mutational and modeling studies that unlike other esterases, the active site is hydrophobic and its activity largely dependent on hormone induction (Fredrikson et al. 1981; Osterlund et al. 1996; Anthonsen et al. 1998). It is proposed that hormone induction triggers structural changes in both regulatory and N-terminal domain, which in turn affects the activity of the enzyme.

HSL hydrolyzes lipids in the form of mono-, di-, and tri-acyl glycerols (MAG, DAG, and TAG) *in vitro* and *in vivo* (Fredrikson et al. 1981; Vossler et al. 1997; Shen et al. 1998). It has been reported that HSL can also hydrolyze organic esters like p-nitro phenyl butyrate (*p*-NPB) *in vitro* (Smith et al. 1996). It has been shown in the literature that limited proteolysis of HSL can destroy the lipase activity (TAG hydrolysis) but not the esterase activity (Smith et al. 1996).

Due to the HSL's direct role in lipid homeostasis, it is often associated with diabetes type-II, obesity and atherosclerosis disease conditions (Ylitalo et al. 2000; Hoffstedt et al. 2001; Teruel et al. 2005; Palou et al. 2009; Ishihara et al. 2010). Researchers have proposed that one of the ways to control abnormal lipid homeostasis in the insulin resistance state is to minimize the hydrolysis of TAG. One of the best ways to hinder the TAG hydrolysis is to inhibit the normal activity of HSL. Though according to some researchers tri-acyl glycerol lipase (ATGL) can also be targeted for the above purpose, HSL is still a best candidate due to its involvement in hormone regulated reaction cascade in adipose tissue (Kim et al. 2006; Schoenborn et al. 2006; Jocken et al. 2008).

4.1.1 Test of IC₅₀s for laboratory synthesized organophosphates (OP) against rat hormone-sensitive lipase (HSL):

Several potent HSL inhibitors have been reported in the literature (**Table 1.3** in **Chapter I**). All of the inhibitors are shown in **Table 1.3** are laboratory synthesized (Claus et al. 2005; Ben Ali et al. 2006). Mostly these inhibitors contain ester groups or lactone rings. However, almost all of the inhibitors reported to inhibit the lipase activity of the enzyme as well (Slee et al. 2003; de Jong et al. 2004; Ben Ali et al. 2006). Though it is well established from mass spectrometric data that these above compounds covalently modify the HSL active site, there is not much information available regarding the initial binding or secondary interactions of aromatic substituent of the inhibitors with active site residues of the enzyme.

Vertesy et. al. has reported the isolation and potency of cyclipostin, a natural product HSL inhibitor (**Table 1.4** in **Chapter I**). Cyclipostin is the first natural product inhibitor ever reported for HSL. The IC_{50} of cyclipostin against HSL is in the low nM range. The core structure of the compound is composed of a seven-membered phosphate ring fused with a five-membered lactone ring. The central P-atom has O-alkyl substitutions of variable C-chain length. Based on the data presented in **Chapter III**, it can be extrapolated that cyclipostin modifies the in HSL active site. In addition, the presence of the long C-chain substitution may facilitate the initial binding of the compound with hydrophobic residues in HSL active site.

Table 4.1 shows the list of compounds that we have tested to date against rat HSL. Except DIFP and compound **6** all other compounds have same core structure featuring a monocyclic seven-membered phosphonate ring and a C-chain at the 5 position. Compound **22a** and **b**, **23a** and **b**, and **24a** and **b** have six, ten and twelve C-chain moieties at their 5 positions, respectively. To evaluate the compounds' potency, the activity of rat HSL in presence of the inhibitors was tested using both esterase and lipase assays (experimental procedure in **Chapter II**). For esterase and lipase assays, *p*-NPB and 9, 10- H^3 -labelled triolein have been used as substrates, respectively. To test the validity of the HSL assay, the IC_{50} of DIFP has been tested using both esterase and lipase assays. The IC_{50} s of DIFP obtained for both esterase and lipase assays closely corroborated with the literature data of 50 μ M (Holm et al. 1989; Holm et al. 1991) and validated the assay procedure.

Table 4.1: IC₅₀s of laboratory synthesized HSL inhibitors.

Compound	Structure	IC ₅₀ (μM)			
		Esterase	Lipase		
			No PC/PI	PC/PI::1:3	PC/PI::1:2
DIFP		30	10	N.A	N.A
6		50	100	N.A	N.A
22a		10	N.A	100	100
22b		>1000	N.A	100	100
23a		500	N.A	150	100
23b		>1000	N.A	400	300
24a		>1000	N.A	350	175
24b		>1000	N.A	80	50
25		>1000	N.A	30	N.A

N.A – Not Applicable.

Compound **6** showed almost 18 and 36 fold less reactivity towards HSL in terms of esterase and lipase activity compared to AChE. This indicates that compound **6** is more specific for AChE active site and behaves more like the conventional AChE inhibitor DIFP. Compound **22a**, **23a**, and **24a** have same diastereomeric structure having the methoxy group and the H₅ on opposite sides of the ring, whereas **22b**, **23b**, and **24b** have methoxy and H₅ on the same side of the ring. Rat HSL showed diastereo specificity towards **22a** and **23a** over **22b** and **23b** in terms of esterase activity. The compounds did not show the same trend in terms of lipase activity. Surprisingly, both **24a** and **24b** showed no potency against rat HSL when esterase activity was tested. The improved potency was noticed in lipase activity when the C-chain length was increased to C₁₂ in **24b**. Both **24a** and **b** did not show any activity in HSL esterase assay. Finally, it is revealed from the result in **Table 4.1** that compounds **22** to **24** do not show a real trend in terms of structure-activity relationship (SAR). The compounds **22** to **24** have the same core structure like compound **9** in **Table 3.1**; **9** being an efficient cholinesterase inhibitor, it was expected that the compounds in **Table 4.1** would at least exhibit some activity in HSL esterase assay.

4.1.2 Effect of liposome composition on inhibitor activity:

It is well established in the literature that the ratio of liposome constituting materials phosphatidylcholine (PC) and phosphatidylinositol (PI) has a considerable effect on the activity of lipase enzymes (Ali et al. 2005; Petry et al. 2005). As mentioned in **Chapter II**, the inhibitors containing long chain C-chain were introduced to the rat HSL in liposome forms. Generally, the ratio of PC/PI was kept 1:3 to form the liposome. It is

not desirable to form large and multi-lamellar liposome entities containing the payload materials due to the limited accessibility of the enzyme. Considering this fact, the liposome composition ratio was changed to 1:2 (PC/PI) and the IC₅₀s of the compounds re-determined. **Table 4.1** shows the IC₅₀s of the compounds embedded in liposome containing PC/PI 1:2. It is revealed from the result that the change in the PC/PI ratio did not improve the potencies of the compounds.

4.2 *In vitro* fluorescence studies of rat HSL's hydrophobic surface exposure upon phosphorylation:

As discussed in **Chapter I**, HSL translocates from the cytoplasm to the lipid droplet upon hormone induced phosphorylation (**Fig. 1.15**). Krintel et al. (2009), has proven *in vitro* that upon PKA induced phosphorylation, the total hydrophobic surface area of HSL increases. This hydrophobic surface area enhancement may play a vital role in HSL's translocation from cytoplasm to lipid droplets *in vivo*. Krintel et al. (2009), has shown that phosphorylation leads to hydrophobic surface exposure but has not dissected the role of different phosphorylation sites in their work. It is possible that the surface exposure is an accumulative result of phosphorylation of all PKA- phosphorylation sites or it is just a single site phenomenon. This dissertation deals with this question by mutating the phosphorylation sites of rat HSL and testing the surface exposure phenomena.

The phenomena of hydrophobic surface exposure has been tested by exposing the protein to 1-anilinonaphthalene 8-sulfonate (ANS), an organic compound that binds with the hydrophobic surface of the protein and exhibits dramatic emission enhancement at 470

nm (detail in **Chapter II**). **Fig. 4.1A** shows that HSL dephosphorylated using protein phosphatases-2A (PP2ase) results in a decrease in the emission of ANS relative to partially phosphorylated HSL as purified from Sf9 cells. This result is consistent with Krintel et al. The same experiment has been done with rat HSL mutated to alanine at both the basal phosphorylation site S565 and regulatory phosphorylation site S563. **Fig. 4.1B** reveals that the partially phosphorylated and completely phosphorylated S563A/S565A double mutant behave similarly. It seems that either both basal and regulatory phosphorylation sites do not have considerable control on the exposure phenomena or it is a cumulative effect that involves the phosphorylation of all four PKA-dependent phosphorylation sites including S659 and S660. It is possible that the basal site S565 may not have any direct influence on the phosphorylation but as it influences the phosphorylation at S563, the indirect contribution of this site towards the exposure phenomena cannot be ruled out.

4.3 *In vivo* studies of rat HSL translocation from cytoplasm to lipid droplets in 3T3-L1 cells:

Though translocation of HSL to the lipid droplets does not always lead to the successful hydrolysis of lipids, the translocation process is one of the most vital steps in the reaction cascade of lipid homeostasis. As discussed in **Chapter I**, an eight amino acid hydrophobic patch (F₇₃₄LSLAALC₇₄₁) at the C-terminal domain of the rat HSL may contribute to the translocation process (Holm et al. 1988). The role of the hydrophobic patch in lipid binding has not yet been demonstrated experimentally and the speculated role of its contribution in HSL's translocation process needs to be tested. In this part of

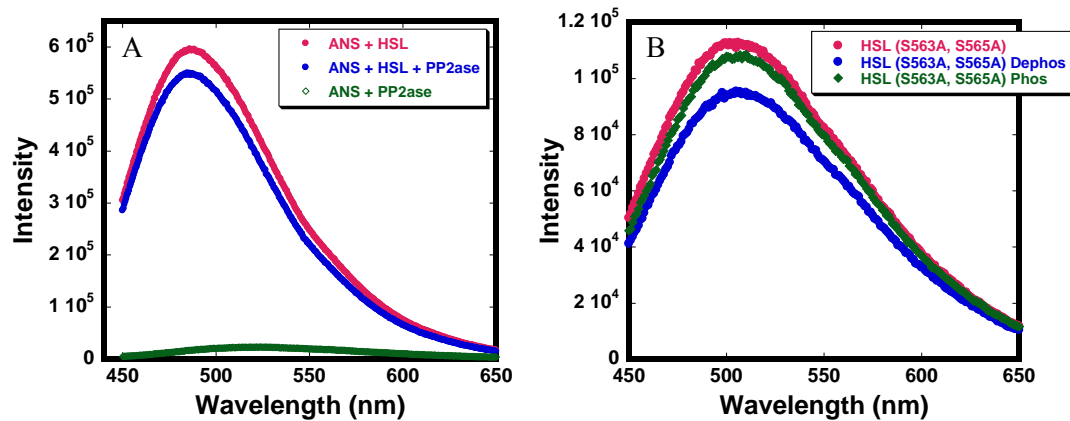


Fig. 4.1: ANS binding to rat HSL to probe the hydrophobic surface exposure.

A: ANS binding has been done with wild type rat HSL at two different conditions; ANS-wild type HSL (red curve) and ANS-PP2ase treated wild type HSL (blue curve) in 50 mM Tris, pH 7.5 at 25°C (see **Chapter II**). ANS has been excited at 380 nm and the emission has been recorded from 450 to 650 nm. The green curve represents the ANS-PP2ase emission. B: Same experiment has been done with double mutant HSL (S563A/S565A). Red, green, and blue curves represent the ANS binding with mutant HSL, PP2ase treated mutant HSL, and PP2ase and okadaic acid treated mutant HSL, respectively.

dissertation, the above hypothesis is examined in 3T3-L1 pre-adipocyte cells.

Researchers have long been using the 3T3-L1 pre-adipocyte cell system to study the different aspects of lipid metabolism (Wolins et al. 2005; Wolins et al. 2006; Granneman et al. 2007). Generally, the pre-adipocyte cells are differentiated to mature adipocytes so that the cells can store the lipid as lipid droplets (experimental detail in **Chapter II**). It has been established that 3T3-L1 pre-adipocytes can easily be transiently transfected to introduce genetic material in the cell for protein expression purposes (detail in **Chapter II**) (Granneman et al. 2007). To follow the translocation process of HSL upon phosphorylation, the protein has been tagged with yellow fluorescent protein (YFP) and the expression has been observed using confocal microscope (**Fig. 2.4**).

As HSL translocates from the cytoplasm to lipid droplets, it is important that the cells mature and form lipid droplets. To pursue the process, after transfection the cells have been chemically differentiated and the lipid droplets are chemically tagged with BODIPY-C₁₂ (detail in **Chapter II**). **Fig. 4.2** shows the co-localization of YFP-HSL and BODIPY-C₁₂ labeled lipid droplets in fully differentiated 3T3-L1 cells.

Using YFP as the potential donor and BODIPY as the acceptor fluorophore; the proximity of the HSL and lipid droplet has been tested by using Forster Resonance Energy Transfer (FRET). As shown in **Fig. 4.2**, FRET has been performed by exciting the donor fluorophore at 488 nm and monitoring the increase in acceptor emission at 510 nm. FRET has also been attempted using the ‘acceptor photo-bleaching’ method, where the acceptor has been photo-bleached at 504 nm and the increase in the donor emission is monitored (**Fig. 4.3**). Unfortunately, not even 5% increase of donor emission has been

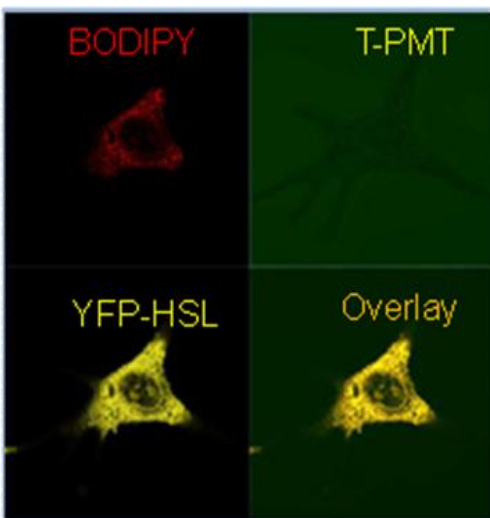


Fig. 4.2: BODIPY-C12 stained differentiated YFP-HSL transfected 3T3-L1 cells.

The YFP-HSL transfected 3T3-L1 cells were differentiated (protocol mentioned in the text) and then the cells were stained with BODIPY-C12 (20 $\mu\text{g/ml}$) for 1 hr at 37°C (protocol in the above text). The cells were washed with PBS three times and confocal image was taken. The picture was taken using Zeiss confocal imaging microscope (CNS, UMSL) with the following parameter set: Track 1 for BODIPY: lens: 63X, laser power master gain = 235, pin hole = 1AU, excitation at 488 nm and emission at 510 nm in Smart setup; track 2 YFP: lens: 63X, laser power master gain = 350, pin hole = 1AU, excitation at 488 nm and emission at 504 nm in Smart setup; track 3: lens: 63X, laser power master gain = 304, pin hole = 1AU, transmitted light (T-PMT) in Smart setup.

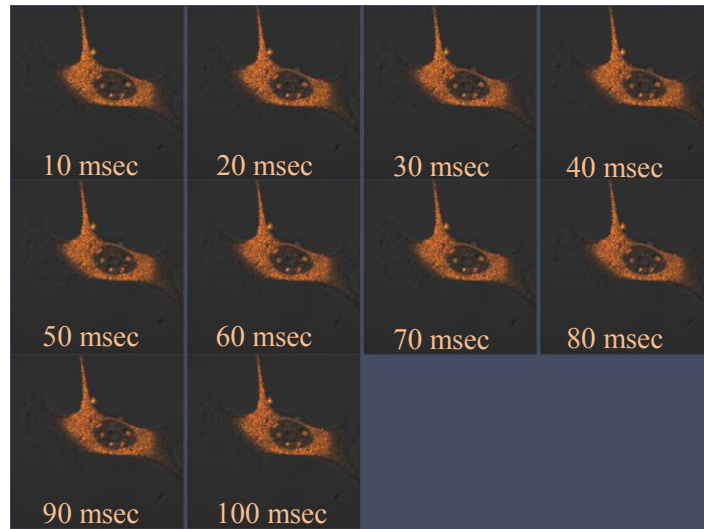


Fig. 4.3: FRET experiment to access HSL translocation to lipid droplet.

Transfection and the lipid staining have been done the same as described in **Fig. 4.2**. The confocal microscope has been set up same as **Fig. 4.2**, except for the FRET experiment, where the three channel mode has been activated. FRET has been performed using the acceptor photo bleaching method, where the donor has been excited at 488 nm and the acceptor has been photo-bleached at 504 nm. The donor emission enhancement was monitored every 10 msec for 100 msec. In the series mode, the stop option was kept 'on' when the intensity increase goes up to 10 %.

noticed in this process, which indicates that for some technical reason FRET has not been successful.

CHAPTER V

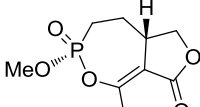
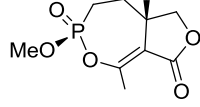
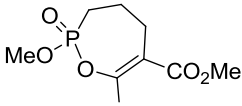
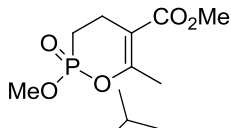
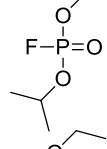
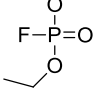
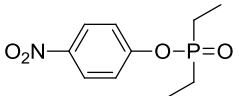
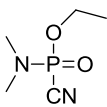
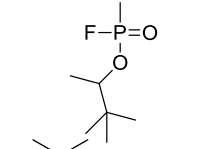
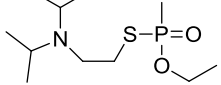
DISCUSSION

5.1 Comparison of potency of laboratory synthesized OPs with the commercially available OPs against human AChE:

The kinetic studies of AChE in presence of different analogs of cyclophostin reveal that both mono- and bi-cyclic compounds are low μM inhibitors and generally exhibit μM inhibition equilibrium constant. Moreover, these classes of compounds behave very similarly to DIFP, a commonly used organophosphate inhibitor for AChE. It is also revealed from **Table 3.2** that they are less potent than DIFP in terms of IC_{50}s , K_{I} , k_2 , and k_2 . Apart from compound **2a**'s species-specific activity that identified the compound as a potential insecticide candidate, it was necessary to compare **2a** and other compounds of its class to the other literature reported OPs.

For the above purpose, the potency of **2a**, **2b**, and **9** were compared with other OPs in terms of the K_{I} and k_{inact} parameters obtained using **Model 2** (simplified version of **Model 1** explained in **Chapter II**) (Walker et al. 2001). From K_{I} and k_{inact} , the k_{i} , a first order rate of inactivation, was calculated and compared with the literature values of k_{i} s of other OPs. The reproducibility of experimental and literature value of k_{i} of DIFP (experimental value $1.4 \text{ e}5 \text{ M}^{-1} \text{ min}^{-1}$ and literature value $1.3 \text{ e}5 \text{ M}^{-1} \text{ min}^{-1}$) authenticated our method (**Table 5.1**). **Table 5.1** shows that **2a**, **2b** and **9** have two orders of magnitude smaller k_{i} than that of the DIFP and three to five orders of magnitude smaller

Table 5.1: Comparison of first order rate of inactivation (k_i) of OPs against human AChE.

Compound	Structure	Kinetic parameters
		k_i ($M^{-1} \text{min}^{-1}$)
2a ^a		9×10^3
2b ^a		2.5×10^3
9 ^a		2.7×10^3
15 ^a		1.4×10^4
DIFP ^{a, b}		$1.4 \times 10^5 / 1.3 \times 10^5$
DEFP ^{a, c}		4.0×10^5
Paraoxon ^{a, c}		9.5×10^5
Tabun ^{a, b}		7.4×10^6
Soman ^{a, b}		9.2×10^7
VX ^{a, b}		1.2×10^8

k_i was calculated from k_{inact}/K_I for each compound using **Model 2 (Chapter II)**.

^a(Dutta et al. 2010); ^b(Worek et al. 2004); ^c(Ordentlich et al. 1993).

than those of tabun, soman, and VX (Worek et al. 2004; Dutta et al. 2010). This result indicates that the **2a** and **9** are much milder and less toxic than the other laboratory synthesized OPs, and can be potential Alzheimer's disease drug candidates.

On the other hand, the low nM potency of the natural and unnatural product of cyclophostin (compound **26** and **27** respectively) (**Table 3.4**) indicated that cyclic phosphate ring system has a unique ability to bind the AChE active site. This opened a new avenue to design potent inhibitors having similar cyclicphosphate-lactone bicyclic entity which was unknown before the analysis done in this dissertation.

5.2 Probable reasons for less potency of compound 22 to 24 against rat HSL:

One of the possible reasons of poor potency of these series of compounds may lie in their structures. The structures of compound **22** to **24** differ far from the naturally occurring potent cyclipostin inhibitors (**Fig. 5.1**). As is obvious from **Fig. 5.1**, the C-chain moiety is attached to the P-center as an alkoxy substituent in cyclipostin, whereas in compounds **22** to **24** the C-chain is attached to the C₅ ring carbon. It is possible that for successful binding as well as covalent modification of the HSL active site, it is essential to have the C-chain at the P-center. To put more light onto this matter, the C-terminal domain of HSL was modeled (**Fig. 5.2**) using the method called secondary structure aided multiple sequence alignment (SSAMSA) using SwissPDB Viewer tool (Guex and Peitsch 1997) (see **Chapter II for details**). Both **24** and cyclipostin were manually docked at the active site. **Fig. 5.3A** and **B** shows the docking results that indicate that if the C-chain is attached at the C₅ position, there will be less probability that **24** will orient in a way that successfully leads to the binding

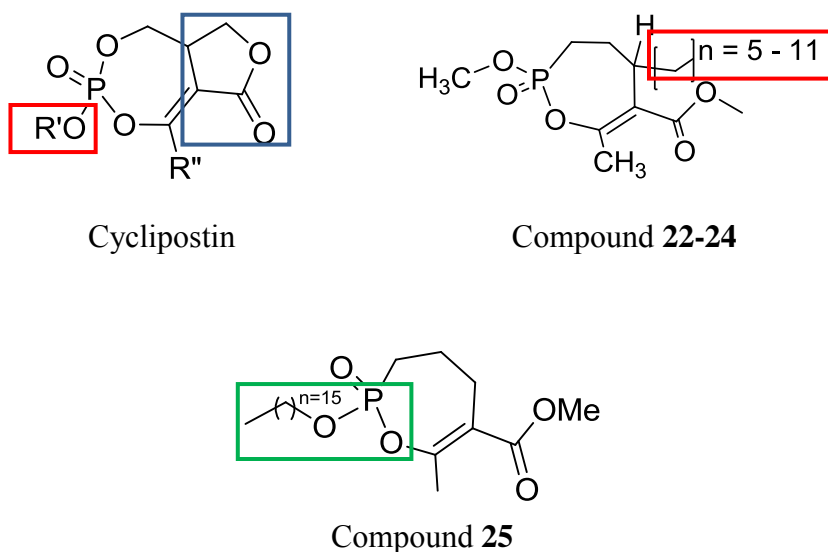


Fig. 5.1: Structural difference of cyclipostin and compound 22-25. Cyclipostin contains the O-alkoxy group having the long C-chain (red square) that is attached to the P-center, whereas the C-chain is attached at the C₅ in **22-24**. Moreover, cyclipostin has a five-membered lactone ring that is absent in **22-24**. Compound **25** is also shown in this figure where there is a C₁₆ C-chain is attached directly to the seven membered ring P-atom (green box). The structure is very similar to the natural product cyclipostin except its monocyclic entity.

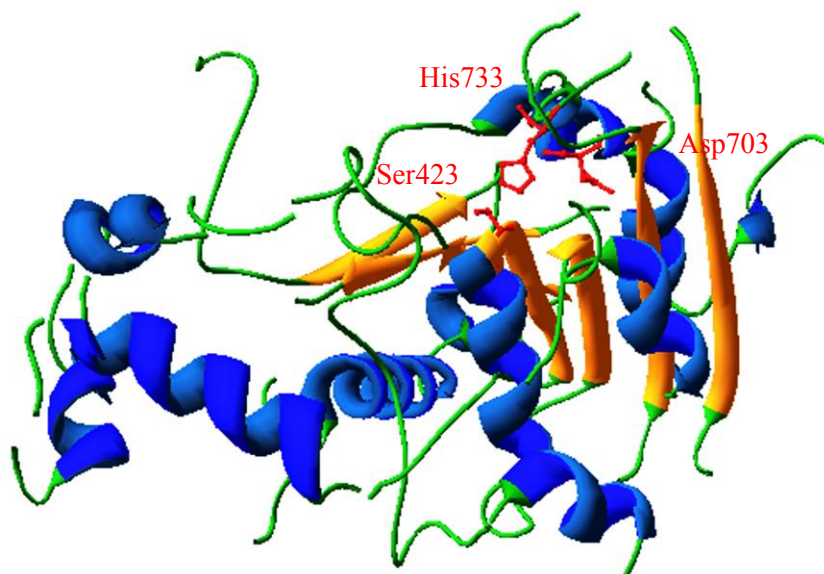


Fig. 5.2: Backbone structure of C-terminal domain of rat HSL. The C-terminal domain sequence (residues 300 to 767) of rat HSL has been fed to the SwissPDB viewer tool and the model has been obtained by using the *Candida rugosa* lipase (CRL) as template. The active site catalytic triad residues are shown in red. The discontinuity at the structure is due to the non-homologous sequence in rat HSL compared to CRL. The analysis is based on structure aided multiple sequence alignment (SSAMSA) which is termed as ‘magic fit’ in Swiss PDB viewer (Guex and Peitsch 1997) (more detail in **Chapter II**).

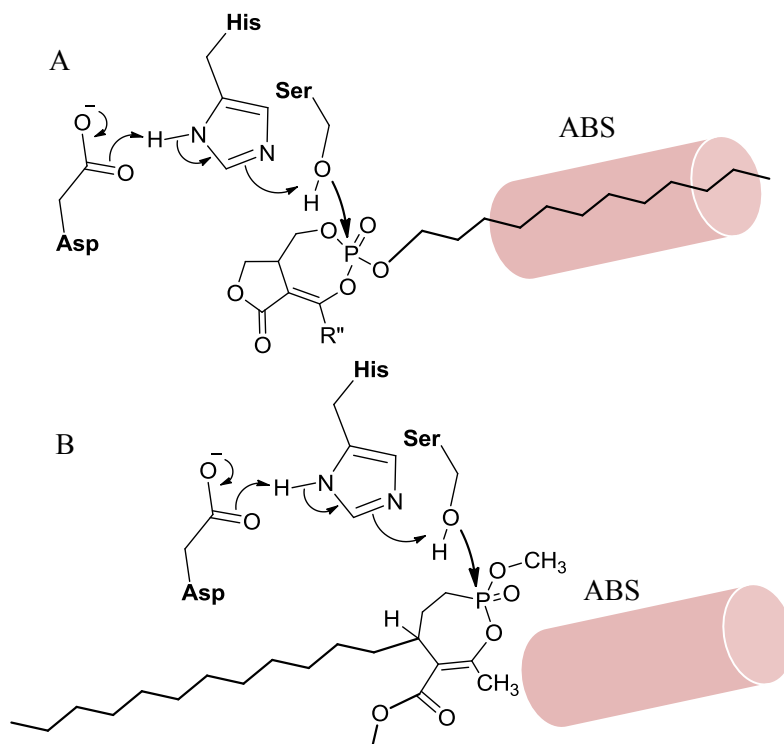


Fig. 5.3: Simplified docking model of cyclipostin and 24 in HSL active site. A: Cyclipostin has been manually docked in the rat HSL C-terminal domain that has been modeled (**Fig. 5.2**) using *Candida rugosa* lipase as a template. The P-center of cyclipostin is within a covalent bond distance of the O-atom of serine (~ 1.65 Å) and the long C-chain directs towards the acyl-binding site (ABS; pink cylinder) (residue 442-453). B: **24** has been docked in rat HSL C-terminal domain. Keeping the serine O-atom P-center distance constant as 1.6 Å, the long C-chain directs opposite to the ABS.

of C-chain to the acyl-binding site (ABS) and as well as the covalent modification at the active site serine. Improved potency of compound **25** (**Fig. 5.1**; **Table 4.1**) supports this above hypothesis.

The improved potency of monocyclic compound **25** (IC_{50} : lipase activity-30 μ M) (**Table 4.1** and **Fig. 5.1**) having C_{16} C-chain attached with O-atom of P-O functionality somehow corroborates with the above hypothesis but the potency still could not reach the nM range against rat HSL. Moreover, the compound did not show any esterase related activity.

Another possible reason for better potency of cyclipostin is that the O-atom (as H-bond acceptor) at the carbonyl function of the lactone ring at the bicyclic entity of the cyclipostin may involve in some secondary interactions with H-bond donor residues at the active site that are absent in **24**.

5.2.1 Compound 24 aggregation in aqueous solution and Dynamic light scattering (DLS) experiment:

It is a well known fact that molecules with long C-chains often aggregate in aqueous solution. If compound **22** to **24** aggregate in the buffer solution used, then it is possible that the aggregated form of the molecules will not be accessible to the enzyme. Compound **22-24** does not carry any charge in their structure which is very similar to triolein, the natural substrate of HSL. In general, the triolein are introduced to the enzyme in the form of liposome, a well-defined aggregated form, otherwise it might aggregate randomly in aqueous solution and could be inaccessible to the enzyme.

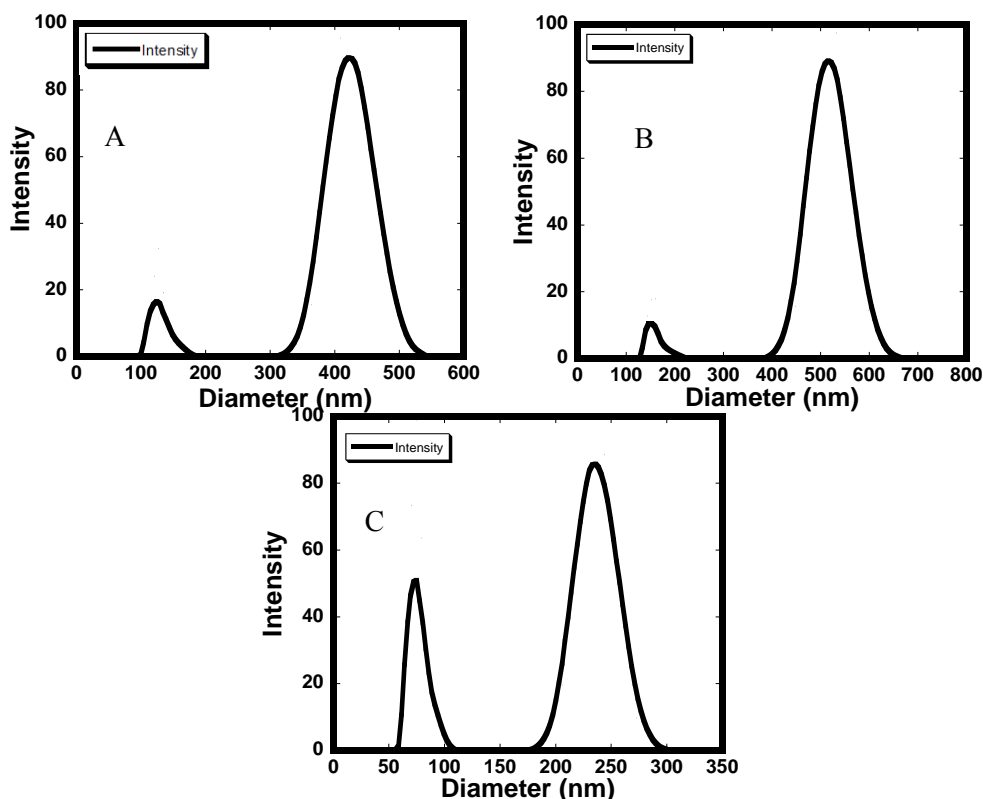


Fig. 5.4: Dynamic Light Scattering (DLS) experiment of **24.** In all of the above three figures, the following experimental conditions are constant: temperature = 25°C, dust cut off = 40.00, run = 4, angle = 90°, assumption of shape = shell, time = 3 mins. A: **24** = 2 μM , average count rate (ACR) = 154.4 cps, polydispersity = 0.217, effective diameter = 311.0 nm and baseline index = 9.3/100%; B: **24** = 125 μM , average count rate (ACR) = 380.4 cps, polydispersity = 0.208, effective diameter = 320.0 nm and baseline index = 9.3/74.4%; C: **24** = 125 μM in liposome having PC/PI=1/3, average count rate (ACR) = 439.5 cps, polydispersity = 0.209, effective diameter = 386.8 nm and baseline index = 6.4/30.19%. The additional peak that is observed at the lower diameter region in all cases is likely a contamination. High contamination observed in C was due to the low dust cut-off selected for the experiment.

Similarly, for compound **22-24** it is possible that due to their aggregation nature the potency of the compounds are underestimated. To determine if aggregation is one of the reasons for reduced potency of these classes of compounds, Dynamic Light Scattering (DLS) experiments (experimental detail in **Chapter II**) was performed on **24b** both in normal and liposome embedded forms. **Fig. 5.4A, B, and C** shows the DLS data of **24** where it is evident that even at 2 μM concentration, **24** has formed some sort of aggregated entity whose average diameter is ~ 450 nm (**Fig. 5.4A**). At 125 μM , the aggregated particle is larger (~ 600 nm) (**Fig. 5.4B**). Surprisingly, liposome-embedded **24** formed smaller particles (~ 250 nm) than the normal one at 125 μM (**Fig. 5.4B and C**). It is evident from the above data that laboratory synthesized analogs of cyclipostin aggregates in the aqueous solution. It is possible that HSL does not have access towards the business end of the molecule due to aggregation that leads to impaired inhibition in presence of this class of inhibitors.

To test the above hypotheses, the synthesis of cyclipostin is necessary. Kinetic, crystallographic and modeling studies of HSL in presence of cyclipostin may bring more light to this issue. This dissertation has contributed towards the initiation of the kinetic studies of analogs of cyclipostin against rat HSL that may help in the search for potential drugs against obesity and diabetes type II.

5.3 Phosphorylation induced translocation of rat HSL:

The biophysical characterization of the conformational change of rat HSL upon hormone-induced phosphorylation may ultimately contribute to the development of potent inhibitor against HSL. **Chapter III** has provided evidence that the

conformational change of HSL during the translocation towards lipid droplets is actually a hydrophobic surface exposure. *In vivo* experiments have been initiated to complement the above observation and multiple mutations have been constructed to identify the region of exposure. Moreover, preliminary data of the effect of phosphorylation on HSL is also provided. It is established that S563 and S565 have very little or no effect on the hydrophobic surface exposure of HSL upon phosphorylation. These results have opened multiple scopes to study the most interesting characteristics of HSL both *in vitro* and *in vivo*.

REFERENCES

- Aldridge, W. N. and E. Reiner (1969). "Acetylcholinesterase. Two types of inhibition by an organophosphorus compound: one the formation of phosphorylated enzyme and the other analogous to inhibition by substrate." Biochem J **115**(2): 147-62.
- Ali, Y. B., F. Carriere, et al. (2005). "Continuous monitoring of cholesterol oleate hydrolysis by hormone-sensitive lipase and other cholesterol esterases." J Lipid Res **46**(5): 994-1000.
- Alonso, D., I. Dorronsoro, et al. (2005). "Donepezil-tacrine hybrid related derivatives as new dual binding site inhibitors of AChE." Bioorg Med Chem **13**(24): 6588-97.
- Anthonsen, M. W., L. Ronnstrand, et al. (1998). "Identification of novel phosphorylation sites in hormone-sensitive lipase that are phosphorylated in response to isoproterenol and govern activation properties in vitro." J Biol Chem **273**(1): 215-21.
- Bandyopadhyay, S., S. Dutta, et al. (2008). "Synthesis and biological evaluation of a phosphonate analog of the natural acetyl cholinesterase inhibitor cyclophostin." J Org Chem **73**(21): 8386-91.
- Barak, D., A. Ordentlich, et al. (1995). "Allosteric modulation of acetylcholinesterase activity by peripheral ligands involves a conformational transition of the anionic subsite." Biochemistry **34**(47): 15444-52.
- Belluti, F., L. Piazzini, et al. (2009). "Design, synthesis, and evaluation of benzophenone derivatives as novel acetylcholinesterase inhibitors." Eur J Med Chem **44**(3): 1341-8.
- Ben Ali, Y., H. Chahinian, et al. (2004). "Might the kinetic behavior of hormone-sensitive lipase reflect the absence of the lid domain?" Biochemistry **43**(29): 9298-306.
- Ben Ali, Y., H. Chahinian, et al. (2006). "Use of an inhibitor to identify members of the hormone-sensitive lipase family." Biochemistry **45**(47): 14183-91.
- Ben-Ari, S., D. Toiber, et al. (2006). "Modulated splicing-associated gene expression in P19 cells expressing distinct acetylcholinesterase splice variants." J Neurochem **97 Suppl 1**: 24-34.
- Bouma, B. N., L. A. Miles, et al. (1980). "Human plasma prekallikrein. Studies of its activation by activated factor XII and of its inactivation by diisopropyl phosphofluoridate." Biochemistry **19**(6): 1151-60.
- Bourne, Y., P. Taylor, et al. (1995). "Acetylcholinesterase inhibition by fasciculin: crystal structure of the complex." Cell **83**(3): 503-12.
- Bourne, Y., P. Taylor, et al. (2003). "Structural insights into ligand interactions at the acetylcholinesterase peripheral anionic site." Embo J **22**(1): 1-12.
- Bracey, M. H., M. A. Hanson, et al. (2002). "Structural adaptations in a membrane enzyme that terminates endocannabinoid signaling." Science **298**(5599): 1793-6.
- Brasaemle, D. L., B. Rubin, et al. (2000). "Perilipin A increases triacylglycerol storage by decreasing the rate of triacylglycerol hydrolysis." J Biol Chem **275**(49): 38486-93.

- Brasaemle, D. L., V. Subramanian, et al. (2009). "Perilipin A and the control of triacylglycerol metabolism." Mol Cell Biochem **326**(1-2): 15-21.
- Brocca, S., F. Secundo, et al. (2003). "Sequence of the lid affects activity and specificity of *Candida rugosa* lipase isoenzymes." Protein Sci **12**(10): 2312-9.
- Callan OH, S. O., Swinney DC. (1996). "The kinetic factors that determine the affinity and selectivity for slow binding inhibition of human prostaglandin H synthase 1 and 2 by indomethacin and flurbiprofen." J Biol Chem **271**(7): 3548-54.
- Casida, J. E., D. K. Nomura, et al. (2008). "Organophosphate-sensitive lipases modulate brain lysophospholipids, ether lipids and endocannabinoids." Chem Biol Interact **175**(1-3): 355-64.
- Casida, J. E. and G. B. Quistad (2004). "Organophosphate toxicology: safety aspects of nonacetylcholinesterase secondary targets." Chem Res Toxicol **17**(8): 983-98.
- Chambers, J. and S. F. Oppenheimer (2004). "Organophosphates, serine esterase inhibition, and modeling of organophosphate toxicity." Toxicol Sci **77**(2): 185-7.
- Clark, J. D., A. R. Schievella, et al. (1995). "Cytosolic phospholipase A2." J Lipid Mediat Cell Signal **12**(2-3): 83-117.
- Claus, T. H., D. B. Lowe, et al. (2005). "Specific inhibition of hormone-sensitive lipase improves lipid profile while reducing plasma glucose." J Pharmacol Exp Ther **315**(3): 1396-402.
- Clifford, G. M., D. K. McCormick, et al. (1998). "Dephosphorylation of perilipin by protein phosphatases present in rat adipocytes." FEBS Lett **435**(1): 125-9.
- Contreras, J. A., M. Karlsson, et al. (1996). "Hormone-sensitive lipase is structurally related to acetylcholinesterase, bile salt-stimulated lipase, and several fungal lipases. Building of a three-dimensional model for the catalytic domain of hormone-sensitive lipase." J Biol Chem **271**(49): 31426-30.
- Cook, K. G., R. J. Colbran, et al. (1983). "Cytosolic cholesterol ester hydrolase from bovine corpus luteum. Its purification, identification, and relationship to hormone-sensitive lipase." Biochim Biophys Acta **752**(1): 46-53.
- Cook, K. G., F. T. Lee, et al. (1981). "Hormone-sensitive cholesterol ester hydrolase of bovine adrenal cortex: identification of the enzyme protein." FEBS Lett **132**(1): 10-4.
- Cook, K. G., S. J. Yeaman, et al. (1982). "Direct evidence that cholesterol ester hydrolase from adrenal cortex is the same enzyme as hormone-sensitive lipase from adipose tissue." Eur J Biochem **125**(1): 245-9.
- Cutler, N. R. and J. J. Sramek (2001). "Review of the next generation of Alzheimer's disease therapeutics: challenges for drug development." Prog Neuropsychopharmacol Biol Psychiatry **25**(1): 27-57.
- de Jong, J. C., L. G. Sorensen, et al. (2004). "Carbazates as potent inhibitors of hormone-sensitive lipase." Bioorg Med Chem Lett **14**(7): 1741-4.
- DeClerck, Y. A., S. Imren, et al. (1997). "Proteases and protease inhibitors in tumor progression." Adv Exp Med Biol **425**: 89-97.
- Donsmark, M., J. Langfort, et al. (2004). "Regulation and role of hormone-sensitive lipase in rat skeletal muscle." Proc Nutr Soc **63**(2): 309-14.

- Dutta, S., R. K. Malla, et al. (2010). "Synthesis and kinetic analysis of some phosphonate analogs of cyclophostin as inhibitors of human acetylcholinesterase." Bioorg Med Chem **18**(6): 2265-74.
- Eckert, S., P. Eyer, et al. (2006). "Kinetic analysis of the protection afforded by reversible inhibitors against irreversible inhibition of acetylcholinesterase by highly toxic organophosphorus compounds." Biochem Pharmacol **72**(3): 344-57.
- Ellman, G. L., K. D. Courtney, et al. (1961). "A new and rapid colorimetric determination of acetylcholinesterase activity." Biochem Pharmacol **7**: 88-95.
- Feller, G., M. Thiry, et al. (1991). "Nucleotide sequence of the lipase gene lip2 from the antarctic psychrotroph *Moraxella* TA144 and site-specific mutagenesis of the conserved serine and histidine residues." DNA Cell Biol **10**(5): 381-8.
- Fredrikson, G. and P. Belfrage (1983). "Positional specificity of hormone-sensitive lipase from rat adipose tissue." J Biol Chem **258**(23): 14253-6.
- Fredrikson, G., P. Stralfors, et al. (1981). "Hormone-sensitive lipase of rat adipose tissue. Purification and some properties." J Biol Chem **256**(12): 6311-20.
- Froede, H. C. and I. B. Wilson (1984). "Direct determination of acetyl-enzyme intermediate in the acetylcholinesterase-catalyzed hydrolysis of acetylcholine and acetylthiocholine." J Biol Chem **259**(17): 11010-3.
- Garton, A. J., D. G. Campbell, et al. (1989). "Phosphorylation of bovine hormone-sensitive lipase by the AMP-activated protein kinase. A possible antilipolytic mechanism." Eur J Biochem **179**(1): 249-54.
- Glynn, P. (1999). "Neuropathy target esterase." Biochem J **344 Pt 3**: 625-31.
- Glynn, P., D. J. Read, et al. (1994). "Synthesis and characterization of a biotinylated organophosphorus ester for detection and affinity purification of a brain serine esterase: neuropathy target esterase." Biochem J **301 (Pt 2)**: 551-6.
- Gonzalez-Sanchez, J. L. and M. Serrano-Rios (2007). "Molecular basis of insulin action." Drug News Perspect **20**(8): 527-31.
- Gorrell, M. D. (2005). "Dipeptidyl peptidase IV and related enzymes in cell biology and liver disorders." Clin Sci (Lond) **108**(4): 277-92.
- Granneman, J. G., H. P. Moore, et al. (2007). "Analysis of lipolytic protein trafficking and interactions in adipocytes." J Biol Chem **282**(8): 5726-35.
- Granneman, J. G., H. P. Moore, et al. (2009). "Perilipin controls lipolysis by regulating the interactions of AB-hydrolase containing 5 (Abhd5) and adipose triglyceride lipase (Atgl)." J Biol Chem **284**(50): 34538-44.
- Greenberg, A. S., W. J. Shen, et al. (2001). "Stimulation of lipolysis and hormone-sensitive lipase via the extracellular signal-regulated kinase pathway." J Biol Chem **276**(48): 45456-61.
- Grober, J., H. Laurell, et al. (1997). "Characterization of the promoter of human adipocyte hormone-sensitive lipase." Biochem J **328 (Pt 2)**: 453-61.
- Grober, J., S. Lucas, et al. (2003). "Hormone-sensitive lipase is a cholesterol esterase of the intestinal mucosa." J Biol Chem **278**(8): 6510-5.
- Groop, L., C. Forsblom, et al. (1996). "Metabolic consequences of a family history of NIDDM (the Botnia study): evidence for sex-specific parental effects." Diabetes **45**(11): 1585-93.

- Guex, N. and M. C. Peitsch (1997). "SWISS-MODEL and the Swiss-PdbViewer: an environment for comparative protein modeling." Electrophoresis **18**(15): 2714-23.
- Harel, M., I. Schalk, et al. (1993). "Quaternary ligand binding to aromatic residues in the active-site gorge of acetylcholinesterase." Proc Natl Acad Sci U S A **90**(19): 9031-5.
- Harel, M., C. T. Su, et al. (1991). "Refined crystal structures of "aged" and "non-aged" organophosphoryl conjugates of gamma-chymotrypsin." J Mol Biol **221**(3): 909-18.
- Hasegawa, M., Y. Tang, et al. (2002). "Differential regulation of gene expression and insulin-induced activation of phosphodiesterase 3B in adipocytes of lean insulin-resistant IRS-1 (-/-) mice." Diabetes Res Clin Pract **58**(2): 79-85.
- Hemila, H., T. T. Koivula, et al. (1994). "Hormone-sensitive lipase is closely related to several bacterial proteins, and distantly related to acetylcholinesterase and lipoprotein lipase: identification of a superfamily of esterases and lipases." Biochim Biophys Acta **1210**(2): 249-53.
- Hillman, G. R. and H. G. Mautner (1970). "Hydrolysis of electronically and sterically defined substrates of acetylcholinesterase." Biochemistry **9**(13): 2633-8.
- Hoffstedt, J., P. Arner, et al. (2001). "A common hormone-sensitive lipase i6 gene polymorphism is associated with decreased human adipocyte lipolytic function." Diabetes **50**(10): 2410-3.
- Holm, C., P. Belfrage, et al. (1989). "Human adipose tissue hormone-sensitive lipase: identification and comparison with other species." Biochim Biophys Acta **1006**(2): 193-7.
- Holm, C., R. C. Davis, et al. (1991). "Expression of biologically active hormone-sensitive lipase in mammalian (COS) cells." FEBS Lett **285**(1): 139-44.
- Holm, C., R. C. Davis, et al. (1994). "Identification of the active site serine of hormone-sensitive lipase by site-directed mutagenesis." FEBS Lett **344**(2-3): 234-8.
- Holm, C., T. G. Kirchgessner, et al. (1988). "Hormone-sensitive lipase: sequence, expression, and chromosomal localization to 19 cent-q13.3." Science **241**(4872): 1503-6.
- Holm, C., T. G. Kirchgessner, et al. (1988). "Nucleotide sequence of rat adipose hormone sensitive lipase cDNA." Nucleic Acids Res **16**(20): 9879.
- Holm, C., T. Osterlund, et al. (2000). "Molecular mechanisms regulating hormone-sensitive lipase and lipolysis." Annu Rev Nutr **20**: 365-93.
- Hotamisligil, G. S., P. Arner, et al. (1995). "Increased adipose tissue expression of tumor necrosis factor-alpha in human obesity and insulin resistance." J Clin Invest **95**(5): 2409-15.
- Ishihara, Y., K. Ohmori, et al. (2010). "Beneficial direct adipotropic actions of pitavastatin in vitro and their manifestations in obese mice." Atherosclerosis.
- Jenkins-Kruchten, A. E., A. Bennaars-Eiden, et al. (2003). "Fatty acid-binding protein-hormone-sensitive lipase interaction. Fatty acid dependence on binding." J Biol Chem **278**(48): 47636-43.

- Jocken, J. W., E. Smit, et al. (2008). "Adipose triglyceride lipase (ATGL) expression in human skeletal muscle is type I (oxidative) fiber specific." Histochem Cell Biol **129**(4): 535-8.
- Johnson, G. and S. W. Moore (2006). "The peripheral anionic site of acetylcholinesterase: structure, functions and potential role in rational drug design." Curr Pharm Des **12**(2): 217-25.
- Johnson, J. L., B. Cusack, et al. (2003). "Unmasking tandem site interaction in human acetylcholinesterase. Substrate activation with a cationic acetanilide substrate." Biochemistry **42**(18): 5438-52.
- Kam, C. M., A. S. Abuelyaman, et al. (1993). "Biotinylated isocoumarins, new inhibitors and reagents for detection, localization, and isolation of serine proteases." Bioconjug Chem **4**(6): 560-7.
- Kassa, J., J. Karasova, et al. (2009). "A comparison of the reactivating and therapeutic efficacy of newly developed bispyridinium oximes (K250, K251) with commonly used oximes against tabun in rats and mice." J Enzyme Inhib Med Chem **24**(4): 1040-4.
- Kidd, D., Y. Liu, et al. (2001). "Profiling serine hydrolase activities in complex proteomes." Biochemistry **40**(13): 4005-15.
- Kim, J. Y., K. Tillison, et al. (2006). "The adipose tissue triglyceride lipase ATGL/PNPLA2 is downregulated by insulin and TNF-alpha in 3T3-L1 adipocytes and is a target for transactivation by PPARgamma." Am J Physiol Endocrinol Metab **291**(1): E115-27.
- Kitamura, T., Y. Kitamura, et al. (1999). "Insulin-induced phosphorylation and activation of cyclic nucleotide phosphodiesterase 3B by the serine-threonine kinase Akt." Mol Cell Biol **19**(9): 6286-96.
- Kitz, R. and I. B. Wilson (1962). "Esters of methanesulfonic acid as irreversible inhibitors of acetylcholinesterase." J Biol Chem **237**: 3245-9.
- Klannemark, M., M. Orho, et al. (1998). "The putative role of the hormone-sensitive lipase gene in the pathogenesis of Type II diabetes mellitus and abdominal obesity." Diabetologia **41**(12): 1516-22.
- Kraemer, F. B. and W. J. Shen (2002). "Hormone-sensitive lipase: control of intracellular tri-(di-)acylglycerol and cholesteryl ester hydrolysis." J Lipid Res **43**(10): 1585-94.
- Krintel, C., M. Morgelin, et al. (2009). "Phosphorylation of hormone-sensitive lipase by protein kinase A in vitro promotes an increase in its hydrophobic surface area." Febs J **276**(17): 4752-62.
- Krintel, C., P. Osmark, et al. (2008). "Ser649 and Ser650 are the major determinants of protein kinase A-mediated activation of human hormone-sensitive lipase against lipid substrates." PLoS One **3**(11): e3756.
- Kropp, T. J. and R. J. Richardson (2007). "Mechanism of aging of mipafox-inhibited butyrylcholinesterase." Chem Res Toxicol **20**(3): 504-10.
- Kryger, G., I. Silman, et al. (1999). "Structure of acetylcholinesterase complexed with E2020 (Aricept): implications for the design of new anti-Alzheimer drugs." Structure **7**(3): 297-307.

- Kurokawa, T., K. Suzuki, et al. (1993). "Cyclophostin, acetylcholinesterase inhibitor from *Streptomyces lavendulae*." J Antibiot (Tokyo) **46**(8): 1315-8.
- Kyte, J. and R. F. Doolittle (1982). "A simple method for displaying the hydrophobic character of a protein." J Mol Biol **157**(1): 105-32.
- Lahiri, D. K., J. T. Rogers, et al. (2004). "Rationale for the development of cholinesterase inhibitors as anti-Alzheimer agents." Curr Pharm Des **10**(25): 3111-9.
- Langin, D., H. Laurell, et al. (1993). "Gene organization and primary structure of human hormone-sensitive lipase: possible significance of a sequence homology with a lipase of *Moraxella* TA144, an antarctic bacterium." Proc Natl Acad Sci U S A **90**(11): 4897-901.
- Liu, Y., M. P. Patricelli, et al. (1999). "Activity-based protein profiling: the serine hydrolases." Proc Natl Acad Sci U S A **96**(26): 14694-9.
- Londos, C., D. L. Brasaemle, et al. (1999). "On the control of lipolysis in adipocytes." Ann N Y Acad Sci **892**: 155-68.
- Londos, C., D. L. Brasaemle, et al. (1999). "Perilipins, ADRP, and other proteins that associate with intracellular neutral lipid droplets in animal cells." Semin Cell Dev Biol **10**(1): 51-8.
- Londos, C., R. C. Honnor, et al. (1985). "cAMP-dependent protein kinase and lipolysis in rat adipocytes. III. Multiple modes of insulin regulation of lipolysis and regulation of insulin responses by adenylate cyclase regulators." J Biol Chem **260**(28): 15139-45.
- Maelicke, A. and E. X. Albuquerque (2000). "Allosteric modulation of nicotinic acetylcholine receptors as a treatment strategy for Alzheimer's disease." Eur J Pharmacol **393**(1-3): 165-70.
- Mallender, W. D., T. Szegletes, et al. (2000). "Acetylthiocholine binds to asp74 at the peripheral site of human acetylcholinesterase as the first step in the catalytic pathway." Biochemistry **39**(26): 7753-63.
- Marcinkiewicz, A., D. Gauthier, et al. (2006). "The phosphorylation of serine 492 of perilipin directs lipid droplet fragmentation and dispersion." J Biol Chem **281**(17): 11901-9.
- Marrs, T. C., P. Rice, et al. (2006). "The role of oximes in the treatment of nerve agent poisoning in civilian casualties." Toxicol Rev **25**(4): 297-323.
- Martin, S., S. Okano, et al. (2009). "Spatiotemporal regulation of early lipolytic signaling in adipocytes." J Biol Chem **284**(46): 32097-107.
- Mignatti, P. and D. B. Rifkin (1996). "Plasminogen activators and angiogenesis." Curr Top Microbiol Immunol **213** (Pt 1): 33-50.
- Millard, C. B. and C. A. Broomfield (1995). "Anticholinesterases: medical applications of neurochemical principles." J Neurochem **64**(5): 1909-18.
- Millard, C. B., G. Kryger, et al. (1999). "Crystal structures of aged phosphorylated acetylcholinesterase: nerve agent reaction products at the atomic level." Biochemistry **38**(22): 7032-9.
- Miyoshi, H., S. C. Souza, et al. (2006). "Perilipin promotes hormone-sensitive lipase-mediated adipocyte lipolysis via phosphorylation-dependent and -independent mechanisms." J Biol Chem **281**(23): 15837-44.

- Moore, D. E. and G. P. Hess (1975). "Acetylcholinesterase-catalyzed hydrolysis of an amide." Biochemistry **14**(11): 2386-9.
- Moore, H. P., R. B. Silver, et al. (2005). "Perilipin targets a novel pool of lipid droplets for lipolytic attack by hormone-sensitive lipase." J Biol Chem **280**(52): 43109-20.
- Musilek, K., J. Kucera, et al. (2008). "Monoquaternary pyridinium salts with modified side chain-synthesis and evaluation on model of tabun- and paraoxon-inhibited acetylcholinesterase." Bioorg Med Chem **16**(17): 8218-23.
- Nachmansohn, D. and I. B. Wilson (1951). "The enzymic hydrolysis and synthesis of acetylcholine." Adv Enzymol Relat Subj Biochem **12**: 259-339.
- Nachon, F., O. A. Asojo, et al. (2005). "Role of water in aging of human butyrylcholinesterase inhibited by echothiophate: the crystal structure suggests two alternative mechanisms of aging." Biochemistry **44**(4): 1154-62.
- Nelson, P. S., L. Gan, et al. (1999). "Molecular cloning and characterization of prostate, an androgen-regulated serine protease with prostate-restricted expression." Proc Natl Acad Sci U S A **96**(6): 3114-9.
- Nilsson, N. O., P. Stralfors, et al. (1980). "Regulation of adipose tissue lipolysis: effects of noradrenaline and insulin on phosphorylation of hormone-sensitive lipase and on lipolysis in intact rat adipocytes." FEBS Lett **111**(1): 125-30.
- Ollis, D. L., E. Cheah, et al. (1992). "The alpha/beta hydrolase fold." Protein Eng **5**(3): 197-211.
- Ordentlich, A., D. Barak, et al. (1993). "Dissection of the human acetylcholinesterase active center determinants of substrate specificity. Identification of residues constituting the anionic site, the hydrophobic site, and the acyl pocket." J Biol Chem **268**(23): 17083-95.
- Osterlund, T., D. J. Beussman, et al. (1999). "Domain identification of hormone-sensitive lipase by circular dichroism and fluorescence spectroscopy, limited proteolysis, and mass spectrometry." J Biol Chem **274**(22): 15382-8.
- Osterlund, T., B. Danielsson, et al. (1996). "Domain-structure analysis of recombinant rat hormone-sensitive lipase." Biochem J **319** (Pt 2): 411-20.
- Pace, C. N., F. Vajdos, et al. (1995). "How to measure and predict the molar absorption coefficient of a protein." Protein Sci **4**(11): 2411-23.
- Palou, M., T. Priego, et al. (2009). "Gene expression patterns in visceral and subcutaneous adipose depots in rats are linked to their morphologic features." Cell Physiol Biochem **24**(5-6): 547-56.
- Pang, Y. P. (2006). "Novel acetylcholinesterase target site for malaria mosquito control." PLoS One **1**: e58.
- Parker, C. W., S. M. Godt, et al. (1967). "Fluorescent probes for the study of the antibody-hapten reaction. II. Variation in the antibody combining site during the immune response." Biochemistry **6**(11): 3417-27.
- Parnetti, L. (1995). "Clinical pharmacokinetics of drugs for Alzheimer's disease." Clin Pharmacokinet **29**(2): 110-29.
- Passolunghi, S., S. Brocca, et al. (2003). "Monitoring the transport of recombinant *Candida rugosa* lipase by a green fluorescent protein-lipase fusion." Biotechnol Lett **25**(22): 1945-8.

- Patricelli, M. P., D. K. Giang, et al. (2001). "Direct visualization of serine hydrolase activities in complex proteomes using fluorescent active site-directed probes." Proteomics **1**(9): 1067-71.
- Pauling, P. and T. J. Petcher (1971). "Inhibitors of acetylcholinesterase. Crystal structure of neostigmine bromide." J Med Chem **14**(1): 1-2.
- Petry, S., Y. Ben Ali, et al. (2005). "Sensitive assay for hormone-sensitive lipase using NBD-labeled monoacylglycerol to detect low activities in rat adipocytes." J Lipid Res **46**(3): 603-14.
- Raclot, T., C. Holm, et al. (2001). "A role for hormone-sensitive lipase in the selective mobilization of adipose tissue fatty acids." Biochim Biophys Acta **1532**(1-2): 88-96.
- Radic, Z., R. Manetsch, et al. (2008). "Probing gorge dimensions of cholinesterases by freeze-frame click chemistry." Chem Biol Interact **175**(1-3): 161-5.
- Radic, Z., N. A. Pickering, et al. (1993). "Three distinct domains in the cholinesterase molecule confer selectivity for acetyl- and butyrylcholinesterase inhibitors." Biochemistry **32**(45): 12074-84.
- Raves, M. L., M. Harel, et al. (1997). "Structure of acetylcholinesterase complexed with the nootropic alkaloid, (-)-huperzine A." Nat Struct Biol **4**(1): 57-63.
- Rawlings, N. D., A. J. Barrett, et al. "MEROPS: the peptidase database." Nucleic Acids Res **38**(Database issue): D227-33.
- Rawlings, N. D., A. J. Barrett, et al. (2010). "MEROPS: the peptidase database." Nucleic Acids Res **38**(Database issue): D227-33.
- Resjo, S., O. Goransson, et al. (2002). "Protein phosphatase 2A is the main phosphatase involved in the regulation of protein kinase B in rat adipocytes." Cell Signal **14**(3): 231-8.
- Reynisdottir, S., M. Eriksson, et al. (1995). "Impaired activation of adipocyte lipolysis in familial combined hyperlipidemia." J Clin Invest **95**(5): 2161-9.
- Robitzki, A., A. Mack, et al. (1998). "Butyrylcholinesterase antisense transfection increases apoptosis in differentiating retinal reagggregates of the chick embryo." J Neurochem **71**(4): p413-20.
- Rondinone, C. M., E. Carvalho, et al. (2000). "Phosphorylation of PDE3B by phosphatidylinositol 3-kinase associated with the insulin receptor." J Biol Chem **275**(14): 10093-8.
- Rosenberry, T. L. (1975). "Acetylcholinesterase." Adv Enzymol Relat Areas Mol Biol **43**: 103-218.
- Rosenberry, T. L. (1975). "Catalysis by acetylcholinesterase: evidence that the rate-limiting step for acylation with certain substrates precedes general acid-base catalysis." Proc Natl Acad Sci U S A **72**(10): 3834-8.
- Rosenberry, T. L. (2010). "Strategies to resolve the catalytic mechanism of acetylcholinesterase." J Mol Neurosci **40**(1-2): 32-9.
- Rosenberry, T. L. and S. A. Bernhard (1971). "Studies of catalysis by acetylcholinesterase. I. Fluorescent titration with a carbamoylating agent." Biochemistry **10**(22): 4114-20.

- Rosenberry, T. L., L. K. Sonoda, et al. (2008). "Analysis of the reaction of carbachol with acetylcholinesterase using thioflavin T as a coupled fluorescence reporter." Biochemistry **47**(49): 13056-63.
- Sanson, B., F. Nachon, et al. (2009). "Crystallographic snapshots of nonaged and aged conjugates of soman with acetylcholinesterase, and of a ternary complex of the aged conjugate with pralidoxime." J Med Chem **52**(23): 7593-603.
- Schoenborn, V., I. M. Heid, et al. (2006). "The ATGL gene is associated with free fatty acids, triglycerides, and type 2 diabetes." Diabetes **55**(5): 1270-5.
- Shafferman, A., C. Kronman, et al. (1992). "Mutagenesis of human acetylcholinesterase. Identification of residues involved in catalytic activity and in polypeptide folding." J Biol Chem **267**(25): 17640-8.
- Shen, W. J., S. Patel, et al. (2010). "Vimentin is a functional partner of hormone sensitive lipase and facilitates lipolysis." J Proteome Res **9**(4): 1786-94.
- Shen, W. J., S. Patel, et al. (2009). "Functional interaction of hormone-sensitive lipase and perilipin in lipolysis." J Lipid Res **50**(11): 2306-13.
- Shen, W. J., S. Patel, et al. (1998). "Mutational analysis of structural features of rat hormone-sensitive lipase." Biochemistry **37**(25): 8973-9.
- Shen, W. J., K. Sridhar, et al. (1999). "Interaction of rat hormone-sensitive lipase with adipocyte lipid-binding protein." Proc Natl Acad Sci U S A **96**(10): 5528-32.
- Shirai, K., N. Matsuoka, et al. (1982). "Effect of phospholipids on lipase activity in rat arterial wall homogenate." Tohoku J Exp Med **138**(2): 131-7.
- Slee, D. H., A. S. Bhat, et al. (2003). "Pyrrolopyrazinedione-based inhibitors of human hormone-sensitive lipase." J Med Chem **46**(7): 1120-2.
- Smih, F., P. Rouet, et al. (2002). "Transcriptional regulation of adipocyte hormone-sensitive lipase by glucose." Diabetes **51**(2): 293-300.
- Smith, G. M., A. J. Garton, et al. (1996). "Evidence for a multi-domain structure for hormone-sensitive lipase." FEBS Lett **396**(1): 90-4.
- Soreq, H., D. Patinkin, et al. (1994). "Antisense oligonucleotide inhibition of acetylcholinesterase gene expression induces progenitor cell expansion and suppresses hematopoietic apoptosis ex vivo." Proc Natl Acad Sci U S A **91**(17): 7907-11.
- Sridhar, G. R., H. Thota, et al. (2006). "Alzheimer's disease and type 2 diabetes mellitus: the cholinesterase connection?" Lipids Health Dis **5**: 28.
- Stralfors, P. and P. Belfrage (1983). "Phosphorylation of hormone-sensitive lipase by cyclic AMP-dependent protein kinase." J Biol Chem **258**(24): 15146-52.
- Stralfors, P., P. Bjorgell, et al. (1984). "Hormonal regulation of hormone-sensitive lipase in intact adipocytes: identification of phosphorylated sites and effects on the phosphorylation by lipolytic hormones and insulin." Proc Natl Acad Sci U S A **81**(11): 3317-21.
- Stralfors, P. and R. C. Honnor (1989). "Insulin-induced dephosphorylation of hormone-sensitive lipase. Correlation with lipolysis and cAMP-dependent protein kinase activity." Eur J Biochem **182**(2): 379-85.
- Su, C. L., C. Sztalryd, et al. (2003). "Mutational analysis of the hormone-sensitive lipase translocation reaction in adipocytes." J Biol Chem **278**(44): 43615-9.

- Sultatos, L. G. (1994). "Mammalian toxicology of organophosphorus pesticides." J Toxicol Environ Health **43**(3): 271-89.
- Sussman, J. L., M. Harel, et al. (1991). "Atomic structure of acetylcholinesterase from *Torpedo californica*: a prototypic acetylcholine-binding protein." Science **253**(5022): 872-9.
- Syu, L. J. and A. R. Saltiel (1999). "Lipotrinsin: a novel docking protein for hormone-sensitive lipase." Mol Cell **4**(1): 109-15.
- Szegletes, T., W. D. Mallender, et al. (1999). "Substrate binding to the peripheral site of acetylcholinesterase initiates enzymatic catalysis. Substrate inhibition arises as a secondary effect." Biochemistry **38**(1): 122-33.
- Sztalryd, C., G. Xu, et al. (2003). "Perilipin A is essential for the translocation of hormone-sensitive lipase during lipolytic activation." J Cell Biol **161**(6): 1093-103.
- Tanaka, M., C. Vedhachalam, et al. (2006). "Effect of carboxyl-terminal truncation on structure and lipid interaction of human apolipoprotein E4." Biochemistry **45**(13): 4240-7.
- Taylor, P. (1998). "Development of acetylcholinesterase inhibitors in the therapy of Alzheimer's disease." Neurology **51**(1 Suppl 1): S30-5; discussion S65-7.
- Teruel, T., R. Hernandez, et al. (2005). "Rosiglitazone up-regulates lipoprotein lipase, hormone-sensitive lipase and uncoupling protein-1, and down-regulates insulin-induced fatty acid synthase gene expression in brown adipocytes of Wistar rats." Diabetologia **48**(6): 1180-8.
- Vertesy, L., B. Beck, et al. (2002). "Cyclipostins, novel hormone-sensitive lipase inhibitors from *Streptomyces* sp. DSM 13381. II. Isolation, structure elucidation and biological properties." J Antibiot (Tokyo) **55**(5): 480-94.
- Vossler, M. R., H. Yao, et al. (1997). "cAMP activates MAP kinase and Elk-1 through a B-Raf- and Rap1-dependent pathway." Cell **89**(1): 73-82.
- Walker, M. C., R. G. Kurumbail, et al. (2001). "A three-step kinetic mechanism for selective inhibition of cyclo-oxygenase-2 by diarylheterocyclic inhibitors." Biochem J **357**(Pt 3): 709-18.
- Wang, H., L. Hu, et al. (2009). "Activation of hormone-sensitive lipase requires two steps, protein phosphorylation and binding to the PAT-1 domain of lipid droplet coat proteins." J Biol Chem **284**(46): 32116-25.
- Watt, M. J., A. G. Holmes, et al. (2006). "Regulation of HSL serine phosphorylation in skeletal muscle and adipose tissue." Am J Physiol Endocrinol Metab **290**(3): E500-8.
- Weill, M., P. Fort, et al. (2002). "A novel acetylcholinesterase gene in mosquitoes codes for the insecticide target and is non-homologous to the ace gene in *Drosophila*." Proc Biol Sci **269**(1504): 2007-16.
- Winkler, U., N. J. Allison, et al. (1996). "Characterization, application and potential uses of biotin-tagged inhibitors for lymphocyte serine proteases (granzymes)." Mol Immunol **33**(7-8): 615-23.
- Wolins, N. E., B. K. Quaynor, et al. (2005). "S3-12, Adipophilin, and TIP47 package lipid in adipocytes." J Biol Chem **280**(19): 19146-55.

- Wolins, N. E., B. K. Quaynor, et al. (2006). "OP9 mouse stromal cells rapidly differentiate into adipocytes: characterization of a useful new model of adipogenesis." J Lipid Res **47**(2): 450-60.
- Wong, L., Z. Radic, et al. (2000). "Mechanism of oxime reactivation of acetylcholinesterase analyzed by chirality and mutagenesis." Biochemistry **39**(19): 5750-7.
- Wood, S. L., N. Emmison, et al. (1993). "The protein phosphatases responsible for dephosphorylation of hormone-sensitive lipase in isolated rat adipocytes." Biochem J **295** (Pt 2): 531-5.
- Worek, F., H. Thiermann, et al. (2004). "Kinetic analysis of interactions between human acetylcholinesterase, structurally different organophosphorus compounds and oximes." Biochem Pharmacol **68**(11): 2237-48.
- Yamaguchi, T. "Crucial role of CGI-58/alpha/beta hydrolase domain-containing protein 5 in lipid metabolism." Biol Pharm Bull **33**(3): 342-5.
- Yeaman, S. J. (2004). "Hormone-sensitive lipase--new roles for an old enzyme." Biochem J **379**(Pt 1): 11-22.
- Ylitalo, K., V. Large, et al. (2000). "Reduced hormone-sensitive lipase activity is not a major metabolic defect in Finnish FCHL families." Atherosclerosis **153**(2): 373-81.
- Yoshida, S. and S. Shiosaka (1999). "Plasticity-related serine proteases in the brain (review)." Int J Mol Med **3**(4): 405-9.
- Zhang, H. H., S. C. Souza, et al. (2003). "Lipase-selective functional domains of perilipin A differentially regulate constitutive and protein kinase A-stimulated lipolysis." J Biol Chem **278**(51): 51535-42.

VITA

Supratik Dutta was born in Burdwan, West Bengal, India on November 29, 1977 to Subinoy Dutta and Gopa Dutta. In 1996 Supratik graduated from the Christian Missionary High School in Burdwan. He entered the Chemistry department of Vivekananda College where he received his Bachelor's degree in Chemistry in 1999. He ranked third in the university examination and entered the Masters' degree program in Department of Chemistry at the University of Burdwan, WB, India. He earned a Masters' in Science with specialization in organic chemistry in 2001 from the same university. After the completion of his Master's degree he worked in Acharya Jagadish Chandra Bose Institute in Calcutta for few years as an institute research scholar. In the fall of 2005 he entered the graduate program at the University of Missouri in St.Louis where he earned his Master's degree in Biochemistry in May 2007.

Permanent address:

Supratik Dutta
56 Puratan Chawk Road, Burdwan,
West Bengal,
India

Publication:

1. **Dutta, S.**, Malla, R. K., Bandyopadhyay, S., Spilling C. D., Dupureur C. M. (2010). "Synthesis and kinetic analysis of some phosphonate analogs of cyclophostin as inhibitors of human acetylcholinesterase." Bioorg Med Chem **18**(6): 2265-74.
2. Bandyopadhyay, S., **Dutta, S.**, Spilling C. D., Dupureur C. M., Rath, N. P. (2008). "Synthesis and biological evaluation of a phosphonate analog of the natural acetyl cholinesterase inhibitor cyclophostin." J Org Chem **73**(21): 8386-91.
